POLITECNICO
MILANO 1863

SCUOLA DI INGEGNERIA INDUSTRIALE
E DELL'INFORMAZIONE

sMAPPER: a database-based simulation framework for modeling and analyzing battery energy storage systems

Tesi di Laurea Magistrale in
Energy Engineering - Ingegneria Energetica

Author: **Jibril Sharafi**

Student ID: 964874
Advisor: Prof. Giampaolo Manzolini
Co-advisors: Enrico Casalini, Luca Moretti
Academic Year: 2021-22

Abstract

Technical difficulties are currently being caused by the growing integration of erratic renewable energy sources into the world's electricity systems. To support the expanding adoption of renewable energy sources, stationary energy storage devices offer a practical and affordable solution. The lifetime, efficiency, and financial returns of energy storage devices provide significant technological and financial problems. Accurate techno-economic modeling becomes essential in order to optimise the economics of projects, both in terms of initial investment and future cash flows. **sMAPPER** (*system-MAPPER*), a comprehensive modeling framework with a focus on analyzing the technical and financial aspects of energy storage technologies, is one of these tools, providing a variety of topologies and system elements embedded in an energy storage application using a modular way based on internal technology and economy database. *sMAPPER* allows for the parametric assessment of the competitiveness of candidate design solutions, where the fitness of the alternative configurations is based on a simulation of the system operation, according to a library of dispatch logics that covers the most common applications targeted by the company (e.g., *PV smoothing*, *Primary Frequency Reserve*, etc.). This thesis demonstrates *sMAPPER*'s capabilities and advantages by offering in-depth understanding of the models and implementations.

Keywords: BESS, lithium-ion, optimizing, modeling, sizing, PV smoothing

Abstract in lingua italiana

Oggigiorno, la crescente integrazione di fonti di energia rinnovabili irregolari nei sistemi elettrici mondiali cause difficoltà tecniche. Per sostenere la crescente adozione delle fonti di energia rinnovabile, i sistemi di accumulo di energia stazionaria offrono una soluzione pratica e conveniente. La durata, l'efficienza e i rendimenti finanziari di tali dispositivi pongono problemi tecnologici e finanziari significativi. Una modellazione tecno-economica accurata diventa essenziale per ottimizzare l'economia dei progetti, sia in termini di investimento iniziale che di flussi di cassa futuri. **sMAPPER** (*system-MAPPER*), un ambiente di modellazione completo incentrato sull'analisi degli aspetti tecnici e finanziari delle tecnologie di accumulo dell'energia, è uno di questi strumenti, che fornisce una varietà di topologie ed elementi di sistema incorporati in un'applicazione di utilizzando un approccio modulare basato su un database interno di tecnologia ed economia. *sMAPPER* consente la valutazione parametrica della competitività delle soluzioni progettuali candidate, dove l'idoneità delle configurazioni alternative si basa su una simulazione del funzionamento del sistema, secondo una libreria di logiche di dispacciamento che copre le applicazioni più comuni a cui si rivolge l'azienda (ad esempio, smoothing fotovoltaico, riserva di frequenza primaria, ecc.) Questa tesi dimostra le capacità e i vantaggi di *sMAPPER* offrendo una comprensione approfondita dei modelli e delle implementazioni.

Parole chiave: BESS, ioni di litio, ottimizzazione, modellazione, dimensionamento, PV smoothing

Contents

1 | Introduction

In previous decades, the introduction of more Renewable Energy Sources (*RES*) capacity to existing power networks served as the primary driver of the global energy transition. This process was strongly aided by both the globally declining cost of wind and solar power generation as well as by local legislation support, including subsidy schemes [1–3]. Following these initial achievements, the energy transition has now begun to encounter new limitations and technological difficulties that necessitate alternative and frequently more site-specific solution methods. Undoubtedly, one of the most effective ways to improve the penetration of *RES* on a global and national level within the power system itself is to connect the power grid to both electric transportation and heating. In addition, as the supply becomes increasingly intermittent and depends more on intermittent sources like solar and wind generation, grid-tied energy storage is discussed as a technically advanced and potentially cost-competitive approach to manage volatility issues [4].

We can categorize front-the-meter (*FTM*) and behind-the-meter (*BTM*) applications for storage integration in power grids [5]. Applications of *FTM* include wholesale energy arbitrage [6, 7], storage-assisted renewable energy time shift [8], and Frequency Containment Reserve (*FCR*) provision [9]. In the context of *BTM* applications, such as Peak Shaving (*PS*) for industrial sites or at electric vehicle charging stations [10] or bill-saving at residential sites through Self-Consumption Increase (*SCI*) with local photovoltaic generation (residential battery storage) [11], a more distributed and locally coordinated power supply is discussed. However, it is essential to examine and optimize the technical characteristics, storage dispatch control, as well as cost/revenue streams throughout the course of the full project lifetime before making a sound investment decision. It is common practice to support these essential steps in the design and operational phase of grid-integrated storage projects by using simulation and modeling tools in conjunction with sensitivity analyses and optimization processes.

Furthermore, a variety of ancillary services are already necessary for electricity infrastructure to run efficiently and dependably as shown in Figure 1.1. To assure supply quality (such as maintaining consistent voltage and frequency), prevent damage to electrical ap-

pliances, and sustain supply to all users, supply and demand must be balanced in real time. All energy systems need some level of flexibility services to enable grid operators to respond to sudden changes in demand or the loss of substantial amounts of supply (e.g. large stations tripping offline, loss of an interconnection). Operators are equipped to quickly restore system equilibrium thanks to flexibility.

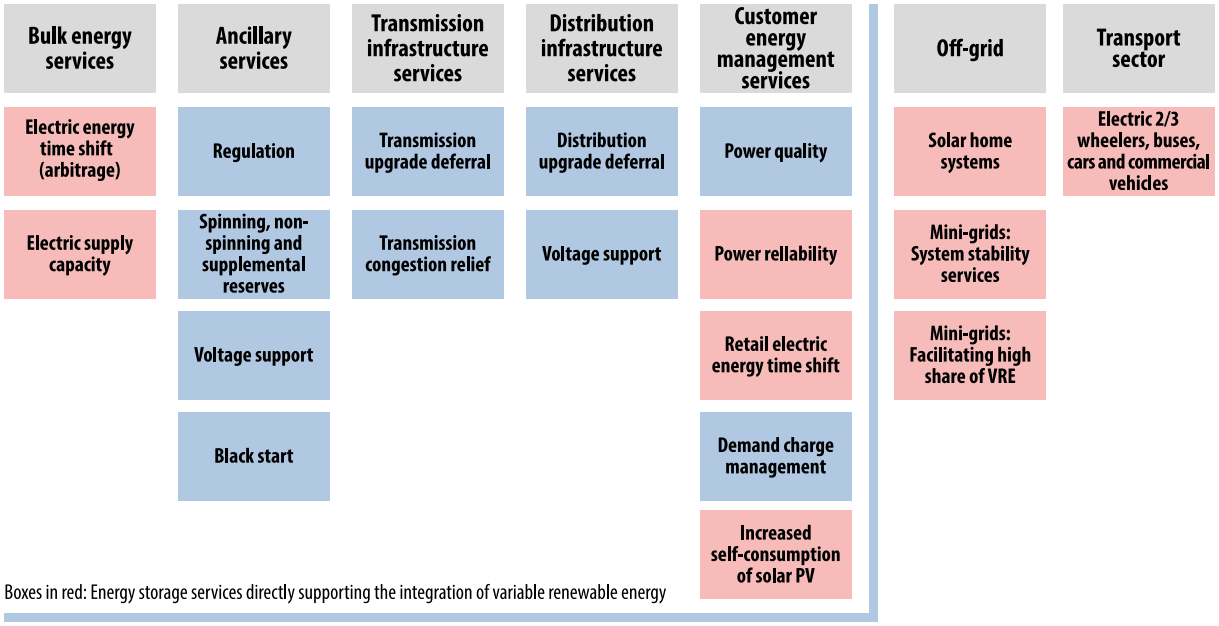

Figure 1.1: Range of services that can be provided by electricity storage [12].

The economics of behind-the-meter storage options, particularly when combined with new photovoltaic (PV) installations, could make this application the biggest driver of battery storage growth in terms of the services battery electricity storage systems could offer. The economic prospects to offer power time-shift services to boost self-consumption or avoid peak demand costs in the residential and commercial sectors are projected to have an impact on the main use case for battery storage through 2030. Additionally, depending on the situation, supplying renewable capacity firming at the utility scale would effectively contribute as well.

Given its rapid reaction capabilities, frequency regulation is another industry where Battery Energy Storage System ($BESS$) is anticipated to become more competitive as costs decline. It is important to note that these are the main services offered by $BESS$ systems. Specific systems will be able to "stack" the value of several services to collect bigger income streams and enhance the economics of $BESS$ projects thanks to their ability to supply multiple grid services in some circumstances. This will be especially crucial in the near to medium term as $BESS$ projects compete in a difficult economy and costs continue to drop. These forecast can be better seen in Figure 1.2, which presents forecasts to 2030

about battery capacity and main use.

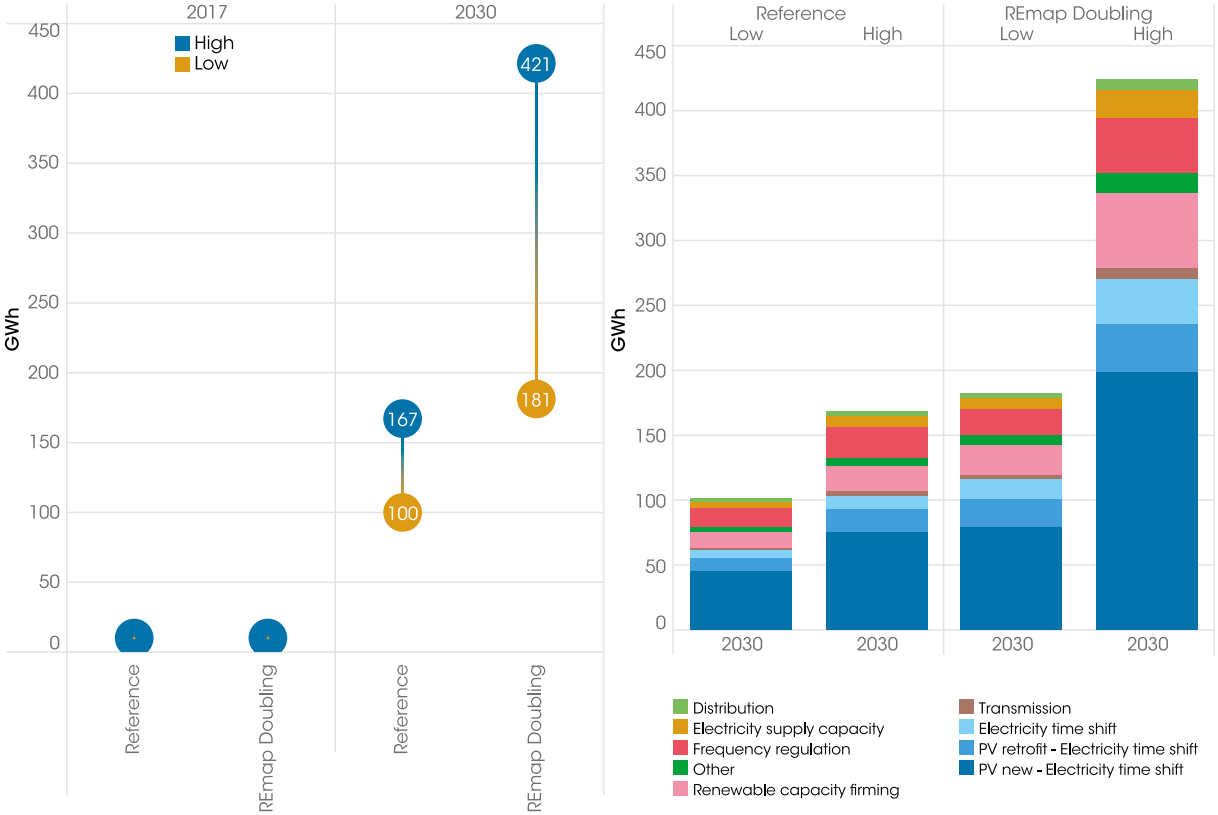

Figure 1.2: Battery electricity storage energy capacity growth in stationary applications by main-use case, 2017-2030 [12].

To help with the aforementioned planning and operating requirements of storage systems, the internal sizing tool **sMAPPER** (*system-MAPPER*) was created. While other tools could be used to partially satisfy the requirements set forth by *NHOA*, developing a proprietary internal tool is a more logical choice given the desire to utilize the internal database and to fine-tune the algorithm in order to properly simulate the *EMS* that would later be put into operation as closely as possible. The goal was to create a thorough modeling framework with an emphasis on examining the technical and financial aspects of the energy storage technology and to provide a variety of topologies and system components embedded in an energy storage application in a modular manner. This is obtained through the integration of user-defined inputs with pre-parameterized component building blocks, calculation methods, result analysis tools, and, more importantly, *NHOA*'s internal technology and economic database. This master's thesis presents the *sMAPPER* methodology.

The results show how even the simpler approach, the *Energetic* one, yield excellent results in line with the case study proposed within reasonable simulation timeframes. The eco-

nomic analysis, while not being robust enough since the economic part of the case study is confidential, gives an insight of the optimal solutions. Nevertheless, other results have to be checked to ensure the compliance of the solutions, such as the number of violations per year. The capability of *sMAPPER* to produce high-level analysis as well as minute per minute simulation plots allow the user to asses every aspect of the project in an accurate manner. Furthermore, the *Engineered* simulation produced even more realistic results, providing an optimal solution very similar to the one built in the study case back in 2019.

Before the framework of *sMAPPER* is further developed, analogous current tools are studied and appraised in Chapter 2. Here, many commercial and open source tools are analysed and compared to *sMAPPER* in order to explain the decision of developing an internal proprietary tool. Then, in Chapter 3 the methodology of *sMAPPER* is presented. It starts from a general description of the structure, and then develops all the models regarding the battery and its peripherals. Furthermore, the economic section, the simulation environment and the PV smoothing application are also described in detail. After that, Chapter 4 presents a case study to demonstrate the potential of *sMAPPER* in a real *BESS* built in 2019 along a PV power plant in Mexico. Lastly, and Chapter 5 closes with a summary of the tool and the results, along with a forecast for additional developments of the tool.

2 | Literature Review

2.1. Similar tools

In a dedicated application scenario, several researchers have examined the sizing and (economically) optimal functioning of a chosen storage system, such as the use of Redox Flow Batteries (*RFB*) for industrial PS applications or the use of lithium-ion batteries (*LIB*) for self-consumption increase (*SCI*) [13, 14]. Other studies compare the suitability of various storage choices for a certain use cases [15, 16]. In the past decade, there was general agreement that the storage technologies that were available at the time do not offer a single perfect candidate that can satisfy all application-specific needs [17]. Nowadays the steeply-falling prices of all energy storage solutions, in particular Li-Ion technologies, have shaped the market in such a way that many companies and research centers started developing tools to assess their usage.

The following gives a brief overview of a number of methods that are illustrated for the techno-economic modeling of stationary storage in grid applications. It should be emphasized that while Table 2.1 outlines some of these tools' key features, this study does not purport to give a comprehensive overview of all tools that might be pertinent in the context matter.

GridLab-D, a universal tool for modeling and evaluating multi-component power system networks is called, was created and made available by the Pacific Northwest National Laboratory (*PNNL*). Its strength is in its capacity to model all of the sub-components in the modeling region by putting up and solving a number of differential equations that describe the physical properties of distinct components. While the tool is undoubtedly effective at simulating a complete microgrid with its varied grid states, it lacks detailed performance models for energy storage systems and application-specific parameterization, making it inapplicable for detailed techno-economic analysis and storage project optimization, which is where this work is concentrated.

The tool **Per-ModAC** created at *HTW Berlin* can be used to do more customized simulations [18]. Performance and efficiency modeling of PV-coupled residential battery storage

Tool name	License type	Developer	Target
SimSES	BSD-3-clause	TUM	Physically motivated energy storage component, system and application behaviour
Homer PRO	Commercial	Homerenergy	Residential/Microgrid modeling - multiple energy systems, multiple application scenarios
GridLab-D	BSD open license	PNNL	Multi-domain state modeling for power distribution system simulation
SAM - System Advisor Model	BSD-3-clause	NREL	Modeling and analysis software for renewable energy projects
StorageVET	Open source	EPRI	Optimization of size and financial evaluation of energy storage
BLAST-BTM-Lite	Commercial freeware (lite version)	NREL	Analysis and modeling of battery degradation
sMAPPER	Internal tool	NHOA	Comprehensive modeling framework with a focus on the technical and financial aspects, making use of the internal database and developing simulations according to *EMS* later put in operation

Table 2.1: Overview of technical and economic modeling tools for energy storage in stationary applications.

systems can be done using this open-source software program. Although the model lacks the ability to examine battery degradation, it is incredibly strong at simulating performance and efficiency for specific battery storage products. More crucially, the current version of this open-source tool cannot be directly applied for cross-application assessments, which is sought for an investor's decision support, and is exclusively limited to a particular residential *BTM* use case.

When it comes to comparing and optimizing the techno-economic performance of storage systems in (micro-)grids, **Homer Pro** and **Homer Grid** are more flexible modeling tools. The tools have been used in numerous scientific publications [19, 20] and support a variety of storage-specific libraries and application-specific modeling capabilities, such as storage-supported renewable energy time shift in island grids as well as peak-shaving and solar-plus-storage calculations in the current professional versions. The software was created by the *National Renewable Energy Laboratory* (*NREL*), but the license for these tools is only available through *Homerenergy* as a commercial product, and it cannot be modified or extended to meet the needs of individual users, particular application scenarios, or regional regulatory frameworks. Applications like the provision of frequency containment reserves and situations for arbitrage marketing, for instance, are not included in the software tools' current iteration.

It is worthwhile to have a closer look at two other tools created by *NREL* and *Sandia National Laboratories* (*SNL*): A robust software package called **BLAST5** (*Battery Lifetime Analysis and Simulation Tool*) is available for both mobile and stationary *BTM* applications. It was developed using *MATLAB*. In stationary *BTM* applications, **BLAST-BTM-robust Lite**'s modeling capabilities for battery performance and lifetime calculations encompass both optimization and fundamental economic calculations. While it is strongly advised that customers interested in PV self-consumption and PS application have a closer look at this tool, the applications (only *BTM*) are obviously constrained and limited. Furthermore, the end-user is unable to modify settings, such as sample time for peak shaving control, because the original code structure is concealed behind a graphical user interface and a proprietary executable file.

The **System Advisor Model** (*SAM*) tool, which is now offered by *NREL*, is built upon a PV modeling framework that was initially established by *SNL*. In its current form, it supports the integration of financial models, such as those used in *Power Purchase Agreement* (*PPA*) computations, and permits the coupling of battery storage with PV systems. What's more, the user interface has been reworked and is now made available as an open-source Python software development kit, enabling others to contribute with their own modifications and improvements. Nevertheless, it does not support other applications such as Primary Frequency Regulation (*PFR*).

There is documentation, instructional videos, and a user feedback forum available for the **StorageVET** tool, which was primarily developed by the *Electric Power Research Institute* (*EPRI*). Since version 2.0 was made public, the tool has been made available as a Python package, and the majority of its useful components are distributed under a *3-clause BSD open source license*. The tools allow the user to run cost-benefit analyses and include different application services like voltage support, retail demand charge reduction, frequency management, and even value stacking by combining numerous services to be delivered by one storage system. Nevertheless, a fairly small number of solutions are now available (*PV*/Internal Combustion Engine (*ICE*) and Battery/Compressed Air Energy Storage (*CAES*)), despite the fact that the interface to the generation and storage technologies provides for a variety of possibilities.

SimSES combines the model accuracy of tools like *SAM* and Per-ModAC with an interface to a variety of applications and energy market scenarios. Furthermore, it can be coupled to grid models to enable Energy Storage Systems (*ESS*) to respond directly to states in a distribution grid, making it possible to perform both a power flow analysis and a thorough simulation of an *ESS* simultaneously. SimSES distinguishes itself from previously listed tools, such as Homer Pro or SAM, by offering a variety of detailed energy

storage systems, including validated and literature-based deterioration models. Additionally, a variety of predefined storage-specific Energy Management System (*EMS*) are created and paired with appropriate economic characteristics, such as auxiliary services and energy trading, to allow end-users to test a system of choice for a chosen application use case. The current code framework is also open source and available for future contributions from other developers throughout the world.

While some of these tools could be used to meet part of the requirements by *NHOA*, the decision to develop a internal proprietary tool is a more sensible choice. Indeed, the desire to use the internal database, as well as to fine tune the algorithm to simulate as closely as possible each different scenario was the thriving force behind this decision. The possibility of developing this in-house tool allows the operation of the *BESS* to be tested even in the sizing phase with the *EMS* that will then be implemented in reality, thus constituting an enormous advantage in terms of real system operation. Thus, even if **sMAPPER** may not hold the same level of technical accuracy as this other methods, it allows an incredible flexibility and modularity that will hold up to the years go by. The capability to merge the internal knowledge that is stored in the database to a simulation tool autonomously is valuable as no other tools would easily make this possible. Furthermore, the implementation of different applications that are a priority for *NHOA* makes *sMAPPER* perfectly suitable for many different project that are alike, reducing the engineering time spent on developing simulations.

s

3 | Simulation Framework

sMAPPER structure consists of mainly two sections: the database reading and importing part, executed in the *Initialize.m* script, and the simulation part, executed in the *Master.m* code. The *Initialize* part, regarding the whole technology and economy database, will mainly be discussed along with its design choices. Afterwards, the simulation environment enclosed in the *Master* part, as well as the different applications are discussed.

3.1. sMAPPER structure

Concerning the structure of sMAPPER, it can be divided, as already described, in two parts. The first one, called *Initialize*, is reported in Figure 3.1. The cylinders represent the outputs of the script, that mainly come from the database. Indeed, the latter is the source of almost all the data that *sMAPPER* will later utilize, except for the *Design* and *Configuration* part that is user defined.

The *Design* script, which is structured in different sections, handles all the different user-input parameters needed for sMAPPER to work properly. For instance, the architecture *AC* or *DC*, the space of solutions to explore or the different values of efficiencies. This file is to be accessed frequently to fine tune the simulation according to the use case.

On the other hand, the *Configuration* script contains the path to all the files in the database, as well as their revision number. This is because as the database gets updated, *sMAPPER* has to be told manually to work with the newer version. The automatic process to retrieve the latest version was not implemented as newer file structure may break the code, thus the need for a manual update to check the compliance.

The scripts regarding the technologies, as well as the economic parameters, are all under different functions but grouped together in the *databaseread.m* function. Their development took an important slice of the overall time as the different files do not have the same structure, and even within the same components differences exists between different manufacturers. Indeed, this part contains the main part about the model developed in *sMAPPER* regarding the batteries, the *PCS*s, the containers, the Power Islands, and the

economic inputs.

The input data is simply already saved in a *.mat* file, thus do not require particular adaptation and can be read directly.

Lastly, all these data is copied in another output, called *Version Data*, that stores all the information regarding the database in order to engrave the all the possible simulation information on a file that will be saved along with the output. This allows to easily and reliably trace back a simulation in completeness.

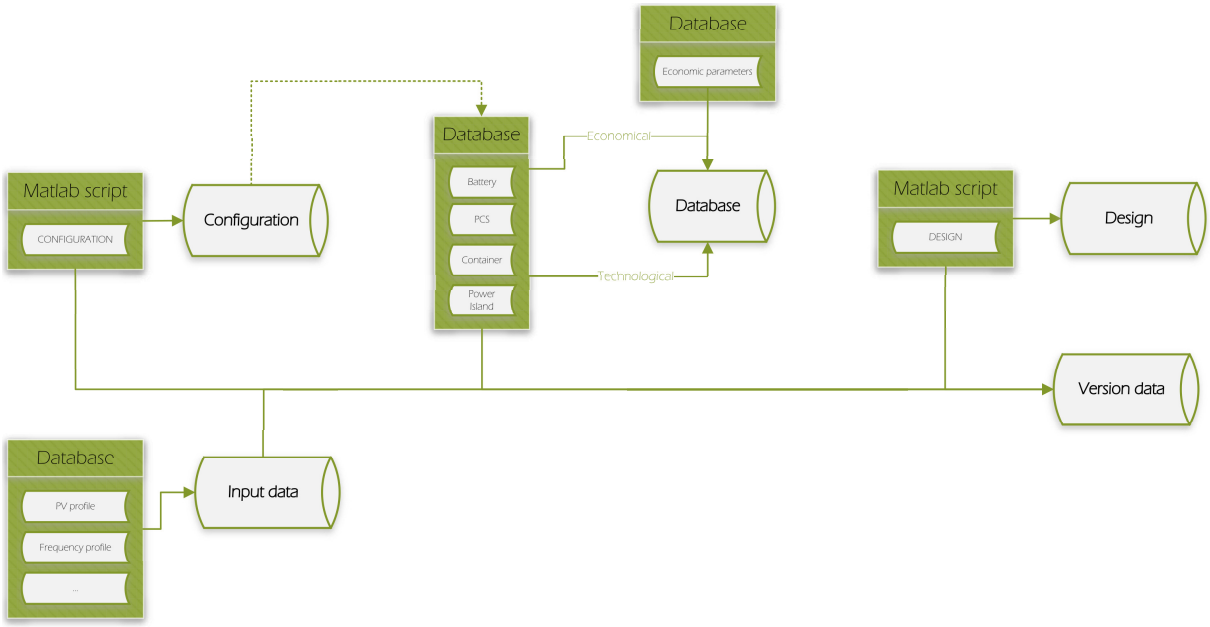

Figure 3.1: *sMAPPER Initialize* part, comprising of mainly the database data gathering.

Then, the *Master* part, represented in Figure 3.2, comes in. Its main objective is to build the environment for the simulation to run according to the models discussed in the next sections.

Firstly, it imports all the database previously developed and adapted for *Matlab*. Then, according to the simulation mode, the Power Island combinations are computed in the *powerislandcombination*. If required by the user, also the input data analysis can be performed prior to the simulation, to have a glance at the data *sMAPPER* will work with.

Lastly, the simulation can run according to the service/application specified in the *Design* script. If available, the *Parallel Computing* toolbox will split the various simulations among the different cores of the machine. At the end of the simulations, an economic analysis is performed showing the best solutions and, if required by the user, various more

detailed plot regarding selected simulations. All the results, both the technical and the economical, are logged in the machine, both in the complete version with year-by-year data and in the averaged version.

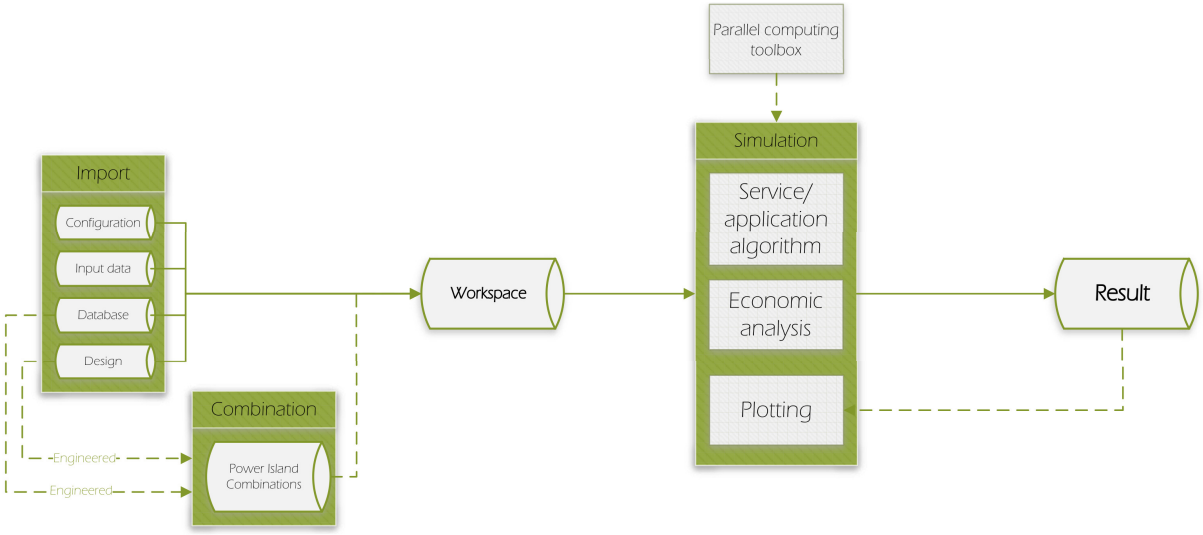

Figure 3.2: *sMAPPER Master* part, comprising of the simulation and results analysis.

3.2. Battery model

In today's market, the structure of a *BESS* is quite standardized: the smallest part is the battery cell, which is grouped in series into modules that are stacked one on top of each other in racks. The racks are then parallelized in variable number according to the project needs. The whole electric system is then centralized in a DC panel. All the battery-related parts are managed by various Battery Management Systems (*BMS*s) and the whole container is protected by security systems such as the fire suppression system. To ensure correct temperatures inside the container, an Heating Ventilation and Air Conditioning (*HVAC*) is always equipped with the *BESS* and is part of what are called auxiliaries. Furthermore, in some configurations, a Power Converter System (*PCS*) is included at the expenses of some battery racks, rendering the system a self-contained unit capable of absorbing or injecting AC power without any other external unit and thus making the whole system exceptionally modular. Figure 3.3 shows an example of a container with its main parts highlighted.

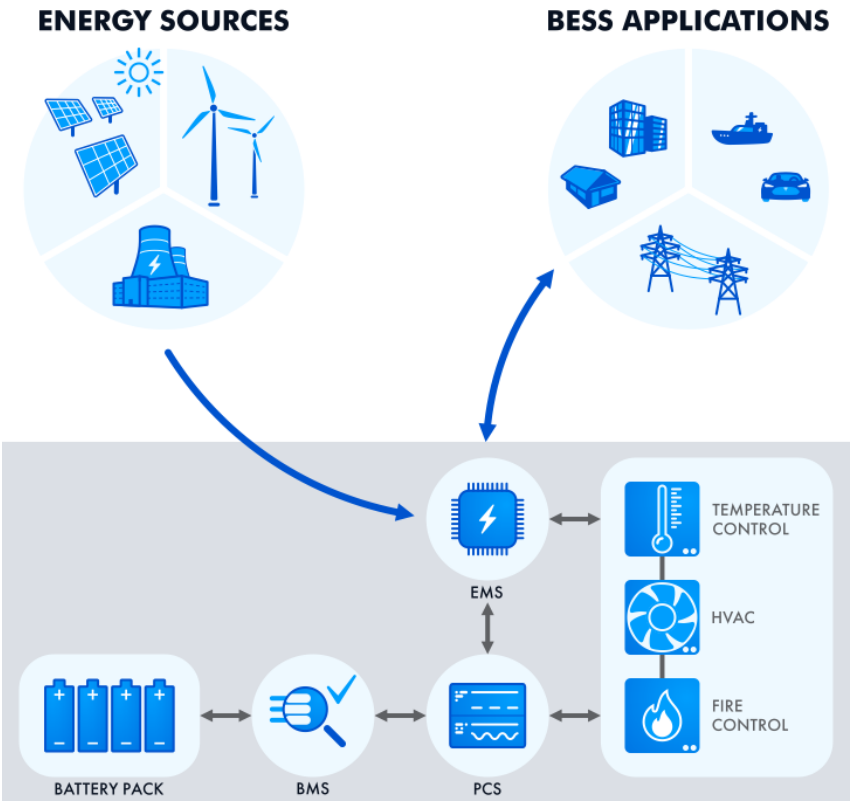

Figure 3.3: Example of Battery Energy Storage System (*BESS*) architecture [21].

3.2.1. Chemistry

As already discussed briefly in the introduction, the principal technology employed in today's energy storage panorama is the lithium ion battery. *NHOA* mainly works with Lithium Iron Phosphate ($LiFePO_4$ or *LFP*) and Lithium Nickel Manganese Cobalt Oxide Cathode (*NMC*) batteries.

NMC is frequently recognised for its high energy density, which affects the cost and design of the enclosure. The cost of the enclosure (structure, cooling, safety, electrical Balance Of System (*BOS*) components, etc.), which varies depending on the battery, is roughly 1.2–1.5 times higher with *LFP* than *NMC* [22]. Because *LFP* is a more stable chemical, its thermal runaway (or fire) temperature threshold is higher than *NMC*'s. But *LFP* and *NMC* also share a lot of similarities: the round-trip efficiencies are comparable, as well as the usual battery performance detriments like temperature and C-rate.

In addition to the technical variations resulting from variations in cell chemistry, there are additionally variations in operational circumstances, pricing, other commercial terms, approach to payment terms, and more. Some of them stem from the fact that the companies' histories and developmental stages differ rather than the actual differences in technology.

Commercially, the initial capex cost of *LFP* batteries is frequently less expensive than that of *NMC*. *LFP* typically costs 20–30% less per kWh, but the total cost of Beginning Of Life (*BOL*) system integration is typically only 5–15% less [22]. Comparing capex based on End Of Life (*EOL*) is more difficult, as it needs to be evaluated on the basis of each product's cycling and calendar performance, warranty and guarantee, ease of expansion, etc.

Operationally, it is preferable to use *LFP* because its operational requirements are more flexible as they allow for a wider temperature range than *NMC* and don't require reefer containers for shipping. Additionally, while *NMC* requires the power battery, a different battery from 2H or 4H use batteries, to support 1C rate (1 hour) application, *LFP* battery products typically support up to 1C operation. In the initial six months, *LFP* batteries deteriorate much more quickly. Due to the possibility that the first shipped batteries could have degraded to, for example, 98% or 96% of *SOH* by the time the last batches are commissioned, this can cause confusion and problems if the projects are large and need to be delivered/commissioned over a few months.

Batteries and other important parts are chosen based on factors like the company, price, other commercials, product fit, project management, supply consistency, and services. Pricing obviously has a lot of significance, but because warranty and supply reliability have recently become more crucial, it is crucial to take product integration fit and safety very seriously

Given this, the two types of batteries will be **treated in the same manner** from a technological point of view, as their minor differences will inherently arise from database without the need to develop different models.

3.2.2. Overall model

The main information regarding each battery model is stored in the database which is kept up-to-date as battery specifics may change, along with the addition of new models. In Tables 3.1 and 3.2 it is shown an example of available information with figurative numbers and names.

Table 3.1 shows the main characteristics, starting from the single cell, moving to the module and up to the whole rack. The main information read by sMAPPER regards the **Rack design energy** [kWh] (which is multiplied by the number of racks per container according to the specific case), as well as the **Max continuous CP-rate**. Table 3.2 reports instead part of the data available about the detailed behaviour of the battery in different operational conditions and degradation states. Among the various tables, the

Battery Information			
Info	Manufacturer	Manufacturer #1	Manufacturer #2
	Tag	Model1	Model4
	Description	Model #1	Model #4
Cell	Cell model	ABC123	DEF456
	Nominal capacity [Ah]	100.00	300.00
	Nominal voltage [V]	3.60	3.20
	Nominal energy [Wh]	400.00	900.00
	Min voltage [V]	3.00	2.50
	Max voltage [V]	4.10	3.65
Module	Module model	XYZ123	ZWT657
	Cells in parallel	2	1
	Cells in series	16	52
	Module design energy [kWh]	10.00	50.00
	Module nominal voltage [V]	60.00	170.00
	Module min voltage [V]	50.00	150.00
	Module max voltage [V]	65.00	190.00
Rack	Rack model	HWK874	BND534
	Modules in series	22	8
	Rack design energy [kWh]	300.00	400.00
	Rack nominal voltage [V]	1280.00	1330.00
	Rack min voltage [V]	1100.00	1170.00
	Rack max voltage [V]	1450.00	1500.00
	Max continuous power [kW]	130.00	190.00
	Max continuous CP-rate	0.45	0.50
	Max peak power [kW]	130.00	190.00
	Max peak CP-rate	0.45	0.50
Bank	Max number of racks in parallel	150	30

Table 3.1: Example of main characteristic in battery database.

DOD		CP-rate		
		0.00	0.25	0.50
Charging method	CP	97.5%	97.5%	96.0%

DC RTE with CP/CP cycle		C-rate		
		0.05	0.20	0.50
SOH	100%	97.9%	96.1%	94.4%
	95%	97.8%	95.9%	94.1%
	90%	97.6%	95.6%	93.7%
	85%	97.5%	95.4%	93.4%
	80%	97.4%	95.2%	93.1%
	75%	97.3%	95.0%	92.8%
	70%	97.1%	94.7%	92.4%
	65%	97.0%	94.5%	92.1%
	60%	96.9%	94.3%	91.8%

SOC_max (Charge)				
	SOH			
CP-rate	100%	90%	80%	70%
0.00	100.00%	100.00%	100.00%	100.00%
0.05	100.00%	100.00%	100.00%	100.00%
0.10	99.00%	98.80%	98.50%	98.30%
0.20	97.60%	97.10%	96.70%	96.20%
0.30	96.20%	95.40%	94.60%	93.80%
0.40	95.40%	94.40%	93.40%	92.40%
0.45	95.10%	93.90%	92.80%	91.70%

Table 3.2: Example of battery datasheet characteristics regarding DOD, RTE and SOC_{max}.

main ones regard the $\mathbf{SOC_{max}}$ and $\mathbf{SOC_{min}}$, in addition to the **Round Trip Efficiency** (RTE). These data is all function of the CP and SOH such that

$$SOC_{min} = f^*(CP, SOH)$$
$$SOC_{max} = g^*(CP, SOH)$$
$$\dagger : DOD = h^*(CP, SOH),\ SOC_{max} = 1 + \frac{DOD}{2},\ SOC_{min} = 1 - \frac{DOD}{2}$$
$$RTE = l^*(CP, SOH)$$

where * indicates a function of a 2 variables lookup table. When the SOC_{max} and SOC_{min} are not directly available (†), the DOD is used in its place and they are derived from the latter assuming a symmetrical distribution.

The battery internal efficiency, where internal indicates before any power converter and thus related mainly to the internal resistance, is represented as $\eta_{internal} = \sqrt{RTE}$ as the RTE itself represents the energy efficiency of a full charge and discharge cycle.

Other information, such as rack heat dissipation, are taken into account but not implemented yet, allowing to add in the future a comprehensive thermal analysis if the data available in the future will allow so.

Power and energy

Due to sMAPPER being a high-level simulation environment, the approach to modelling the power and energy flows is based only on the active power method. This technique allows to avoid computing all the voltages and current, as well as waveforms and power factors. While such approach does not allow to evaluate in detail the battery usage and voltage curves, it greatly simplifies the computational burden as well as reducing the layers of complexity of the whole simulation framework.

In fact, taking into account the voltages and currents would require in-depth knowledge of the working principles of each single inverter model, together with developing an electrical schematic of the whole system. Furthermore, other problems would arise due to lack of detailed physical properties of the system, such as the internal resistance of each single battery cell which also varies due to ageing.

Active and reactive powers could be implemented in the model, but as the reactive power by definition does not play a role in the energy depleted or absorbed by the battery, it would only be of matter when sizing the electrical components. Nonetheless, this task is already being done in the database during the design and sizing process of the different containers types since both the *PCS* and the *HVAC*, along with the whole *BESS*, are rated in MVA instead of MW.

Nevertheless, the voltage and current limits are ensured to be respected as the code implements boundaries regarding the maximum allowable *CP* depending on the current *SOC* and *SOH*. Furthermore, the battery is never allowed to exceed the prescribed *SOC* limits given by both the use case (where the user can impose a certain *DOD*) and the database.

Thermal model

All of the aforementioned storage processes' performance, efficiency, and ageing are sensitive to thermal conditions. Utility-scale *LIB* stationary *ESS* are free-standing, outdoor installations that are exposed to the elements. The industry standard today for protecting delicate electrical components from unfavourable environmental conditions is to install entire energy storage systems inside standard shipping containers. Modularity, scalability, ease of logistics, compliance with road-transport regulations, and the capacity to plan and optimise land use are all advantages of such a configuration. These containers are also specially equipped with insulation to prevent heat transfer to or from the environment and to maintain a consistent operating temperature for the internal components. Due to the internal resistance to current flow during operation, LIBs produce heat. Technology

based on lithium-ion batteries is particularly susceptible to unfavourable changes in cell temperature and deteriorates more quickly when used outside of their ideal temperature ranges.

Nevertheless, despite the importance of a thermal model, a realistic implementation of it would pose a considerable challenge. The aspects to take into considerations are many:

- **Ambient temperature**: this could either be available as a constant user-specified temperature model, that would introduce a great simplification, or a location-specific model. The latter would indeed require integrating external tools, such as Greenius developed by the German Aerospace Center (*DLR*) [23], and thus more developing time.
- **Irradiance**: despite the ambient temperature being the main parameters, in many locations the irradiance plays a non-negligible part. Taking into account this aspect would both require, as for the ambient temperature, integrating external tools, as well as knowing the absorbivity, reflectivity and geometric features of the containers.
- **Ambient wind, natural convection and rain conditions**: the containers are installed in the open environment and as such, they experience all kinds of different weathers. The difference in natural convection in different ambient condition influence greatly the thermal dissipation.
- **Products transmittance**: this parameter is key in understanding the natural heat dissipation process. This value, non-standardized, requires a relative database linked to *NHOA*'s products which is not currently available for *sMAPPER*.
- **Thermal bridges, latent heat**: this aspects, while being minor, add up in the whole thermal model and increase the complexity.

While all of these problems could be assessed, a proper thermal model would indeed require a lot of effort while not providing substantial difference to the high-level analysis that *sMAPPER* provides. For this model to be robust and durable over time for *NHOA*'s sake, all the relative data would need to be available as a database kept updated as the technologies and manufactures change. Nevertheless, this possibility is open for future improvements of this tool.

Therefore, the thermal dissipation is **entirely dealt through the *HVAC* system**. Its maximum auxiliary consumption per container is documented in the database, and it includes the thermal dissipation given by the batteries as well as the *PCS* and other various electrical components. A more detailed description is provided in the relative subsection further below.

3.2.3. Self-discharge

Typically, lithium-ion battery cells have excellent charge retention, allowing them to cycle with nearly 100% round-trip coulombic efficiency. This results in a very low self-discharge rate (C/50,000 or less), making it challenging and time-consuming to measure precisely. Furthermore, it is additionally influenced by temperature, past cycling history, duration, and state of charge. In particular, the key variables are the starting SOC and the temperature, the latter doubling the self-discharge rate every 10°C [24]. Moreover, the process of self-discharging has not to be mistaken for the capacity fade (battery ageing) as the effect on the battery is the similar over long resting periods. To add complexity, it is difficult to generalise results because different chemistries and manufacturers exist. Figure 3.4 shows some examples of how the self-discharge rate varies with different storage temperatures, while also depending on the resting period length.

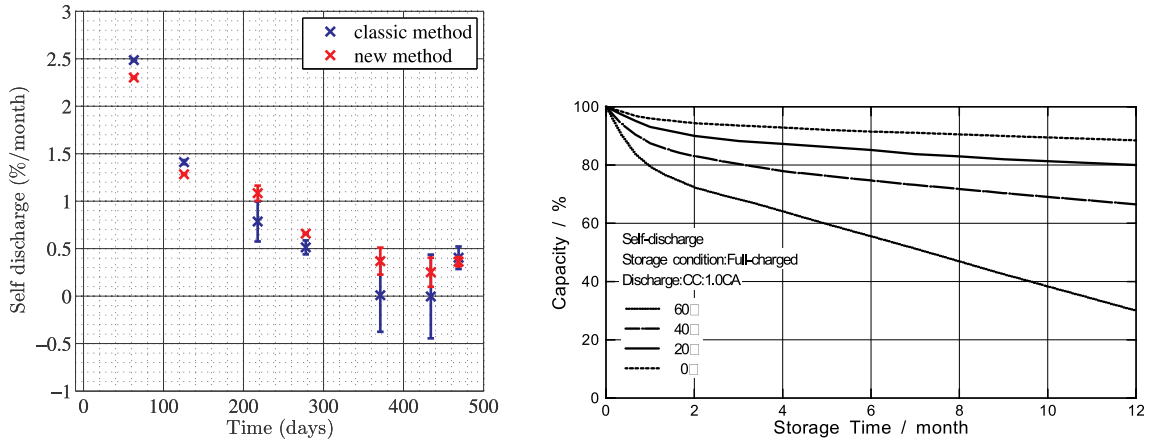

(a) HAL Open Science [25]. (b) SANYO [26].

Figure 3.4: Examples of self-discharge rate behaviour from different sources.

Due to this, various methods have been implemented to quantify the self-discharge rate of lithium-ion battery cells [25, 27, 28]. Regardless of the procedure followed, there is agreement on the influence of the above-cited key variables but not on the results obtained. Different periods of publications show different state-of-art knowledge of lithium-ion batteries, which is why results vary widely within different year other than within different manufacturers/researchers. Some of the few sources that address directly the self-discharge problem in lithium-ion batteries are reported in Table 3.3. The main thing that can be taken out from the latter is how much the values differ, even from sources from the same period. This is also because the typical self-discharge rate is not constant, but rather a monotonically decreasing function that diminishes with lower voltages (lower SOC).

Source	Self-discharge [%/month]	Conditions	Notes
Sanyo	3%	$100\%_{SOC}$, 20°C	From 2006 [26]
Quest Battery	0.3%	Not specified	From 2010 [29]
Battery University	5% in 24h, then 1-2%	Not specified	From 2021 [24]
IEEE Conference	0.5 - 2.5%	$65\%_{SOC}$, 60°C	From 2016 [25], extrapolated from chart
Storing Energy	3%	Not specified	From 2016 [30]
Keysight	0.5 - 1%	Not specified	From 2021 [31]
DNK	5 - 10%	Not specified	From 2018 [32]

Table 3.3: Overview of different self-discharge rates according to various sources.

This means that, in the most sensible form, the self discharge rate is a 2-variable function such that $\%_{self-discharge} = f(SOC, T)$ for a single battery chemistry or, more precisely, single battery model.

Moreover, an analysis was done on the impact of the different constant self-discharge rates at different cycles per year. The left y-axis in Figure 3.5 shows the relative number of cycles in the case with the self-discharge included to the simulation with respect to the simplified case with no self-discharge. The study was performed in *MATLAB* developing a one year sample loop with a 1-minute timestep, implementing a basic *SOC* restoring method and charging/discharging the battery with pseudo-random values (negative offset plus a seeded random value). The sensitive analysis on the different self-discharge rates and cycles per year was done with the same random values, to ensure consistency in the different runs. The results shows how, intuitively, the self-discharge influence (that is, the cycles per year relative to the simplified case) increases as the self-discharge rate increases. The band of results around the y-value of 1, present up to self-discharge rates of $\sim 5\%_{SOC}$/month at down to 60 cycles per year, represents simulations with outcomes approximable to the simplified case. Typically, to properly make use of batteries, the number of cycles per year is higher than 90, making even higher values of self-discharge rates less impactful. Additionally, according to the previous Table 3.3, the most typical self-discharge rates already all fall inside the aforementioned band, meaning that the influence is **negligible** in most real-world cases.

Furthermore, the approach used on *sMAPPER* to rely as much as possible on *NHOA*'s databases would fail here as not even manufacturers provide detailed information on this matter.

Despite this, it was chosen to add the possibility to take into account the self-discharge

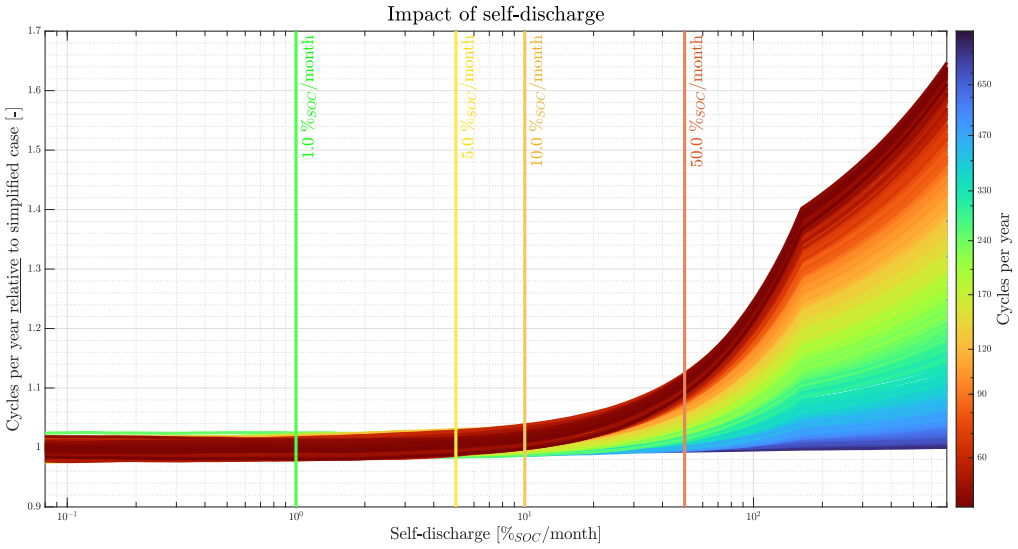

Figure 3.5: Self-discharge influence at different battery cycles per year and different discharge rates.

behaviour in *sMAPPER* through an user input value. This value is set to 0 by default due to the aforementioned reasons, but can be adjusted accordingly if the case study requires so.

3.2.4. Battery degradation

Literature review

Due to usage and exposure to the environment, lithium ion cells deteriorate [33–36]. The cells' capacity to store energy, meet energy needs, and ultimately survive is compromised by this degradation. Any system using Li-ion cells as its power source needs to be aware of how much energy the battery can store and how much power it can deliver at any given time. In order to estimate and predict current and future energy storage capacity and power capability, methods and models that make use of the measurements and parameters that are currently available are needed. This is because it is difficult to infer the rates of capacity and power fade from operational data in a practical system. Numerous physical and chemical processes that have an impact on the electrodes, electrolyte, separator, and current collectors of Li-ion batteries can lead to cell degradation [37–41]. Figures 3.6a and 3.6b shows the main mechanisms at work during the cell degradation.

Theoretical models and empirical models can both be used to predict battery degradation. Studies on theoretical degradation [43–48] typically concentrate only on the most preva-

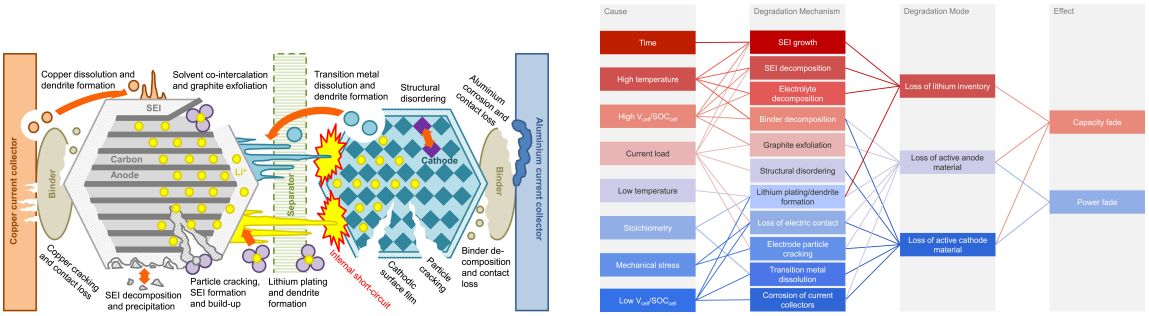

(a) Degradation mechanisms.

(b) Cause and effect of degradation mechanisms and associated degradation modes.

Figure 3.6: Degradation process in Li-ion cells [42].

lent mechanisms, such as the formation and growth of the Solid Electrolyte Interphase (*SEI*) [49, 50] or electronic contact loss through particle cracking [51, 52] due to the variety of causes, rates, and interdependencies of these degradation mechanisms. However, at the planning stage, there is no information available regarding the specific cell conditions; one can only predict the *BESS*'s operating pattern. There are still not enough theoretical studies connecting operation-level observations to the molecular-level degradation processes [53, 54]. Therefore, it is challenging to establish a direct connection between the charging and discharging patterns and the molecular-level activities taking place within the battery cells.

Storage planning and operations studies can more easily be incorporated with empirical models [55–59]. Each of these empirical degradation models is designed for a particular *BESS* application where the *BESS* operating region is constrained and an accurate model based on a few degradation experiments is possible. Experimental data that they are based on have limitations for empirical models. Therefore, a model created for one application scenario may not be applicable to another. For instance, empirical battery degradation models for *EV* frequently presumptively use a consistent daily charging schedule. The performance of a battery used for frequency regulation, where the *BESS* follows a stochastic charging and discharging signal, is unlikely to be predicted by a model of this kind. For each new application, battery ageing experiments must be carried out in order to obtain an accurate empirical model of battery degradation. Such tests would need to be conducted beforehand using pricey test facilities and would take months or even years.

Some paper [60] suggests a semi-empirical battery capacity degradation model designed for off-line battery life assessments to circumvent these issues, combining theoretical analyses with experimental observations to produce a model that is applicable to other operating conditions. Nevertheless, all these approaches come short when it comes to differentiate

ageing between different battery models of the same chemistry and/or manufacturers.

sMAPPER database

As shown in Figure 3.7a obtained from *NHOA*'s database, the State of Health (SOH) over the years varies widely within the same battery manufacturers even when the battery chemistry is the same. Needless to say, this is a result of many factors, mainly being the various operational conditions. In Figure 3.7b and 3.7c it is shown, for two different manufacturers, two different models of batteries and their relative ageing according to different study cases. For each one of them, the manufacturers provide simulation data according to the required specifics and operational condition. It has to be noted that the information obtained from the manufacturers does not represent real-world ageing data, but rather simulation results from proprietary internal tools. As such, it is not always possible to extrapolate correlations between the input variables and the output (SOH). Furthermore, the available data does not cover any possible operational conditions that *sMAPPER* may encounter as it relies on data from past projects with specific requirements.

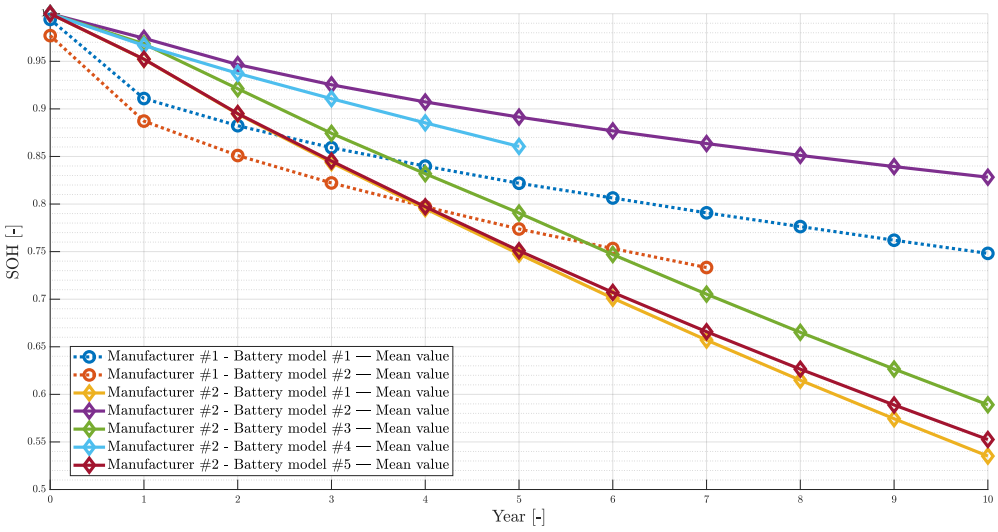

(a) Comparison between different manufacturers and battery models (average across all different operating conditions).

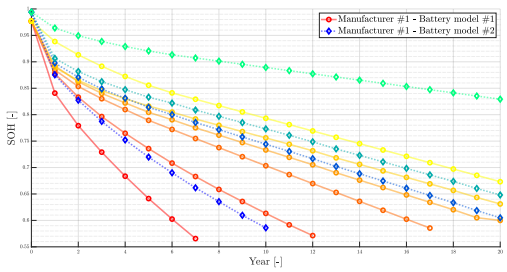

(b) Manufacturer #1, two battery models, various operating conditions.

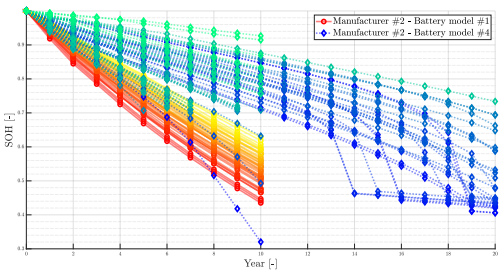

(c) Manufacturer #2, two battery models, various operating conditions.

Figure 3.7: Different battery degradation data from various operating conditions, taken from two different manufacturers.

Table 3.4 reports an example of *NHOA*'s battery ageing database for a particular battery model. The data has been modified to protect *NHOA*'s internal database while keeping a similar trend to preserve the input-output correlation. As input data, the main parameters at play are **Cycles [#/year]** (or better yet, the **Eq. Cycles [#/year]**), **Charging C-rate, Discharging C-rate, and Depth Of Discharge (*DOD*)**. Yet, other parameters come into play in the evaluation of a battery degradation, such as **Center SOC, restSOC, and restTime**. Indeed, looking closely at Table 3.4, it is clear how, even while maintaining constant the above mentioned main parameters, the *SOH* varies widely. Taking as an example **Simulation 1** and **Simulation 2**, the only difference between these two cases is the restSOC which varies from 20% to 80%. Yet, the *SOH* difference just in the first year varies from -3.00% to -5.10%, and reaching a final

value of respectively 60.80% and 50.40%. Clearly, the influence of the restSOC is not negligible according to the simulations, but yet finds difficult real-world applications due to the complexity in simulating and taking into account such aspect. The same reasoning applies for the Center SOC and the restTime.

INPUT DATA										
Battery data	Simulation 1	Simulation 2	Simulation 3	Simulation 4	Simulation 5	Simulation 6	Simulation 7	Simulation 8	Simulation 9	Simulation 10
Project	Project #1	Project #1	Project #1	Project #1	Project #1	Project #1	Project #1	Project #2	Project #2	Project #2
Year	2018-12	2018-12	2018-12	2018-12	2018-12	2018-12	2018-12	2021-05	2021-05	2021-05
Battery model	Model #1	Model #1	Model #1	Model #1	Model #1	Model #1	Model #1	Model #1	Model #1	Model #1
Cycles [#/year]	1500	1500	1500	1500	1000	1000	300	1000	300	1000
Charging C-rate	0.300	0.300	0.300	0.300	0.300	0.300	0.350	0.350	0.800	0.800
Discharging C-rate	0.350	0.350	0.350	0.350	0.350	0.350	0.550	0.550	1.000	1.000
DoD	50.0%	50.0%	50.0%	50.0%	75.0%	80.0%	90.0%	25.0%	90.0%	25.0%
Eq. Cycles [#/year]	750.00	750.00	750.00	750.00	750.00	800.00	270.00	250.00	270.00	250.00
Center SOC	50.0%	50.0%	75.0%	75.0%	50.0%	50.0%	50.0%	50.0%	50.0%	50.0%
restSOC	20.0%	80.0%	20.0%	80.0%	20.0%	80.0%	60.0%	60.0%	60.0%	60.0%
restTime	11.00	11.00	11.00	11.00	11.00	11.00	22.00	22.00	22.00	22.00
Temperature [°C]	23	23	23	23	23	23	23	23	23	23
State of Health (SOH)										
Year	Simulation 1	Simulation 2	Simulation 3	Simulation 4	Simulation 5	Simulation 6	Simulation 7	Simulation 8	Simulation 9	Simulation 10
0	100.00%	100.00%	100.00%	100.00%	100.00%	100.00%	100.00%	100.00%	100.00%	100.00%
1	97.00%	94.90%	94.20%	92.00%	96.60%	94.30%	97.70%	98.10%	97.30%	98.10%
2	92.60%	88.50%	88.80%	84.50%	90.70%	86.50%	93.60%	95.40%	93.70%	95.40%
3	88.20%	82.90%	84.00%	78.70%	85.60%	80.20%	90.00%	93.20%	90.20%	93.30%
4	84.30%	77.80%	79.20%	72.60%	80.50%	74.00%	86.70%	90.50%	87.20%	91.60%
5	80.50%	72.80%	74.60%	66.90%	75.50%	67.70%	84.10%	88.00%	84.50%	90.00%
6	76.40%	67.80%	70.30%	61.70%	70.50%	62.00%	81.70%	85.80%	81.80%	88.00%
7	72.30%	63.30%	65.90%	56.90%	65.60%	56.40%	79.40%	83.80%	79.50%	86.10%
8	68.30%	58.70%	61.80%	52.20%	60.90%	51.30%	77.10%	82.00%	77.30%	84.40%
9	64.60%	54.50%	57.90%	47.80%	56.40%	46.50%	75.20%	80.20%	75.20%	82.80%
10	60.80%	50.40%	54.10%	43.70%	52.30%	41.80%	73.30%	78.50%	73.10%	81.40%

Table 3.4: NHOA battery ageing database.

Due to the above mentioned reasons and the general approach of *sMAPPER*, the parameters taken into account for the battery ageing mechanism in the multi-year simulations are:

- **DOD**: computed as $DOD = SOC_{max} - SOC_{min}$, where SOC_{max} and SOC_{min} are respectively the maximum and minimun values of SOC during the current year
- **C-rate**: computed as the aggregated average C-rate in charging and discharging, only accounting for values of $|P_{BESS}| > 0$, such that

$$C_{rate} = \frac{\overline{P_{BESS}}}{E_{nominal_0}}, \ \overline{P_{BESS}} = avg(|P_{BESS_{non-zero}}|)$$

  where $P_{BESS_{non-zero}}$ represents the non-zero values of power as the C-rate is determined based only on the working time of the battery. The nominal capacity for the C-rate is referred to the installed capacity as the power rating of the *BESS* does not decay with ageing.

- **Eq. Cycles**: computed as the throughput divided by the nominal battery capacity, such that

$$Cycles = \frac{\int |P_{BESS}| \, dt}{2E_{nominal}}$$

where the factor 2 at the denominator accounts for the fact that a full cycle requires a complete charge-discharge. The nominal capacity for the cycles is referred to the actual capacity including the ageing.

SOH measurement process

There is no agreed-upon method in the industry for determining *SOH* because the battery capacity does not correspond to a specific physical quality. Therefore, the latter is here defined according to the **Constant Power - Constant Power** (*CP-CP*) method. This technique requires the battery to undergo a complete charge-discharge cycle while always complying with the *CP* constraint, meaning that the procedure would keep going only as long as the *BESS* could hold up to the nominal power. The cycle starts with the battery empty, and charges it till the battery voltage limits kick in and limit the current (and thus the power). Then, after some delay, the discharge process begins, until the lower voltage limits halt it. In Figure 3.8 the *CP-CP* method is compared with more common the Constant Power - Constant Voltage - Constant Power (*CP-CV-CP*). The latter, shown in dotted lines in the chart, lets the power in charge and discharge to fall below the nominal one, enabling the battery to fully charge/discharge, effectively allowing more throughput. This clearly results in an higher capacity as during the charge process the *SOC* reaches almost 100% while in *CP-CP* it was stopped preemptively. Moreover, during the discharge process the *SOC* also reaches lower values, close to 0. Finally, to evaluate the effective capacity of the system, the integral of the measured power during the discharge is computed as it represent the case with the lower capacity compared to the charge process. The values next to the arrows inside Figure 3.8 show the values of cumulative energy of the whole *CP-CP* procedure, and their difference represents the effective capacity of the system.

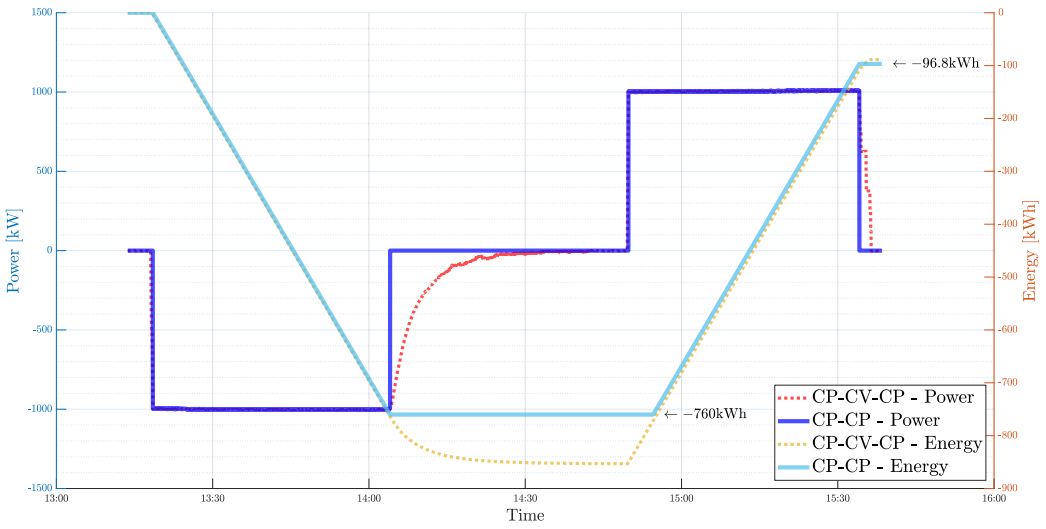

Figure 3.8: *CP-CP* method compared to the *CP-CV-CP*.

This technique is employed in the year-zero test, during the commissioning phase, along with the yearly test to periodically check the compliance with the project requirements and forecasted ageing. Figure 3.8 represents a real-world yearly test performed by *NHOA* on a 14 months old *BESS*, with the values normalized to match a maximum power of $1MW$.

Then, according to the proposed *CP-CP* method, the SOH is defined simply as

$$SOH = \frac{C_{current}}{C_{installed}}$$

where C denotes the capacity in energy measured via the *CP-CP* process.

Validating ageing estimation

To evaluate *NHOA*'s battery ageing database, a validating process has been performed by analysing the data from fully-operational *BESS*s commissioned years prior to this thesis. The information is gathered through the use of a Battery Management System (*BMS*), an electronic system that, among many other features, monitors the state and reports the data of the battery pack(s). In particular, any of the aforementioned factors (individually or in combination) may be used by the designer of the *BMS* to determine the *SOH*, defining arbitrary weights for each of them:

- Internal impedance

- Capacity
- Voltage
- Self-discharge
- Number of charge–discharge cycles
- Age of the battery
- Temperature of battery during its previous uses

Nevertheless, as the definition of how the *SOH* is evaluated is generally a trade secret, it is not possible to extrapolate comprehensive formulas/correlations. Furthermore, manufacturers are still improving and detailing the best method for calculating the *SOH* during plant operation, so the results obtained are not completely reliable.

In Figure 3.9 it is reported the *SOH* data continuously collected by the *BMS* of two different *BESS*s over their lifetime. Apart from some outliers in Project #1, comparing the degradation of the two different systems it is clear how the *SOH* behaviour is quite fictitious as it is highly unrealistic a stair behaviour like the one shown. Indeed, it is a result of the above-mentioned estimation process performed by the *BMS* in the background.

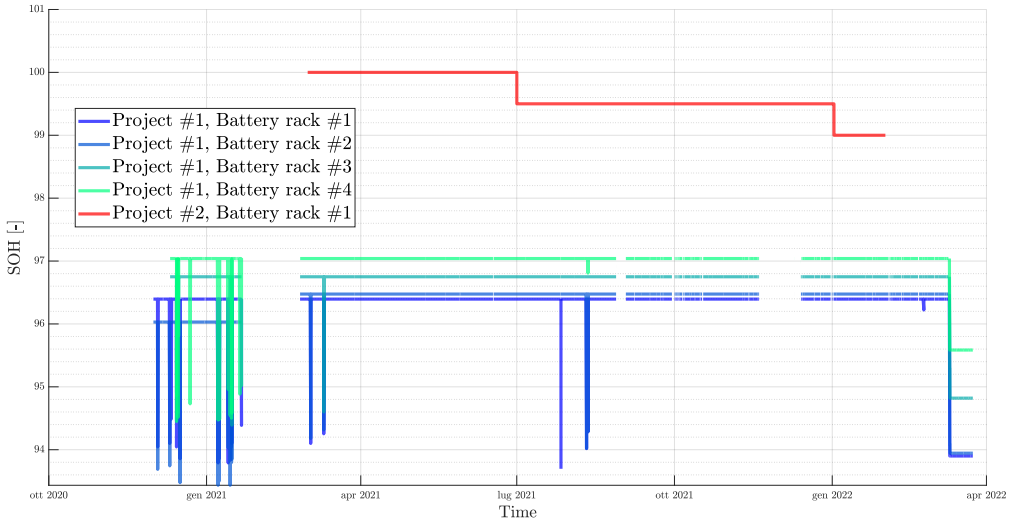

Figure 3.9: *SOH* data gathered by the *BMS* from two different projects.

Therefore, validating the ageing database based on the *BMS* data is not feasible for the above-mentioned reason. Even so, the lack of access to diversified projects and the short operational life would have made the validation valid only for a couple of battery models and for a couple of years, and could not be extended to the whole database.

Luckily, the yearly test data from one project was recently available and allowed a reliable validation of a single battery model ageing database after more than one year from the commissioning, proving how manufacturers degradation curves provided for different operational conditions seem trustworthy. The exact results can not be reported, but the relative lost usable energy at the end of the first year was very close to the guaranteed value by the manufacturer.

The data, obtained with specialized tools and cross-validated between different measurement equipment, allow for very thorough analysis of the *BESS* performances. The downside is that the system has to cease operation for a full working day and request charge/discharge profiles from the grid, as well as requiring specialized personnel to perform the test. Thus, these tests are performed only on a yearly basis to ensure that the project minimum capacity warranties are fulfilled while minimizing the downtime.

sMAPPER approach

As a result of all of this, the available solutions were mainly two:

- **Literature** approach: using an electro-chemical based method and exploiting publicly accessible correlations and parameters.
- **Database** approach: take advantage of the existing *NHOA*'s battery ageing database.

While the literature approach would ensure a deeper understanding (and maybe accuracy) of the ageing mechanism, the act of choosing one of the many theoretical and/or empirical methods would require further studies and analysis, as well as needing to keep it up-to-date as *NHOA*'s battery chemistries and manufacturers may change in the years.

On the other hand, the database approach allows *sMAPPER* to work flawlessly in the future as it is already used and maintained up-to-date by other sectors in the company. Furthermore, as proved by the validation test, the database, which is made up of manufacturers' ageing curves, is reliable and represents the most empirical way to estimate batteries' degradation.

Thus, as the general approach of *sMAPPER* is to model everything to be as close to reality as possible while making use of the internal knowledge and information, the **database** approach is implemented. Nevertheless, this poses the challenge of how to interpolate/extrapolate the degradation data from many curves, if the space of all the operational conditions is rather sparse given the variables making up the ageing estimation are *DOD*, C-rate and Eq. Cycles, as well as the current *SOH* (or alternatively the current year). Figure 3.10a represents how different different battery models even from

the same manufacturer may have different data sizes, while two examples are reported in Figure 3.10b and Figure 3.10c that respectively show a sparse and dense database.

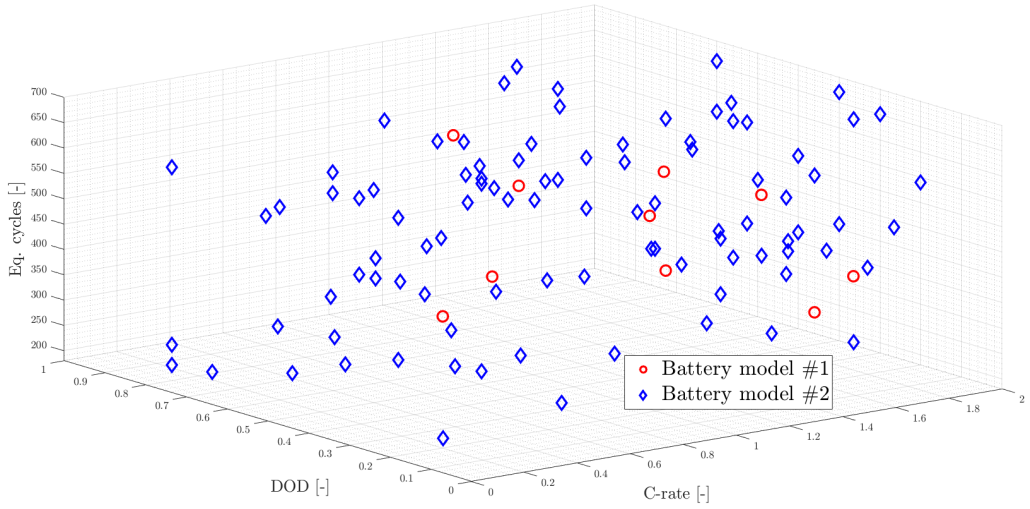

(a) Comparison between sparse and dense space. Each point represents an available simulation with ageing data in the database.

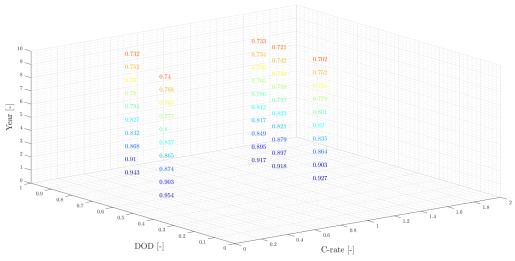

(b) Sparse data example. The eq. cycles variable has been left out for drawing reasons.

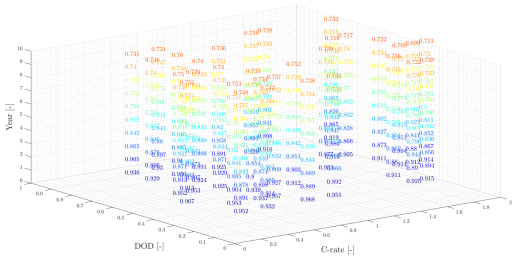

(c) Dense data example. The eq. cycles variable has been left out for drawing reasons

Figure 3.10: Example of different data densities in the ageing database, showing how non-homogeneous knowledge can lead to sparse and ineffective information.

The techniques available to estimate the ageing according to the operational condition in *sMAPPER* are two:

- **Complete**: create by interpolation and extrapolation a complete 4-dimensional map containing values of SOH degradation per year ($SOH_t - SOH_{t-1}$) as function of the main parameters plus the current year. This approach, which was difficult to implement, yielded terrible results as the data is not spread homogeneously, and thus the wide gaps in the 4D lookup table were filled with linear interpolation data. Furthermore, this method wrongfully assumes each of the parameters is weighted

equally in importance.

- **Simplified**: the data from the database is kept in the original shape, being just averaged with respect to the non-main parameters, namely center SOC, restSOC, and restTime. Then, during the run, the degradation is accounted taking the curve of the current year from the database with the closest values of the operational parameters. This method is based on the minimum square distance of the normalized difference. This technique induces errors, but on the same level as the complete method while avoiding all the complexity.

After testing both methods and noticing that the complete yielded poor results compared to the overhead required, the **simplified** approach was implemented. The *SOH*, and therefore the battery capacity, is updated at the end of each year according to the given operational conditions.

3.3. System periphery

The whole *BESS* relies on many auxiliaries and periphery components to work properly and reliably. All of them are modeled based on the database's information. Hereafter, all of them will be discussed in detail in their relative section.

3.3.1. PCS

The Power Conversion System (*PCS*) is a multi-functional inverter/converter device that offers bidirectional power conversions ($AC \leftrightarrow DC$) for electrical energy storage. This component is present in every system and can either be installed inside the container itself, along with their batteries in another section, or be in a separate container/cabinet outside to provide more modularity. In Figure 3.11 it is shown an example of architecture where the *PCS* is enclosed by a separate unit.

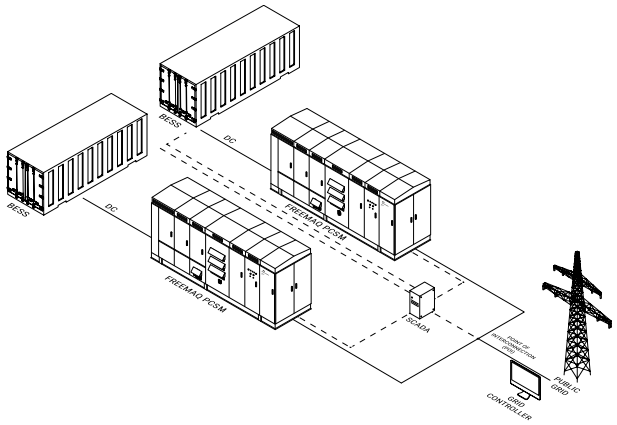

(a)

Figure 3.11: Example of *BESS* with external *PCS* [61].

NHOA makes use of different *PCS* models. For all of them, a dedicated database is available with information about the main parameters rated on both *AC* and *DC* side, along with its stand-by and auxiliary consumption. The latter is taken into account indirectly through the auxiliary consumption of the product, which comprises also the *PCS*. Furthermore, lookup tables are available for the charge and discharge efficiency operation of the converter as a function of both the *DC* voltage and the load. Figure 3.12 shows how the main parameter influencing the efficiency is the load, while the *DC* voltage has little to no impact on the output.

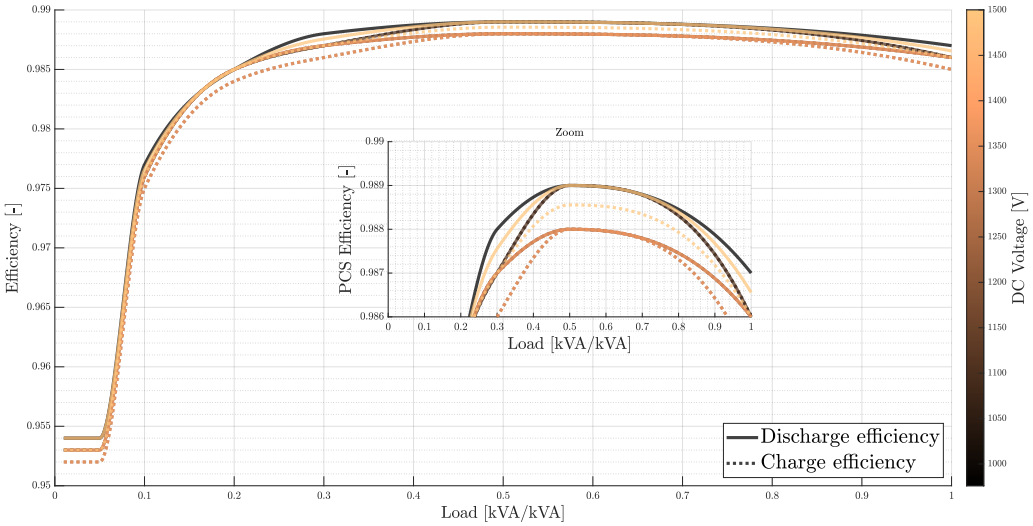

Figure 3.12: PCS efficiency as function of load and *DC* voltage.

Thus, the 2D lookup table is averaged over the different voltage levels such that the

efficiency can be expressed as

$$\eta_{PCS} = f(\alpha)$$

where α represents the *PCS* load in terms of $\frac{kVA}{kVA_{nominal}}$, which due to the previous assumptions, becomes $\frac{kW}{kW_{nominal}}$.

3.3.2. Container

As already stated above, utility-scale *LIB* stationary *ESS* are free-standing, outdoor installations that are exposed to the elements. The industry standard today for protecting delicate electrical components from unfavourable environmental conditions is to install entire energy storage systems inside standard 20-foot or 40-foot shipping containers. Modularity, scalability, ease of logistics, compliance with road-transport regulations, and the capacity to plan and optimise land use are all advantages of such a configuration. Information from the database is available for the different container models, and Table 3.5 reports an example with figurative numbers and names.

Main parameters				
Info	Container type	Energy	Hybrid	
	Tag	Model1	Model2	
	Application	Energy-intensive	Power-intensive	
Power room	Compatible PCS	-	PCS #2	
	Max number of PCS	0	2	
Battery room	Compatible battery module	Manufacturer #1	Manufacturer #1	
	Max number of banks	2	2	
	Modules per string	8	15	
	Max number of strings per bank	12	10	
	Number of strings	10	-	
	Number of banks	2	-	
Auxiliaries	Total maximum auxiliary consumption	65.00	60.00	kVA
	Maximum consumption per bank	2.2	-	kVA
	Maximum consumption per rack	3.2	-	kVA

Table 3.5: Example of two container models in the database.

As stated before, the thermal dissipation is entirely dealt through the *HVAC* system. Its maximum auxiliary consumption per container is documented in the database, and it includes the thermal dissipation given by the batteries as well as the *PCS* and other various electrical components. The maximum consumption is related to the maximum load of the whole system and occurs when the batteries work at maximum *CP*. When the batteries are idle though, the consumption is not supposed to be null. Thus, the auxiliary load consumption follows a quadratic function, where the base load is dictated by an user-input percentage of the maximum load. The quadratic relation is implemented

based on the quadratic correlation between the current (power, and thus load) and the losses following Ohm's law. The function can then be written as

$$P_{auxiliaries}(\alpha) = P_{auxiliaries,stand-by} + (P_{auxiliaries,maximum} - P_{auxiliaries,stand-by}) * \alpha^2$$
$$P_{auxiliaries,stand-by} = \beta * P_{auxiliaries,maximum}$$

where α represents *BESS*'s load in terms of $\frac{P_{BESS}}{P_{BESS,installed}}$, while β indicates the base load percentage with respect to the maximum one. The latter has a default value of 5% which is the average value according to multiple real-case scenario, but it can be changed if the study case requires so.

Indeed, the main parameters are the **Total maximum auxiliary consumption** and the **Max number of modules**. The latter is obtained multiplying the max number of banks by the modules per string and by the max number of string per bank. This allow to compute the maximum possible energy content of the container knowning the module nominal energy in kWh.

The "max" next to the number of modules in Table 3.5 indicates that fewer racks are allowed to be installed inside the container, leading to a smaller capacity but freeing up space. This is particurarly important with respect to future planning as due to battery ageing the capacity of the *BESS* may fall below the prescribed level, thus needing a capacity augmentation to abide to the project's terms. This concept, called *Top-Up* strategy, will later be discussed in the *Future Improvements* section, as its implementation requires a great effort due to the many challenges it presents.

The different possible quantity of modules inside a container lead to different combinations that are grouped into different Power Islands. The latters represent the main product that contain all the components and containers and their different variation. They will be discussed in detail in the next sections.

3.3.3. Skid

The output from the *PCS* unit, while being *AC*, has a voltage level too low to be injected into the grid. Thus, before the Point of Common Coupling (*PCC*), a transformer has to be fitted to step-up the low voltage to the medium or high voltage required by the grid. This task is usually performed by self-contained unit called Medium Voltage Skid (*MV* skid).

The *MV* skid is a compact turnkey platform made from high resistance galvanized steel with all the medium voltage equipment integrated, including a pre-wired outdoor power transformer, *MV* switchgear, oil spill tank with rainwater filter, and built-in fast power connection to different containers and *PCS* enclosures. With between 480 V - 690 V in the low voltage range and 12 kV to 36 kV in the high voltage range, this compact platform usually achieves power outputs between 1000 kVA and 4000 kVA. Its simplicity to be transported and delivered into remote sites makes it the optimal solution for *EPC* (Engineering, Procurement and Construction). Moreover, the Twin Skid exists to meet the requirements of large scale *BESS*, achieving power outputs between 3000 kVA and 8000 kVA.

Figure 3.13a shows an example of *MV* skid by *Power Electronics*, while Figure 3.13b reports a typical schematic for a skid connected to an inverter and to the grid.

(a) MV skid appearance.

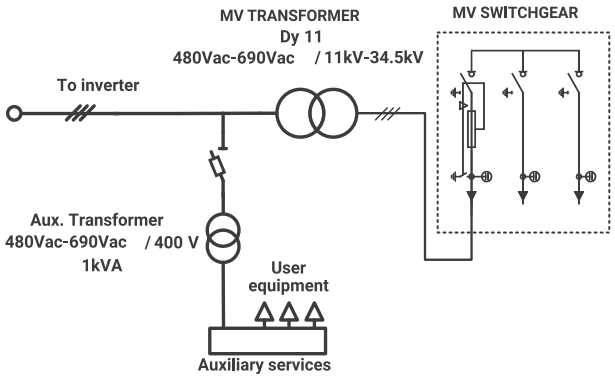

(b) MV skid electrical schematic.

Figure 3.13: Examples of an MV skid, by *Power Electronics* [62].

This component yields very high efficiency values, above 98% and typically around 99% [63]. These values, while not being constant, do not follow a particular pattern or behaviour. Indeed, since transformer efficiency is very difficult to generalise (as it depends

very much on supplier, power, and voltage levels, which are all characteristics that easily change from design to design) and differs by only a few tenths of a percentage point, the approach followed by *NHOA* is to consider a constant efficiency from a database point of view. Furthermore, not taking this approach would significantly increase the computational time as the *MV* skid efficiency is taken into account at every timestep and a lookup table requires a significant overhead. The benefit would be marginal due to the very high and quasi-constant value of efficiency.

For the above mentioned reasons, it has been chosen to implement the MV skid with a **constant user-set efficiency**. This allows to tune the efficiency according to the use case. Furthermore, a customizable *HV* skid with is implemented by default but set to unitary efficiency to account for those scenarios where the *PCC* requires high voltage.

3.3.4. Power Island

All the aforementioned components and sub-systems are grouped together under a single product called **Power Island**. A Power Island is an engineered solution comprised of different sub-systems that together form the *BESS*. Different models of Power Island exist, and each of them is suitable for different applications. Although they all share the standard shipping container format, the components inside as well as the capacity and installed power vary widely. The number of different possible combinations allow for a great deal of pre-engineered solution ready to be used for each different study case. Indeed, for each different Power Island number (namely, the model) different sub-Power Islands models exist with different combinations of battery, *PCS*, and *MV* skid models and quantities, as well as different topologies. In Table 3.6 is reported an example with figurative numbers and names that shows how the same Power Island number has widely different combinations in terms of installed power and capacity, leading to different possible power-to-energy ratios $[\frac{1}{h}]$.

Power Island	
PCS enclosure model	PCS Model #1
Battery enclosure model	Battery Model #1
Max. # of PCS	1
Max. # of Energy Islands	2
Battery model	Battery Model #1 - 0.5C
Battery tag (as per Tech Database)	BatteryModel1
Max. c-rate	0.5
Battery module capacity [kWh]	50.00
# battery modules per rack	10
# of PCS per enclosure	2
PCS model	PCSModel1
Max. # of battery racks per Energy Island	28
Min. # of battery racks per Energy Island	16

Design combinations						
# PCS	**1**	**1**	**1**	**1**	**1**	**1**
# Energy Island	**1**	**1**	**1**	**2**	**2**	**2**
# battery racks per enclosure	**16**	**22**	**28**	**16**	**22**	**28**
Apparent power [MVA]	4.00	4.00	4.00	4.00	4.00	4.00
Nominal AC, LV power [MW]	3.0	4.0	4.0	4.0	4.0	4.0
Nominal DC storage capacity [MWh]	6.0	8.0	10.0	12.0	16.0	21.0
Power-to-energy ratio [1/h]	0.50	0.50	0.40	0.33	0.25	0.19
Min operating cos(phi) @ nominal power	0.75	1.00	1.00	1.00	1.00	1.00

Table 3.6: Example of Power Island data in the database.

Each component can either be a result of internal developments and engineering process,

or be a third-party turnkey product that come in the format of external cabinets. This concepts applies to batteries, that can either be stacked into racks or directly bought as single cabinet/container, as well to *PCS* and *MV* skid.

This flexibility allows for very versatile and modular projects that scale up without difficulties and require less engineering since a good deal is already done while developing the different Power Islands. The Power Islands can then be parallelized to achieve any scale desired by connecting them via the *MV* voltage lines, while linking their control systems to obtain a centralized hub to operate the different *BESS*s as a whole single power plant.

Having already analyzed and described all the different sub-systems, the Power Island in *sMAPPER* is modeled just as an enclosure (or, in *MATLAB* code format, a struct) that contains all the needed information about its components. The only information related directly to the Power Island regards the number of battery racks and *PCS* per enclosure, as well as the total number of enclosures. In this way, the installed capacity and power are obtained. Then, the simulation will provide results for a discrete or non-discrete number of Power Islands, according to the type of simulation run. The latter will be discussed later.

3.3.5. Economic inputs

To evaluate the different possible solutions, an accurate economic and financial analysis has to be performed. All the main general information, along with the more detailed ones about the different products, are stored and kept up to date in *NHOA*'s database. In fact, the latter is divided into two sections: **General** and **Power Island**.

The general section contains the main information which comprises typical investments parameters such as inflation rate or margin. In Table 3.7 an example is reported. These values can be easily accessed and changed according to the different projects, time horizons and interest rates. The exchange rate, automatically updated, is present to standardize all the different currencies used with the different components into $ (*USD*).

Item	Tag	Unit	Value	Notes
Inflation rate	IR	-	1.0%	*To be evaluated based on the country*
Discount rate	DR	-	6.0%	*Based on the client WACC*
System integrator margin	SIM	-	10.0%	*% of battery+BoS+PCS+EMS+transformer+grid connection*
Developer overhead	DOH	-	5.5%	*% of battery+BoS+PCS+EMS+transformer+grid connection+system integrator margin+EPC*
Developer margin	DM	-	6.5%	*% of battery+BoS+PCS+EMS+transformer+grid connection+system integrator margin+EPC*
Exchange rate	ER	[$/€]	1.002	

Table 3.7: Example of general economic data in the database.

The other section regards everything else related to the Power Islands which follows the same structure as Table 3.7. The database has data for all the different models

of the components and sub-systems, ranging from the battery to the *PCS* to the *MV* skid. Furthermore, the cost of the Energy Management System (*EMS*), Engineering, Procurement and Construction (*EPC*) and *EMSplus* (which represents a further overhead to include for some Power Islands) are all included and are adjusted according to the different Power Islands. The various costs may be provided per unit ($\frac{\$}{u}$) or per capacity ($\frac{\$}{kWh}$).

At last, all these information is gathered by *sMAPPER* which aggregates all the different costs to put a figure on each Power Island. The computation is done according to the exact components model employed in the relative Power Island, multiplied by their quantity. This process produces a struct in *MATLAB* that holds, for each Power Island, all its economic information, as well as the main one which is the total overall investment cost.

All the different solutions are plotted prior to each run, and and example is reported in Figure 3.14. The different markers represent combinations of battery racks, *PCS*s and containers that end up on some trend-lines. For instance, it is clear how the Power Island #1 follows the line at $CP = 1$ up to a certain point, where then the nominal capacity grows more than the nominal power, leading to lower *CP*s. This happens especially with Power Island #2, where after following the 2h line, it becomes flat as the nominal power of the PCS is saturated and adding other battery racks only increases the installed capacity. The color, which represents the cost per installed power [$\frac{\$}{kWh}$], is the most important metric when looking at the different solutions. It is apparent that higher *CP BESS*s require an higher expenditure, and that increasing the installed capacity leads to lower costs due to the presence of economies of scale and fixed costs such as *EPC*.

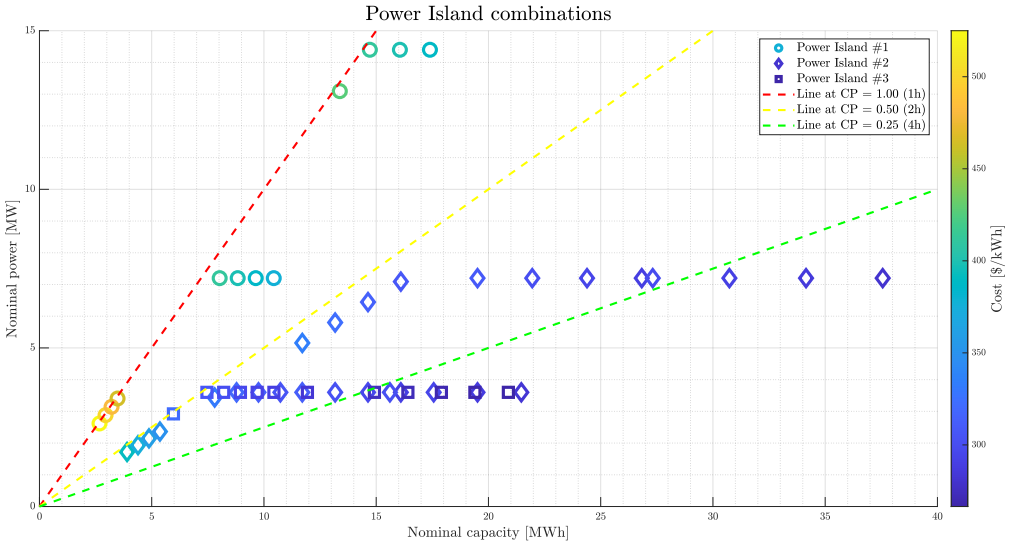

Figure 3.14: Cost space of different Power Island solutions for a particular range of *BESS* capacities.

Although Figure 3.14 greatly shows the different solutions that will later be explored by *sMAPPER* in the simulation, an important piece is missing from the chart: the number of free battery racks. Indeed, looking closely at the figure, some solutions have divergent costs even though the nominal capacity and power are similar. The reason behind it is that the containers are not fully utilized in those cases, leading to higher overall costs due to the non fully-exploited space inside. This information is visible only by adding another axis to the previous chart. In Figure 3.15 it is plotted the aforementioned chart. Indeed, it is clear how Power Islands with fully utilized containers lead to the most efficient pricing.

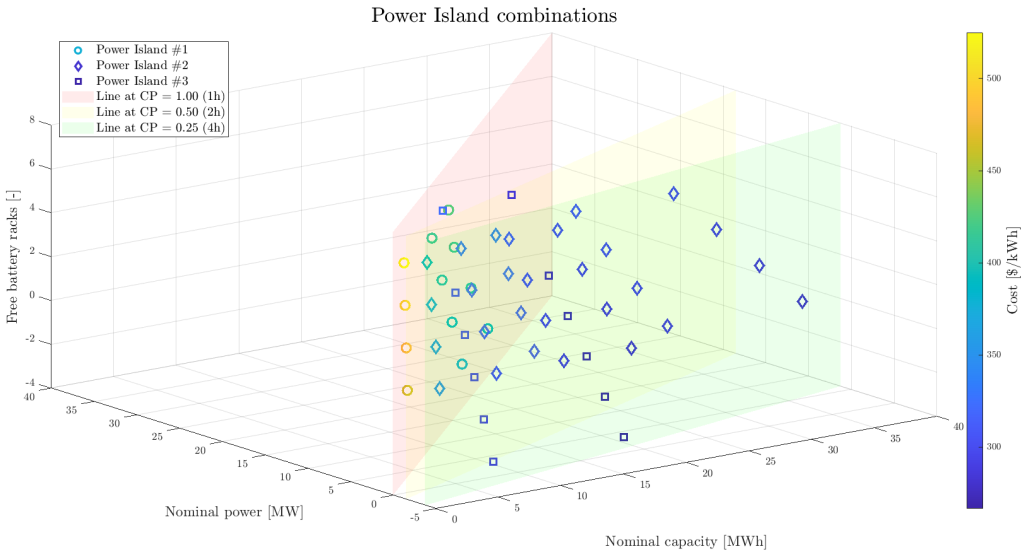

Figure 3.15: Cost space of different Power Island solutions for a particular range of *BESS* capacities, including the number of free battery racks.

The latter is of particular importance when accounting for the Top-Up strategy, which requires swapping batteries and revamping the *BESS* without installing new containers, but rather by filling the empty battery racks left when first building the whole system. Even if this strategy is not implemented yet for reasons discussed in the Further Developments section, it is a good piece of information when assessing all the possible solutions.

As *sMAPPER* runs simulations on all the points in the previous charts, when exploring a wide space of solutions the computational time may be too high. Because of this, a filter has been implemented that picks the best solutions (that is to say, with the lowest cost) in a 3D-space around all the points. The filter works by first trying a whole range of different ϵ values, and picking up on the number of points removed according to the relative ϵ. The function, which can be expressed as $\%_{filtered} = f(\epsilon)$, is then inverted such that the input is the a required fraction of filtering (for instance, to keep only 30% of the total number of solutions). The inverted function, which has the shape of $\epsilon = f^{-1} = g(\%_{filtered})$, is obtained by finding the closest epsilon that yields the required filtering which, in the end, is used to set the distance for the filtering process itself. Then, the same figures with nominal capacity and nominal power are plotted, but with considerably less solutions. In Figures 3.16a and 3.16b an example is reported in both the 2D and 3D version with 50% of filtering.

For what concerns the exterior costs, such as the ones relative to the specific application, they are also included in the economic database. For instance, for a *PV* smoothing

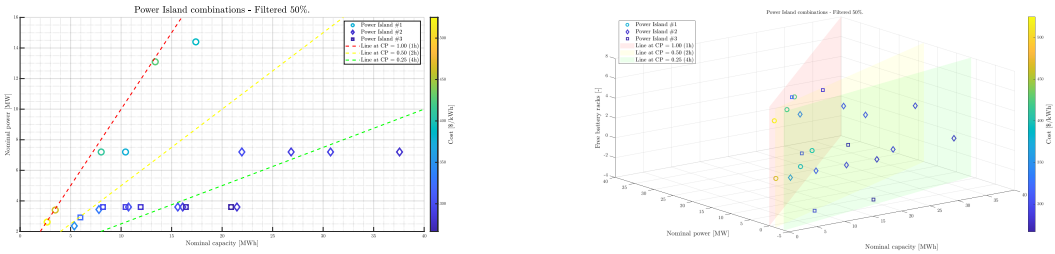

(a) Cost space 2D filtered.

(b) Cost space 3D filtered.

Figure 3.16: Cost space of different Power Island solutions for a particular range of *BESS* capacities filtering 50% of the solutions.

application it is possible to define both the violation cost per minute, as well as the remuneration per MWh of injected energy into the grid.

The operative costs and revenues are then computed during the simulation on a year basis. Then, the cash flow is computed taking into account all the different sources. Finally, the main economic parameter, the Net Present Value (NPV), is calculated (among many other, such as payback time) as such

$$NPV = C_0 + \sum_{t=0}^{T} \frac{CF_t}{(1+r)_t}$$

where:

- C_0 = net initial investment expenditures
- T = total time period count
- t = current year
- CF_t = cash flows of each period
- r = discount rate or interested rate required of the investment

According to the use case, the key parameter for the economic assessment can be either the NPV or the payback time, being the former the default one. In the PV smoothing application, but it is applicable in other scenarios as well, the NPV is compared to the no-*BESS* scenarios, which is taken as base case. Then, those results, along with many other, are logged and eventually charted to compare them over the simulation years.

3.4. Simulation part

Following the description of all the different components and sub-systems, it is needed to address the simulation modes, as well as how the workspace interacts with the run itself. After the *Initialize* part has been run, all the database data gets stored inside *MAT-files*, which are binary *MATLAB* files that store workspace variables and come in handy thanks to their ease of use and fast access. All the various databases revision numbers, the current *sMAPPER* version, as well as the date of the last edit of the file are saved as well, allowing the user to backtrack precisely what information where used for a particular run, even later in time.

The first step of the *Master* script is to import all the data previously saved. This is done by simply importing the various databases through the *load* function in *Matlab* for the *.mat* files. The workspace, that contains all the variables in memory, is shaped such that only a handful of structs exist. In this way, the code can be well-ordered and it is possible to arrange the whole structure in different functions with clearly defined inputs and outputs. Then once the environment is set, the simulation continues onto the input data analysis, which is explored further down in the *PV* smoothing application.

3.4.1. Simulation mode

As *sMAPPER* has many capabilities, the simulation time requires an important amount of time depending on the space of solutions to explore. To overcome this problem, two simulation modes with different computational times have been developed: **Energetic** and **Engineered**. The differences, mainly lying in simplifications of the overall *BESS* model, will be discussed hereafter.

Energetic

This mode derives its name from the idea that an *Energetic* approach implies a more high-level analysis, with less interest to the single components and more to the overall system. Indeed, this method introduces many simplifications to achieve a computational time significantly lower. First and foremost, this method does not develop all the different Power Islands with each component. Instead, given a range of nominal capacity [MWh] and different CPs, it generates simulations according to all the different possible combinations of them. This means that the main characteristics of the *BESS* do not represent a real world system, but rather a continuum of solutions. For this reason, this approach would also be referred as the "continuous" one, rather than "discrete". Indeed,

the results, when interpolated to produce a finer space of solutions, provide smooth curves and spaces allowing to easily gather important information from the simulation.

As the Power Island is not modelled, all the different components and sub-systems do not rely on the database, but rather on fixed constants given by the user. For instance, the auxiliaries do not depend on the load, but rather consume a fixed percentage of energy of the overall installed capacity. Along the same line, also the battery degradation is defined as a constant.

As the components and the sub-systems are not modelled, there would be no direct way to assess the cost of the whole *BESS*. For this reasons, the user has to input three different costs: the cost per capacity installed $[\frac{\$}{kWh}]$, the cost per installed power $[\frac{\$}{kW}]$ and the *EPC* overhead as a percentage of the whole system cost. The values, tuned to match as closely as possible the different shapes the different Power Islands cost curves have, needs to be updated manually according to the use case and to the current market prices.

While this method is obviously not accurate enough to produce reliable simulations, it is very handy when it is needed to first assess the optimum range of possibilities where the optimum may land. As a matter of fact, this simulation takes few seconds per year simulated, allowing in a handful of minutes to have results which roughly resemble what an a more accurate simulation would provide in hours. This allows future more detailed runs to search a smaller solution space and thus lower the overall time required.

Engineered

On the contrary, this approach models everything as it has been discussed before, taking all the necessary information from the database and using all the different equations and relations between them to produce a detailed analysis of the *BESS*, from the high-level to the components and sub-systems. In this way, the simulation output is much more reliable and accurate while being much slower to compute, in the order of 2 to 5 times more with respect to the *Energetic* simulation. All the different variables and struct which represents the components in code language gather the necessary information from the database by using the component tag, which is unique.

Apart from this, the *Engineered* approach follows the various hypothesis described above in the previous sections. The equations and formulas used will be discussed further down as they are application-specific. It has to be noted that from a simulation point of view, the two methods follow the exact same algorithm and code, while only differing in the phase pre-simulation that defines all the variables and components. Here, the *Engineered* approach will use functions and lookup tables rather than constants.

Last but not least, a significant effort was put to optimize the code. Due to the huge amount of data present in the workspace and they way it was structured in structs, tables and lookup tables meant the overhead for each line of code became important. This is because, as the simulation runs on the whole year minute per minute, each small *Matlab* call to a inner-struct would require time only to locate that resource. That is why many variables were copied into local variables and lookup tables functions transformed with the *griddedInterpolant* function, which is significantly faster.

3.4.2. Simulation generation

Prior to run the simulation itself, a generation process has to be performed to create the right environment for the simulation. This requires to gather and group all the different simulation parameters and characteristics into a single table, and to assign to each unique combination of simulation number that will last to the results, to ensure consistency across input-output data. This happens whether the simulation mode is the *Engineered* or the *Energetic* one. Nevertheless, the former produces a wider table as more information has to be saved, such as Power Island number or Power Island combination. Furthermore, for both modes, the table includes the specific cost of the solution to easily be spotted when analysing the data.

To explore all the different required solutions the user input prior to the simulation, the function *allcomb* is used. In Table 3.8 an example is reported where, starting with the nominal energy, the nominal power and the photovoltaic installed power, those values gets combined in such way that all the possible combinations are present. The f on top of the arrow in the middle of the tables indicates the function *allcomb*. Then, a loop code loops through every simulation number to simulate the required application or service.

Nominal energy [MWh]	Nominal power [MW]	PV DC peak [MW]
10	0.25	50
30	0.5	100
50	1	

$\xrightarrow{f}$

Simulation number	Nominal energy [MWh]	Nominal power [MW]	PV DC peak [MW]
1	10	2.5	50
2	10	2.5	100
3	10	5	50
4	10	5	100
5	10	10	50
6	10	10	100
7	30	7.5	50
8	30	7.5	100
9	30	15	50
10	30	15	100
11	30	30	50
12	30	30	100
13	50	12.5	50
14	50	12.5	100
15	50	25	50
16	50	25	100
17	50	50	50
18	50	50	100

Table 3.8: Example of input parameters combination to explore all the different possible solutions.

This method, which can be seen as a sensitivity analysis, will later be discussed in the future developments sections as it allows, theoretically, to impose a sensitive analysis on almost every aspect the user requires.

After all the environment is ready, the simulation can start. The code is structured in such a way that it is possible to use the *Parallel Computing Toolbox* by *Matlab*. This needful tool allows to run multiple simulations at once on the same computer, splitting the loop among the available processors in the machine running the code, be it a laptop or be it a Virtual Machine (VM). Depending on the system capabilities, the code will effectively run from a minimum of double the speed, up to 16x or 32x faster.

3.5. Application: PV smoothing

Along with the database, the core part of *sMAPPER* regards the applications. In fact, *sMAPPER* is developed with the intent to build a solid modeling framework, and then build on top of it different modules, which can be different services or applications related to the specific need. The algorithm implemented (namely, the *EMS*) is the same that later will be installed in operation for the *BESS*, allowing for a great deal of realism of the simulation. It has to be noted that once an application is developed, implementing new ones is easier as most of the equations regarding the *BESS* can be applied regardless of the service. What mostly changes is the underlying algorithm concerning the power dispatch, as well as the *SOC* management strategy. Furthermore, also the various constrains may change accordingly. Nevertheless, the economic analysis should remain quite similar, apart from the specific fees and remuneration policies. Hereafter, the application concerning the PV smoothing is discussed, and it is the one implemented in the case study.

Globally, photovoltaic (PV) power has dramatically increased over the last ten years. In actuality, between 2007 and 2018 the global PV power capacity increased by more than 5000% [64]. In terms of levelized cost of energy ($LCOE$), utility scale PV production is currently one of the most economical generation technologies [65–67]. This growth pattern is therefore anticipated to continue in the future. In some areas, the ratio of solar to conventional power generation has increased significantly as a result of the rise in PV power. This may result in problems due to the solar resource's inherent erraticness, particularly in cloudy conditions [68, 69].

The PV covered area and cloud speed are the two main factors that affect the ratio of change in the PV plant's power output [68, 70–72]. For various locations and plant sizes, output power variations of up to 90%/min have been documented [70, 73–75]. These types of power fluctuations can result in grid quality issues with frequency or

even voltage stability [69, 75–77]. To limit the maximum permitted rate of change for PV plants, various Transmission System Operators (TSOs) have established regulations [78–82]. According to the Puerto Rican grid code [78], the ramp-rate (RR) limit tolerance range can range from 1%/min for the most restrictive scenario in Mexico [79] to 10%/min.

Installing an energy storage system (ESS), which can include flow batteries, super capacitors, fuel cells, Li-ion batteries, or a combination of them, is the conventional method for reducing PV fluctuation [83]. Thanks to their technological advancement, performance, and anticipated price decrease, lithium-ion batteries are the most appropriate ESS technology [84, 85]. However, the addition of an ESS raises both the project's initial investment and the overall cost of the energy produced [66, 86, 87]. Therefore, in order to prevent the PV $LCOE$ from becoming less competitive, it is crucial to reduce the additional costs associated with the use of batteries. The initial cost of the EES and the battery life are the two main determinants of the increased $LCOE$.

Each ramp-rate strategy's intrinsic qualities have a significant impact on both of these variables. The moving average filter [86] and the traditional ramp-rate control [71] are two of the smoothing techniques that are most frequently studied [71, 88]. The latter continuously assesses the variation in PV power and charges or discharges the ESS when the desired smoothing is surpassed. The battery needs to be able to absorb and discharge the energy required by the worst possible positive or negative fluctuation because it is impossible to predict what the next fluctuation will look like [71]. *sMAPPER* implements the traditional one, but if the case requires so a low pass filter may be coded easily.

With regard to the simulation, a violation happens whenever the AC power injected in the PCC is lower or higher than the allowed ramp-rate. As the timestep of the simulation is of 1 minute, the violation fee is represented as a single cost per violation $[\frac{\$}{violation}]$, which inherently becomes a cost per minute (of violation).

Regarding the remuneration, it is a simple constant price per energy injected into the grid $[\frac{\$}{MWh}]$ which can be easily set according to the market or the signed contracts. In the future, with the correct knowledge, it may be possible to implement an hourly pricing tariff.

Moreover, a PV clipping ratio is included as often the inverter is not sized according to the PV DC peak power, but rather to a lower value accepting the fact that few hours per year the power may be curtailed due to the power saturation of the inverter. This is done mainly to reduce the size and cost of the inverter. This value, user customizable, is defaulted to 1 but can be increased if one wants to take into account this aspect.

Indeed, a degradation factor in the PV power output is implemented to take into account the ageing of the modules. Many manufacturers provide degradation warranties that are mostly linear. For this reason, it was chose to implement a constant value that updates each year the peak DC power output of the photovoltaic. Setting on the value is more difficult instead, as degradation values differ depending on the technology used, the manufacturer and the year of production [89, 90]. Furthermore, when designing a PV plant, data about the modules are widely available along with the ageing warranties. Thus, the value should be changed according to the use case. Nevertheless, a value of 0.70% per year with respect to the nominal value was chosen as default as it seemed to be a number close to today's industry standards.

3.5.1. Input data analysis

As already introduced, the input data analysis function serves the purpose of giving the user a first impression of the data *sMAPPER* is going to work with. This is crucial as it allows to spot any particular key information in the data and plan accordingly. Jumping straight to the simulation part without being familiar with the data can lead to wrong assumptions or to draw off-target conclusions.

The PV smoothing, as the name suggests, implies using data from the power output of a photovoltaic power plant. The application concerns the smoothing of the power output as, due to its spiky nature, lead to instability in the grids. In this case, which concerns a $100MW$ PV power plant, the data spans a whole year and has a timestep of 1 minute. It is provided in a *.mat* file with the values normalized to values of [0, 1].

Figure 3.17 analyses three main aspects of a PV plant:

- **Seasonal trend**: the four colors, representing the different seasons, show how, on average, the power is distributed throughout the day. The trend-lines have a band around them that represent the standard error (SE). This chart gives a first glance at the overall data.
- **Sorted distribution**: this single curve shows in a pretty straightforwardly how the PV power is distributed, in a sorted way and with the x-axis representing the hours per year. In this manner, one can easily understand for how many hours the power plant works above (or below) a certain power level.
- **Sorted derivative**: this chart, while being more complex, gives a very useful insights directly related to the PV smoothing itself. To obtain such plot, the data is first differentiated and then sorted. Subsequently, two black dotted bands are

drawn that represent the maximum allowable rise or drop in power in one minute, and outside there regions two colored patches appear. The green one represents the moments where the power increase is too great to be injected, and thus can be absorbed by a *BESS* or be curtailed. On the other hand, the red patch represents the points in which the power drops suddenly, and a *BESS* is required to try to smooth that out via injecting more power in the grid. Should not this be enough, a violation will occur with its relative cost. Therefore, the chart allows to eyeball what the base case would yield in terms of energy curtailed and violations, as well as the required size of *BESS* to reduce at minimum the fees.

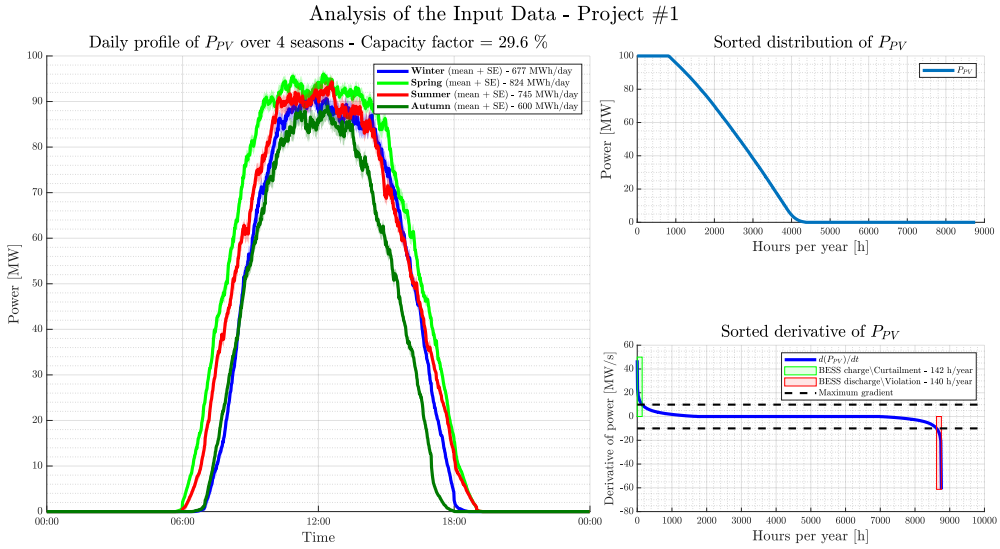

Figure 3.17: Analysis of the distribution of the input data, part 1.

In contrast, Figure 3.18 shows a simpler chart that compares the average distribution of fraction of daily generation. This plot is supposed to give more insights on the hourly distribution of the different season. This may be relevant when planning also to implement a Peak Shaving (*PS*) service along with the *PV* smoothing. Indeed, it is clearly visible how, in this example data, during spring and summer the distribution has a wider base and thus would require less energy shifting, opposed to the winter months that yield their energy content mainly during the peak hours.

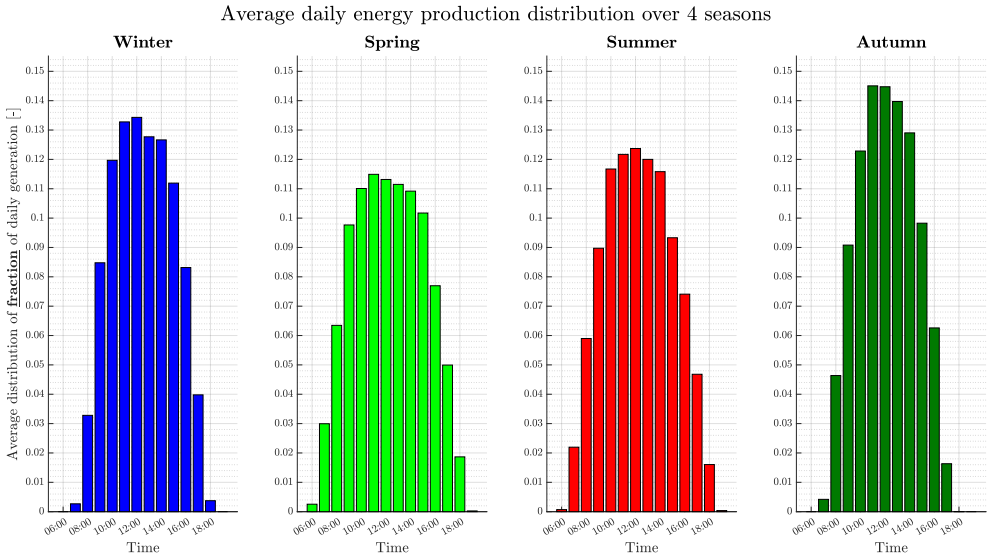

Figure 3.18: Analysis of the distribution of the input data, part 2.

3.5.2. SOC management

As with any application or service involving the use of a battery, a *SOC* management strategy needs to be implemented to ensure the readiness of the *BESS* to perform its duty. Therefore, a *SOC* restoring technique that resembles a hysteresis cycle has been implemented that works as following according to a flag variable called *hysteresis flag*:

- hysteresis flag = **0**: in this mode, the *SOC* management is disabled. To enter this mode, some conditions need to be met: the hysteresis flag was equal to 1 and the *BESS* has reached an energy level lower than the target one or the hysteresis flag was equal to -1 and the *BESS* has reached an energy level higher than the target one, such that

$$hysteresisFlag^{\text{t-1}} == 1 \land SOC^{\text{t}} < SOC_{target}$$
$$\lor$$
$$hysteresisFlag^{\text{t-1}} == -1 \land SOC^{\text{t}} > SOC_{target}$$

- hysteresis flag = **1**: in this mode, the *SOC* management forces the battery to discharge with a fixed percentage of the *BESS* installed power, set by default to 10% but customizable. This low value was chosen to allow the battery to achieve a lower mean CP over the year. If the case study requires a more aggressive *SOC* restoration to ensure higher reliability of the system, different values should be chosen. To enter this mode, the battery has to exceed a superior threshold, typically

set to 70% but modifiable. This does not mean that the battery will never reach SOC levels higher than the superior threshold, but rather that this limit is the point where the battery SOC would be too high to reliably perform its duty. Thus, the condition is the following:

$$SOC^{t} > SOC_{target,superior}$$

- hysteresis flag = **-1**: this mode is the exact same as the previous one, but in reverse as it forces the battery to charge. The condition is the following:

$$SOC^{t} < SOC_{target,inferior}$$

Whenever no one of the conditions are met, the hysteresis flag will just be the same as the previous timestep.

In Figure 3.19 it is shown an example of SOC behaviour during a simulation. It is clear that when the battery exceeds the dotted black lines, which represents the threshold, the battery SOC changes according to a fixed slope that is defined by the aforementioned value of 10%. Needless to say, during those phases the $BESS$ is still able to work as intended in the PV smoothing application.

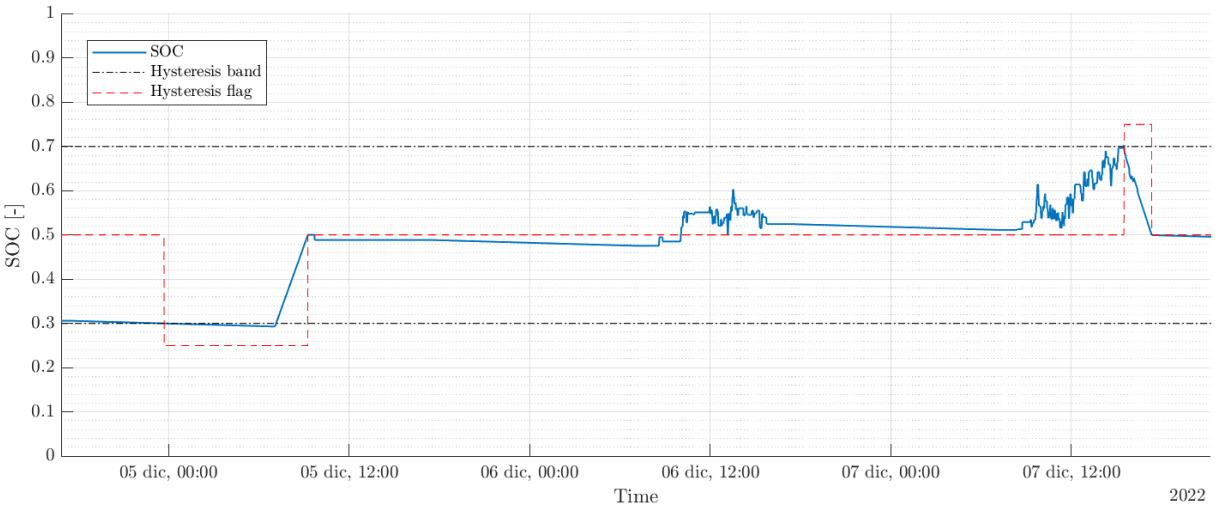

Figure 3.19: Example of SOC management in a simulation with both the charge and discharge phase.

3.5.3. Architecture

For this application, the possible topologies are mainly two, and are named *AC* or *DC* depending on the coupling method. Hereafter, the different topologies are represented along with their various working operations.

Firstly it is shown the *AC* coupling. In Figure 3.20 it is shown a scheme with all the different components and sub-systems and with the whole system working in normal operation, with the *BESS* at idle. The inclusion of two *MV/HV* skid is to account for all the possible different scenarios, as the coupling always happens at MV voltage but the *PCC* may require *HV* instead. The battery is followed by the internal efficiency box, which does not represent a physical component but rather is a way to model the inefficiency related to the battery itself before any conversion process. Furthermore, the auxiliaries are included after the as typically they work by spilling some of the power by connecting to the MV voltage for ease of installation.

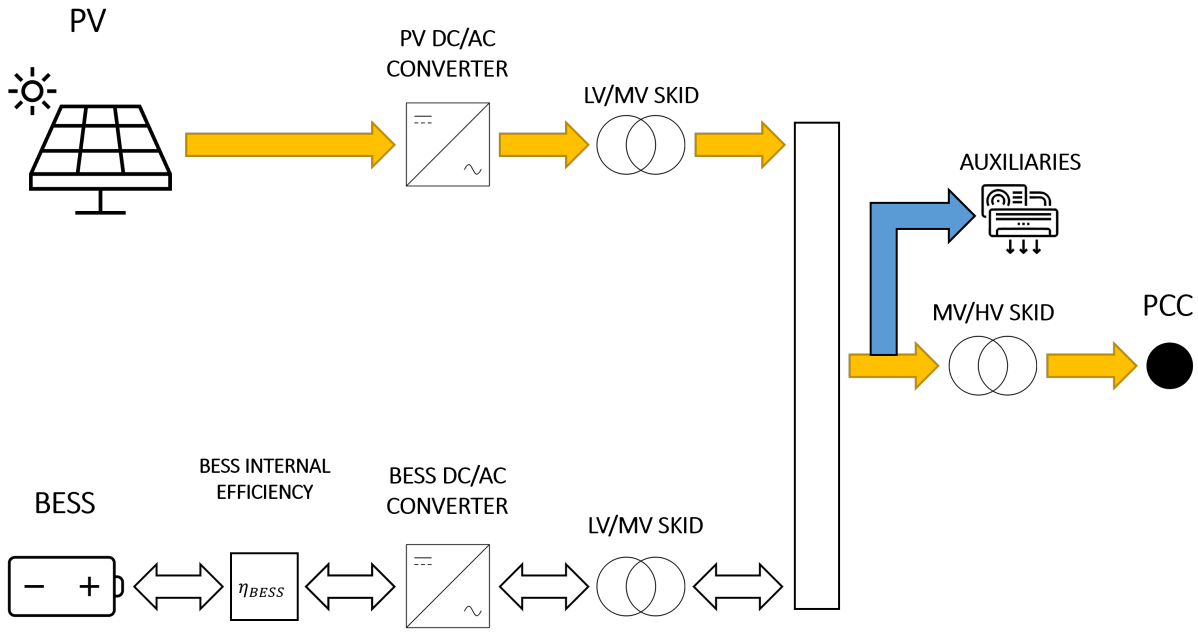

Figure 3.20: *PV* smoothing architecture with *AC* coupling with *BESS* in normal operation.

In Figures 3.21 are represented the 4 main operational modes of the whole system. In the top two figures, Figures 3.21a and 3.21b, it is shown the battery intervention in case the *PV* would exceed the ramp limit. In the bottom two figures, Figures 3.21c and 3.21d, the *SOC* management is shown that kicks off whenever the battery energy level has drifted outside the prescribed boundaries.

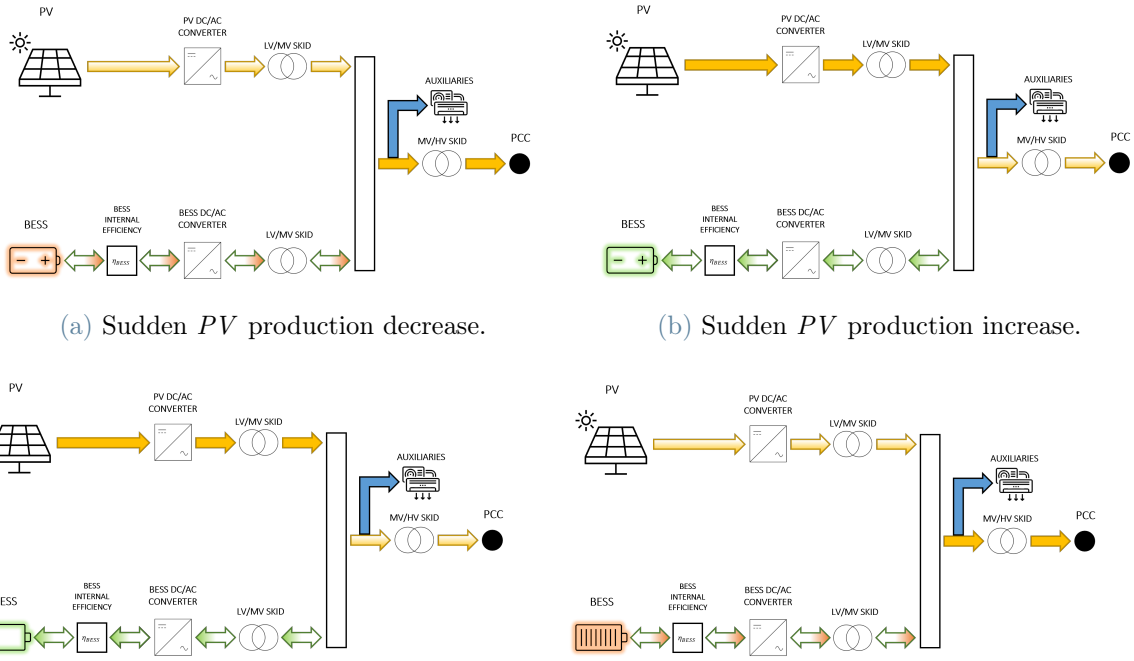

(a) Sudden *PV* production decrease.

(b) Sudden *PV* production increase.

(c) SOC management, charging *BESS*.

(d) SOC management, discharging *BESS*.

Figure 3.21: *PV* smoothing architecture with *AC* coupling with *BESS* in various operation modes.

Then, it is shown the *DC* coupling. In Figure 3.22 it is shown a scheme with all the different components and sub-systems. The inclusion of two *MV/HV* skid is to account for all the possible different scenarios as for the *AC* coupling. In this case, though, the battery and the *PV* are followed by a DC/DC conversion process. The latters are usually mutually exclusive, and the architecture with the converter only the battery side is the most used one. Concerning the operational modes shown in Figures 3.23a, 3.23b, 3.23c, and 3.23d, they follow the exact same structure as the *AC* architecture.

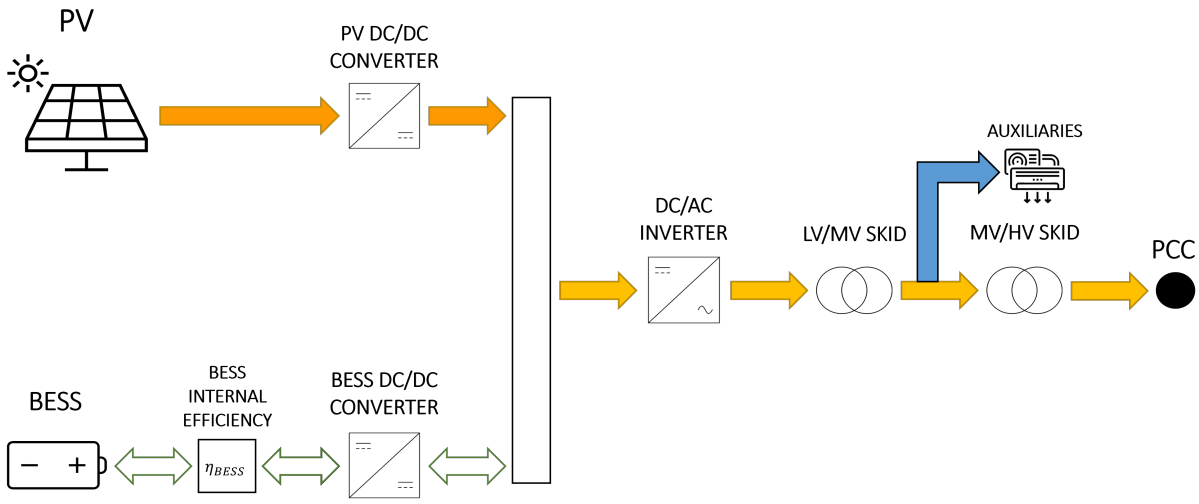

Figure 3.22: *PV* smoothing architecture with *DC* coupling with *BESS* in normal operation.

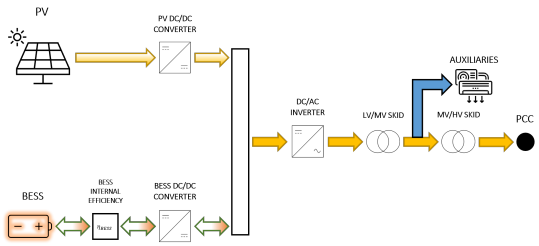

(a) Sudden *PV* production decrease.

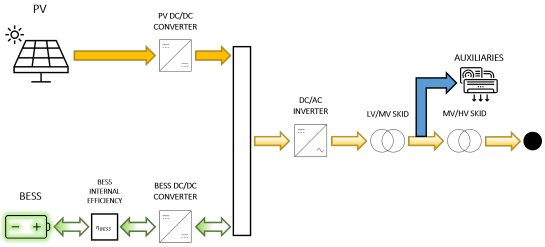

(b) Sudden *PV* production increase.

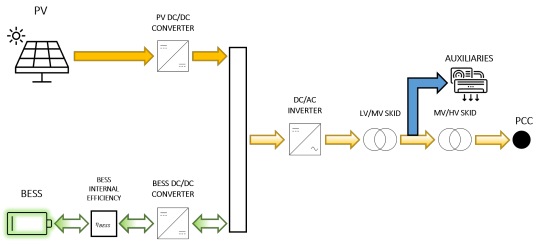

(c) SOC management, charging *BESS*.

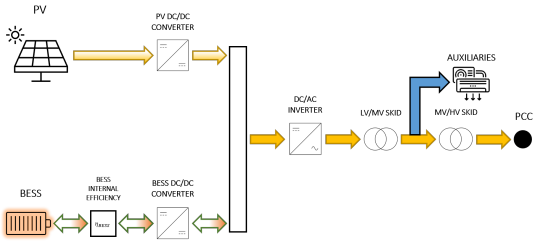

(d) SOC management, discharging *BESS*.

Figure 3.23: *PV* smoothing architecture with *DC* coupling with *BESS* in various operation modes.

Lastly, it is shown a side-by-side comparison between the two topologies in Figure 3.24.

Each of them has its own advantages and disadvantages, which can be listed as:

- **AC**:

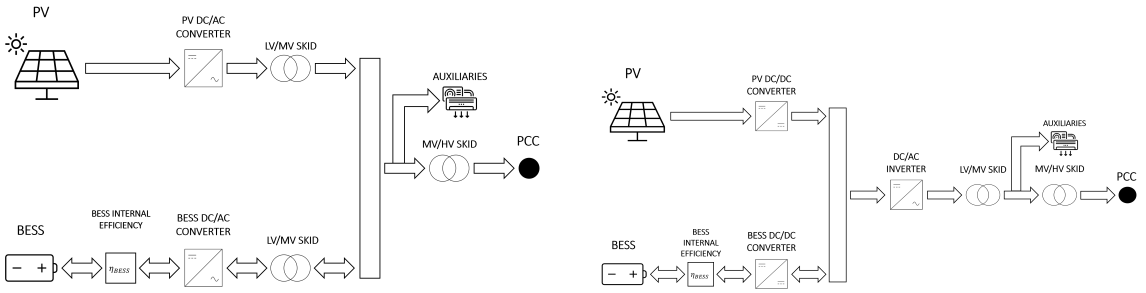

(a) *AC* coupling structure. (b) *DC* coupling structure.

Figure 3.24: *PV* smoothing architectures comparisons between *AC* and *DC* couplings.

- Advantages:
  - Retrofitting: An existing *PV* system can be easily upgraded with additional *AC*-coupled batteries to increase capacity.
  - Flexibility: The placement of the inverters and batteries is not constrained for installers. Any kind of inverter can be used with AC coupling.
  - Resiliency: If one inverter fails, the ability to install other inverters and batteries in different places reduces the likelihood of a power loss. The combined power from several inverters is greater, and battery problems have no effect on power generation.
- Disadvantages:
  - Cost: Due to the usage of several inverters, *AC*-coupled systems are more expensive than *DC*-coupled systems.
  - Lower efficiency: The stored energy is changed three times: from *DC* current to *AC* current to power the building, from *AC* current to *DC* current to charge the battery, and finally from *DC* current to *AC* current once more. There is a little amount of energy lost during each conversion.
  - Supply limitations: Since *AC BESS*s lack transformers, they are unable to handle the surge loads caused by numerous appliances, and they are not intended for usage off-grid.

- **DC**:
  - Advantages:
    - Affordability: Due to the use of a single inverter for the solar panels and

batteries and the lack of additional components like voltage transformers and switchgear, *DC*-coupled systems are often less expensive than AC-coupled systems.

* Higher efficiency: *DC BESS*s only convert the current once, as opposed to several conversions in *AC* systems, which results in lower energy losses and higher efficiency.

* Oversizing: Solar panels can produce more electricity than the inverter's rated capacity using *DC*-coupled systems. In contrast to an AC-coupled system, where the extra energy is lost, this method can use it to charge the battery, an EV charger, or any *DC* load.

– Disadvantages:

* Limited flexibility: Compared to an *AC* system, installers have less degrees of freedom because the inverter must be placed close to the battery.

* Less resiliency: In a *DC*-coupled system with a single inverter, both the solar power and the battery capacity are lost in the event of an inverter failure.

As already analyzed by others [91], the best performing *PCS* layout was found to be *DC*-coupling with a *DC-DC* converter at the battery side, followed by *AC*-coupling, under the same input-output conditions (irradiance, *PFR*, and dispatching settings). The *DC*-coupling with *DC-DC* converter at the *PV-side* arrangement has the lowest performance. Different conversion stages involved in the energy flow from *PV* to battery during *PFR* service during the day and from battery to grid during energy shifting during the evening were responsible for the various performances.

Regardless of the theoretical best configuration, all of them are available to perform simulations on all the different case scenarios that may arise.

3.5.4. Algorithm

The algorithm, after having initialized all the different variables, starts firstly with checking if the power produced by the *PV* at the next timestep is greater than the ramp rate limit. If this is the case, then just injects the maximum power. Otherwise, the *BESS* comes into play to absorb the excess or to provide the missing power. Then, according to the *hysteresisFlag* (which represents the *SOC* management), if the battery is forced to charge or discharge, it tries to absorb or inject some of the total power to restore the *SOC*

to the target level. Lastly, according to the current *SOC*, it defines the *hysteresisFlag* for the next timestep according to the aforementioned conditions.

If the simulation mode is *Energetic*, many steps of the algorithm are skipped as the efficiencies, as well as some constraints are constant. This lines are omitted through the use of flags and ifs. Indeed, this is what makes the *Energetic* mode way lighter, as all the functions and lookup tables are what slows down the overall run.

On the other hand, if the simulation mode is *Engineered*, during each step of the algorithm the efficiencies are computed. This is done via functions such as $\eta_{BESS,internal} = f(\frac{P_{BESS,DC,real}}{E_{nominal}}) = f(CP)$, where the subscript *real* indicates the power before the internal efficiency according to the structures seen in Figures 3.24, which in turn are lookup tables with linear interpolation. The *CP* is computed as $CP = \frac{P_{BESS,DC,real}}{E_{nominal}}$, where P is the instantaneous *BESS* power, while $E_{nominal}$ represents the capacity installed at Beginning Of Life (*BOL*). This is because the power does not fade over the years, and as such the CP should be computed according to the nominal capacity not to exceed the battery max *CP* rating at *BOL*.

An issue arises when computing the internal efficiency of the batteries: as the $\eta_{BESS,internal}$ is a function of the power, but the power is computed after accounting for the efficiency such that $P_{BESS,DC,real} = P_{BESS,DC} * \eta_{BESS,internal}$. Because of this, the efficiency function is an implicit one, and an iterative process would be needed to find the right value, starting from a guess and refining it until the value has an acceptable accuracy. While this would be the correct way to solve it, it would immensely lengthen the simulation time while yielding no results accuracy improvement. The implemented way is instead to guess the closest value and then computing the $P_{BESS,DC,real}$. The guesses usually can be the $P_{BESS,DC}$, which will be very close to the output value, or the $P_{BESS,DC,nominal}$ which account for the worst case load.

As a consequence, exact equalities and inequalities could not be computed. Thus, a threshold value was introduced to account for this, with the value being 0.1% of the installed power. This resulted in any difference being smaller than that one, to be treated as 0.

Regardless, there is another step in computing the $P_{BESS,DC,real}$ that ends up being the correct ones: accounting for limits and boundaries. Indeed, to ensure that the batteries always work within the correct region, *min* and *max* functions are implemented. For instance, in the case of the *BESS* forced to discharge due to the *SOC* management:

$$P_{BESS} = min(P_{BESS,nominal}, P_{BESS,max}(E^{t-1}), P_{BESS,available}, P_{BESS,max}(SOC, SOH))$$

$$P_{BESS,nominal} = \text{from database}$$

$$P_{BESS,max}(E^{t-1}) = \frac{E^{t-1}}{dt}, dt = \frac{1}{60}$$

$$P_{BESS,available} = P_{BESS} + P_{PCC,available} * \eta_{BESS \rightarrow PCC}$$

$$P_{BESS,max}(SOC, SOH) = CP_{max}(\frac{E^{t-1}}{E^{y}_{nominal}}, SOH^{y}) * E_{nominal,BOL}$$

where t indicates the current timestep and y the current year. The $P_{PCC,available}$ indicates the amount of available power that can be injected into the grid (to force the battery discharge) while still remaining inside the allowed ramp rate. This kind of equations are repeated multiple times during the simulations for all the different needs and are extended even to the PV. Furthermore, all the different efficiencies, which are put into functions prior to the simulation, are computed like $\eta_{PV \rightarrow PCC} = f(\frac{P_{PV}}{P_{PCS,nominal}})$. This allow ease of coding and maintenance as it is clear the function of the efficiency, while not filling the code the database functions and data.

Lastly, at the end of every timestep, the actual $P_{BESS,DC,real}$ is computed and the $BESS$ energy content is updated. The *hysteresisFlag* is also computed to decide the SOC management mode for the next timestep. After the simulation has run for 1 complete year, the economic assessment and the various KPIs are computed, as well as re-calculating all the initial parameters and variable for the next year. Here, the SOH along with other parameters that change over the years are computed.

4 | Case Study

The case study analysed in this thesis regards a PV smoothing project that will be discussed hereafter.

4.1. Baja California Sur, Mexico

The case study analysed in this thesis regards a project commissioned by NHOA in 2019 located in Baja California Sur, Mexico. The BESS is integrated to the $23MW_{AC}/31.2MW_p$ *Sol de Insurgentes PV* plant. Figures 4.1b and 4.1a show the location of the site and, in particular, the location of the *MV/HV* substation, where the *BESS* is installed. The

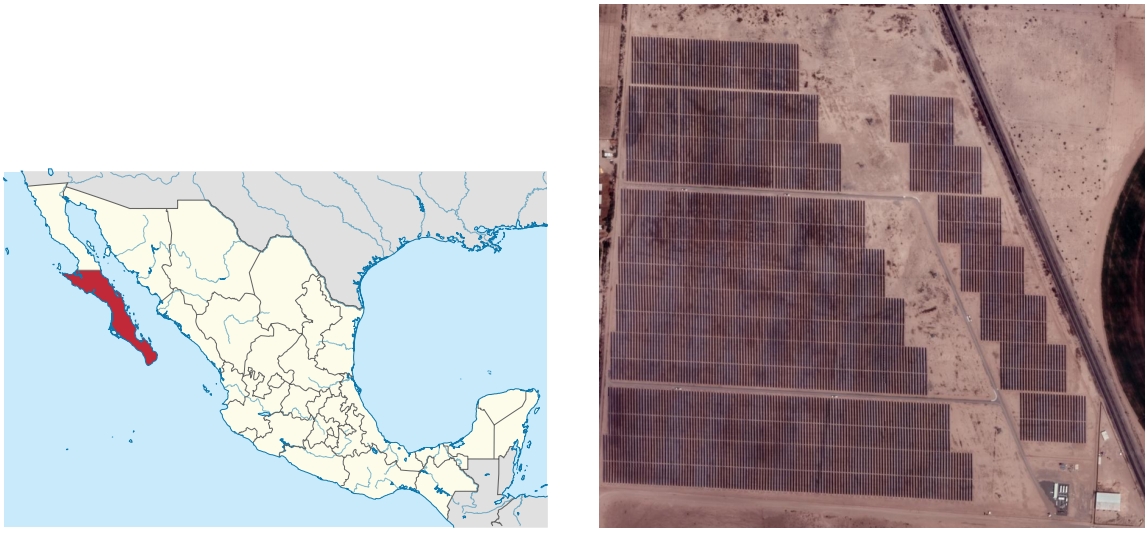

(a) Mexico region. (b) Google Earth aerial view.

Figure 4.1: Site location.

Table 4.1 resumes the main geographical data of the site.

Sol de Insurgentes BESS is a lithium-ion based storage system, $5.4MVA$ / $3.168MWh$ rated power and energy installed. The storage system is supported by dedicated Power Conversion Systems (*PCS*), that consists of NHOA' proprietary 4-quadrant converters. Table 4.2 resumes the main technical features of the *BESS*.

Location	Info
Project typology	PV + BESS
Latitude	25° 12' 2.25" N
Longitude	111° 45' 9.53" O

Table 4.1: Site data.

Characteristic	Value
Installed PCS power	5.4 MVA
Battery technology	Lithium-ion NMC
Installed battery capacity @BOL	3.168 MWh
Battery max continuative C-rate	2C
Useful AC battery capacity @EOL 10 years	>1.25 MWh

Table 4.2: Main technical features of BESS.

The *BESS* is composed of:

- n.3 identical 40ft High-Cube containers
- n.3 2 MVA *LV/MV* Oil Natural Air Natural (*ONAN*) transformers, for connection to the MV switchgear of the substation
- n.1 EMS cabinet, with the Energy Management System (*EMS*)

Each container is composed of n.2 separate rooms, the Battery Room and the *PCS* Room, respectively containing the batteries and the Power Conversion Systems (*PCS*). The *BESS* will be parallel connected to the *PV* plant through a *MV* switchgear at 34.5kV, then, the *PV* + Storage plant will be connected to the 115kV Grid with a single Point of Connection (*POC*). *BESS* limit of supply are the *MV* terminals of *LV/MV ESS* transformers.

Information about the economic part of the project are confidential and thus cannot be reported.

4.1.1. Issues

The battery market is a rapidly changing one, and manufacturers, as well as models and chemistries, change frequently according to the different trends. In this case, the battery used, which are rated at 2C or 30 minutes, are not anymore present in the utility scale market. Indeed, nowadays's market is moving towards bigger capacity batteries both for the lower price per kWh and for the ability to exploit power intensive applications, such as the PV smoothing, along with other energy intensive application, such as Peak Shaving. This allows the investors to make better use of the systems, while keeping the price lower as usually batteries with rating between 0.5C and 1C are used. For these reason,

NHOA's database does not contain data regarding batteries more than 1C. This means that the *Engineered* mode will not be able to propose a solution as the presented one. Nevertheless, it is interesting to analyse how with the current battery models employed by *NHOA sMAPPER* will cope, and the relative best solutions proposed. On the other hand, in the *Energetic* mode, which allows to search any desired capacity and power, it will be possible to explore 2C solutions.

Furthermore, the information about the PV power plant is not directly available as *NHOA* involvment in the project regarded only the *BESS* system, not the photovoltaic part. Indeed, some data about the power plant was available online, reporting the use of 300W peak power panels [92]. Thus, the chosen PV degradation rate was chosen taken from different datasheet of modern $300W$ photovoltaic panels and its value is set to 0.70 $\frac{\%}{year}$ as it represents a mean value in the current industry [93].

On the same page, as the data about the PV power plant is not directly available, the economic part has to be assessed through the use of open information. The data found regarding the remuneration per energy injected in the grid is at 50.7 $\frac{\$}{MWh}$ [94]. This value, which represents the average contract price of all the different winners of the Clean Energy Auction for energy in Mexico in 2016. On the other hand, regarding the violation price for the ramp rate, no information was anywhere to be found, so the price has been set 100 $\frac{\$}{MWh}$. This price, while not being backed up by any number, is one that was found to produce results in line with the real projects pricing and design solutions.

In reality, the violation price does not always exists, but rather a limit on the amount of violations per year is stipulated. All this information is usually is confidential and thus only estimates can be achieved. According to the *Deutsche Gesellschaft für Internationale Zusammenarbeit (GIZ) GmbH* who drafted a document titled *Electrical Energy Storage in Mexico*, an option would be to express a requirement towards the performance and fulfillment ratio of the grid service. An example of this could be that any *PV* plant must guarantee a maximum ramp of 10% of nominal power per minute and that this requirement must be met during 99.9% of the time. While the ramp is known for the study case, the violation minutes is not. Thus, while this will not be hard-coded as a proxy for discerning the acceptable runs from the others, it will still be taken into account when selecting the optimal solution.

Lastly, most of the economic parts and details are not public and thus cannot be reported here. For this reason, the economic analysis for this case study will be weaker, but supported by other *KPI*s to seek the optimal solution. Nevertheless, the main economic parameter will be reported for both the *Energetic* and *Engineered* modes. The costs, while

tuned to be similar to *NHOA*'s ones, are not supposed to be taken as exactly realistic values due to the aforementioned reasons.

4.1.2. Input data analysis

The data utilised in this project is the same used in the sizing process of this *BESS* in 2019. It is a 1 minute timestep data, as required by *sMAPPER*. The input analysis function, described in the previous chapter, allows to inspect how the data is shaped. In Figure 4.2 are represented the three main aspects of a PV plant: Seasonal trend, sorted distribution and sorted derivative. From the sorted derivative plot, it is possible to know how many hours per year the no-BESS scenario violates the ramp rate limit, which in this case amounts to 266 $\frac{h}{year}$ in curtailment, and 264 $\frac{h}{year}$ in violation. These are to take as the worst-case scenarios for any simulation. Furthermore, looking at the bottom-right plot, it is clear how an optimal BESS size in terms of installed power would be something around the 3 to 5 MW, as higher values would only fall in the steeper region of the curve which yields diminishing returns. Indeed, the installed power of *Sol de Insurgentes* is of 5.4 MVA, close to this eyeballed value.

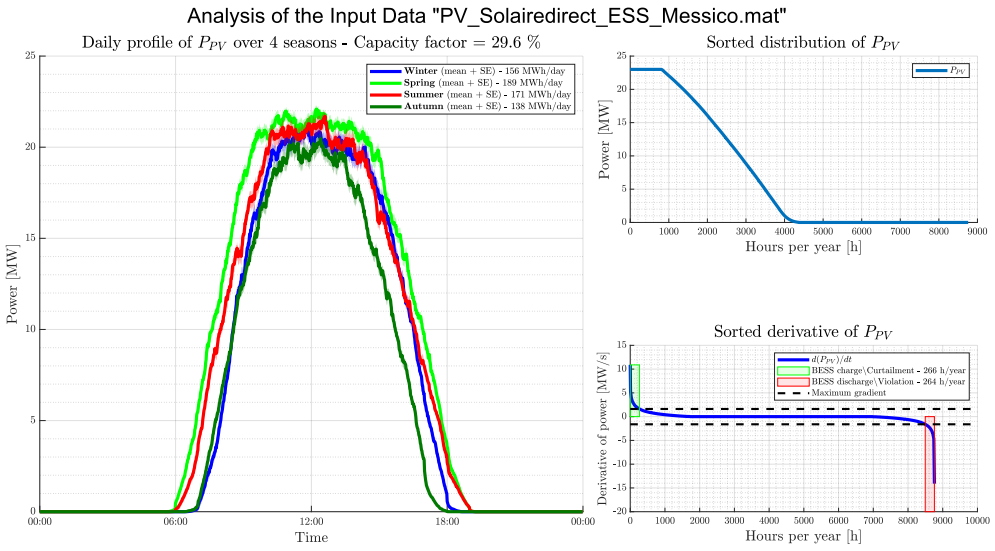

Figure 4.2: Analysis of the distribution of the input data in the case study, part 1.

In contrast, Figure 4.3 shows a simpler chart that compares the average distribution of fraction of daily generation, and for this study case it is not too relevant. Nevertheless, this may be interesting when planning also to implement a Peak Shaving (PS) service along with the PV smoothing.

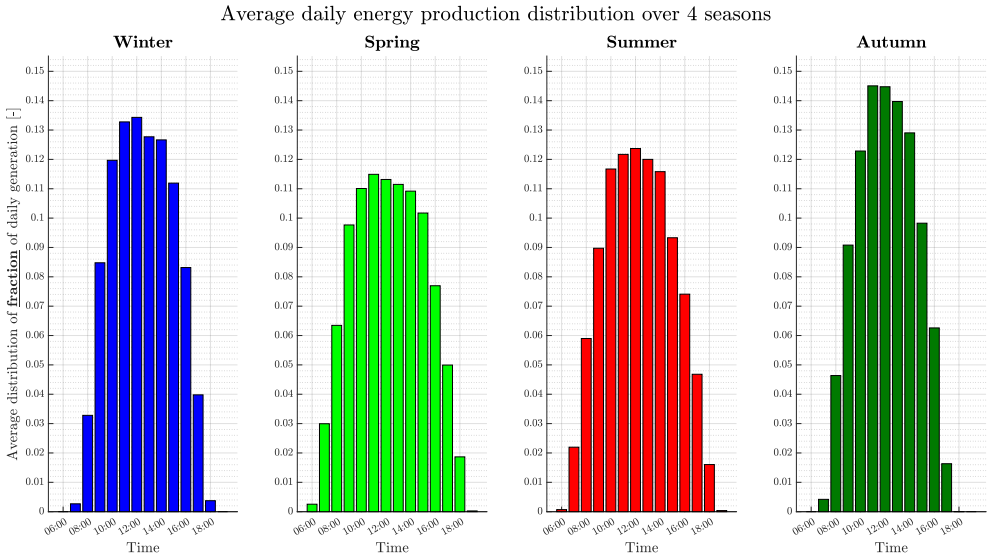

Figure 4.3: Analysis of the distribution of the input data in the case study, part 2.

4.1.3. SOC management strategy

The *SOC* management strategy employed is the same as the one introduced in the previous chapter. The values employed are reported in Table 4.3. The power offset introduced during the *SOC* restoration mode is active as percentage of the nominal power, and its value of 10% has been chosen after some sensitivity analysis on different runs. The *SOC* target is simply 50% as is it the most reasonable value in this type of application. The hysteresis band, which represents the amplitude of the hysteresis threshold for the *SOC* restoration strategy and is symmetric with respect to the target level, has a value of 20% which results in a band of 30-70 %. This amplitude seemed to be the best one when it came to the trade off of reliability of the *BESS* while keeping the battery cycling at a lower value.

Parameter	Value
Power offset	10 %
Hysteresis band	20 %
SOC target	50 %

Table 4.3: Parameters of the SOC management strategy.

4.1.4. Energetic

As stated previously, the first step to find the optimal solution is to run the *Energetic* simulation. In this mode, it is possible to set the space of solutions to explore, as well as the different efficiencies. In this case, the size of nominal capacities at *BOL* analysed was between 1 and 5 MWh, while the possible *CP* are 0.5, 1 and 2. The photovoltaic was put at $23MW_{AC,LV}$ as the size was already given and no sensitive analysis was necessary. This means that all the solutions spanning from 1 MWh and 0.5 MW to 5 MWh and 10 MW are analysed, with a discrete step of 0.1 MWh each.

Regarding the efficiencies, since the photovoltaic input data was already given in AC LV side its conversion efficiency was put to 1. Regarding the BESS, its internal efficiency was put to 98%, while the efficiency to the *PCC* (not including the internal one) was set to 96%. Their product leads to an overall efficiency of 94%, value in line with the one used by *NHOA* while designing this *BESS*. For the same reason, the MV skid was set to 99% efficiency, while the HV skid is not present and thus set to 1. Moreover, as the coupling is on the AC side, the DC/DC converter efficiency is set to 1 as it does not exists. All this values, along with the different economic parameters, are reported in Table 4.4. All the different values are set to mimic as closely as possible the behaviour of the *Engineered* mode as it is the more realistic and reliable one.

Parameter	Value
Degradation per year	2%
Cost per kWh	210 $/kWh
Cost per kW	50 $/kW
EPC percentage	30%
Container auxiliaries	0.0012 MW/MWh

Efficiency	Value
PV to PCC	1
PV to BESS	1
BESS to PCC	96%
BESS internal	98%
PV inverter	1
PV DC/DC converter	1
BESS DC/DC converter	1
MV skid	99%
HV skid	1

Economic	Value
Inflation rate	1%
Discount rate	6%
Margin	22%
Fixed costs	30000 $/year
O&M	2 $/kWh*year

Table 4.4: *Energetic* parameters of the simulation.

Overall, the simulation explored 123 simulations (41 steps in nominal capacity from 1 to 5 MWh, and 3 different *CP*s per step) and took total of $\sim 7000s$. Considering that each simulation ran for 10 years, each year took 6 seconds on average to compute. Considering that each year, apart from all the variables and parameters initialization, has to loop through 525,600 minutes, the simulation is fast. At the end of the simulation, all the results (the full ones, comprising of all the years information, and the compact ones, which average each simulation per the 10 years) are logged into the result folder. Then, a pop-up window appear to ask the user what simulations among all of them is required to be plotted in detail, and for which years.

It has to be noted that prior to this simulation, another one with the same parameters was run, exploring a wider but emptier space of solutions (2 to 20 MWh with 2 MWh step, with CPs of 0.5 and 2). This simulation, which only took about 20 minutes, allowed to understand that the space that should be explored is up to 5 MWh as reported by Figure 4.4. The latter shows the *NPV* difference (that is, the difference between the base case and the one with the *BESS* implemented) for all the range of explored solutions. The results are interpolated on the grid to produce smoother lines and to show the location of the optimum more clearly. The red line on the top-right indicated the line where the solutions with the *BESS* implemented are actually worse than the base case. Lastly, the stars indicate the top 10 best solutions, and the *CP* lines of value 2C, 1C, 0.5C and 0.25C are plotted as well. Indeed, it is clear that the best solutions for this power intensive application lay on the 2C line.

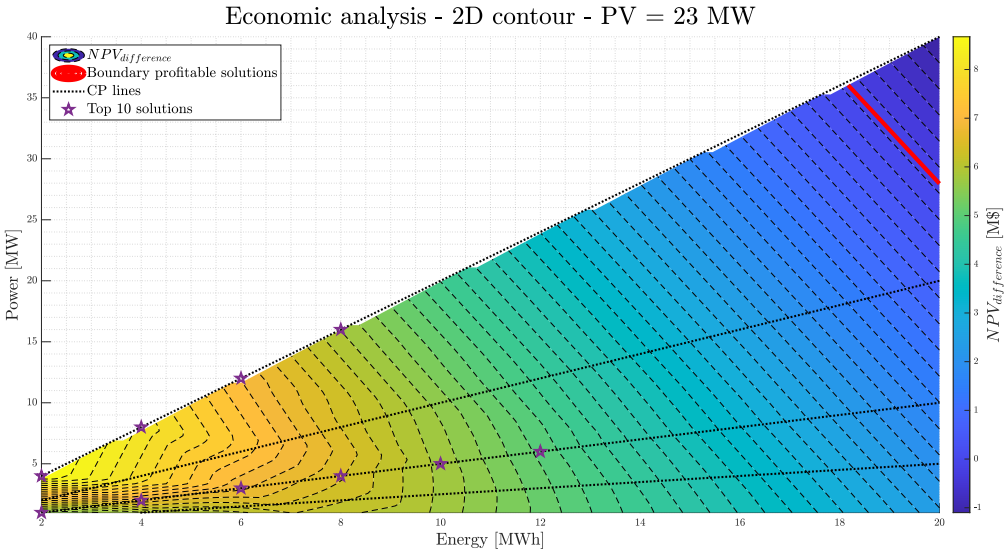

Figure 4.4: Energetic mode, contour map of the simple case.

After this simpler simulation has been quickly analysed, the main energetic simulation previously explained has been run. Its main results are reported hereafter. Firstly, the same chart as before is proposed in Figure 4.5 but looking at a smaller and denser part of the solution space with respect to the previous one. Indeed, here the lines are smoother due to the higher numbers of point to interpolate on. The best solutions, which lie on the 2C line as stated before, lie around the 2-2.5 MWh nominal capacity mark, leading to 4 to 5 MW in nominal power. This result is already close to the one proposed and commissioned by *NHOA* in the end. Nevertheless, as costs have widely changed over the years, it would be difficult to recreate the exact same economic conditions as the ones in

2019 and thus the same optimal results.

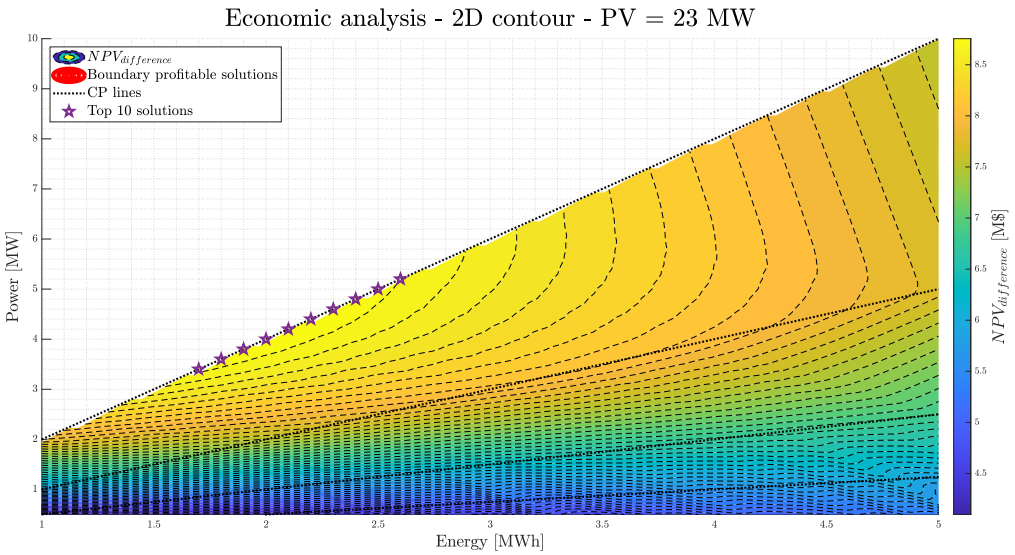

Figure 4.5: Energetic mode, contour map.

Reported in Table 4.5 are the main result, where most of the simulations were not reported for space reasons. They are averaged over the 10 years for each simulation, and selected among all the other result data column that is logged from *sMAPPER*. The first three columns represent the simulation characteristics, while the other ones represent the results. Indeed, the most important column is the violations per year because, as aforementioned, the *NPV* approach to determine the best solution is not a strong one as it relies on current economic estimates. Instead, the amount of violations per minute, which should not exceed the 0.1% of the total time, is a great metric. Indeed, the green rows represent those cases. It is clear how increasing in capacity leads to better results, but it is interesting to see that the first simulation able to cope with the 0.1% constraint has a nominal power exactly the same as the one requested by the project. This shows how even the *Energetic* simulation proves to be useful to assess the problem in rapidity.

Simulation number	Nominal energy [MWh]	Nominal power [MW]	Violations [min/year]	Eq. cycles [cycles/year]	Mean CP [-]	DOD [-]	PV produced DC [MWh]	PV curtailed DC [MWh]
1	1	0.5	8314	134.4	0.246	0.660	57484.2	335.7
3	1	2	2794	310.2	0.803	0.810	57674.4	145.5
31	2	1	5685	107.5	0.253	0.595	57578.6	241.3
32	2	2	2762	152.6	0.423	0.595	57674.5	145.4
33	2	4	684	191.8	0.564	0.673	57731.9	88.0
48	**2.5**	**5**	**373**	**159.8**	**0.479**	**0.657**	**57740.3**	**79.6**
62	3	3	1348	118.0	0.344	0.530	57714.4	105.5
63	**3**	**6**	**194**	**136.7**	**0.416**	**0.598**	**57744.4**	**75.5**
78	**3.5**	**7**	**98**	**119.6**	**0.366**	**0.600**	**57746.4**	**73.5**
91	4	2	2723	76.4	0.220	0.473	57673.6	146.3
92	4	4	663	95.6	0.281	0.485	57732.4	87.5
93	**4**	**8**	**50**	**105.7**	**0.327**	**0.621**	**57747.2**	**72.7**
107	**4.5**	**4.5**	**480**	**87.4**	**0.257**	**0.465**	**57737.3**	**82.6**
108	**4.5**	**9**	**27**	**95.3**	**0.293**	**0.616**	**57747.9**	**72.1**
122	**5**	**5**	**362**	**80.8**	**0.236**	**0.471**	**57740.9**	**79.0**
123	**5**	**10**	**12**	**86.4**	**0.266**	**0.567**	**57748.1**	**71.8**

Table 4.5: Results averaged over the 10 years of the Energetic simulation.

Regarding the economic part, even though it is clear that everything relies on the violation fee, it is interesting to see that the best solutions may not coincide with the ones with the fewer minutes of violations per year. Indeed, the higher investment costs would not be payed back by such projects. To better visualize this, the economic results are reported in 4.6. The best case in terms of NPV cumulative after 10 years, is highlighted in yellow on the last columns, and in fact does not coincide with a case compliant with the 0.1% constraint. The remuneration, which depends almost only on the installed PV power plant and the irradiation data, is pretty much constant, as the only losses in remuneration come from the few hours of curtailment per year which amount to very little energy. On the other hand, the violation cost can skyrocket when the *BESS* is not suitable for the application, as seen in the first rows.

Simulation number	Nominal energy [MWh]	Nominal power [MW]	Violations [min/year]	Cost [$/kWh]	Remuneration [$/year]	Remuneration loss [$/year]	Violation cost [$/year]	NPV cumulative [$]
1	1	0.5	8314	430.4	$ 2,873,198	$ 14,007	$ 831,370	$ 8,210,888
3	1	2	2794	567.8	$ 2,882,072	$ 5,133	$ 279,360	$ 10,480,647
31	2	1	5685	430.4	$ 2,877,102	$ 10,103	$ 568,460	$ 8,917,909
32	2	2	2762	476.2	$ 2,881,573	$ 5,633	$ 276,220	$ 10,099,855
33	2	4	684	567.8	$ 2,884,159	$ 3,046	$ 68,400	$ 10,831,452
48	**2.5**	**5**	**373**	**567.8**	**$ 2,884,261**	**$ 2,945**	**$ 37,300**	**$ 10,679,802**
62	3	3	1348	476.2	$ 2,882,866	$ 4,340	$ 134,840	$ 10,231,002
63	**3**	**6**	**194**	**567.8**	**$ 2,884,161**	**$ 3,045**	**$ 19,440**	**$ 10,471,251**
78	**3.5**	**7**	**98**	**567.8**	**$ 2,883,971**	**$ 3,235**	**$ 9,800**	**$ 10,225,246**
91	4	2	2723	430.4	$ 2,880,475	$ 6,730	$ 272,280	$ 9,327,051
92	4	4	663	476.2	$ 2,883,140	$ 4,066	$ 66,320	$ 10,049,804
93	**4**	**8**	**50**	**567.8**	**$ 2,883,730**	**$ 3,476**	**$ 4,950**	**$ 9,957,757**
107	**4.5**	**4.5**	**480**	**476.2**	**$ 2,883,084**	**$ 4,122**	**$ 48,010**	**$ 9,888,726**
108	**4.5**	**9**	**27**	**567.8**	**$ 2,883,482**	**$ 3,724**	**$ 2,650**	**$ 9,680,668**
122	**5**	**5**	**362**	**476.2**	**$ 2,882,963**	**$ 4,243**	**$ 36,150**	**$ 9,697,158**
123	**5**	**10**	**12**	**567.8**	**$ 2,883,221**	**$ 3,984**	**$ 1,170**	**$ 9,397,083**

Table 4.6: Economic results averaged over the 10 years (except for the NPV cumulative) of the Energetic simulation.

To further understand the impact of the violation cost, another simulation with the same parameters and conditions was run, only changing the violation cost from $100\frac{\$}{min}$ to $30\frac{\$}{min}$. The comparison with the case presented above are reported in Figures 4.6a, 4.6b, 4.6c, and 4.6d. The top two contour plots show how, intuitively, reducing the violation cost reduces the space of optimal solutions and pushes the optimum towards smaller systems. Instead, from the bottom two charts it is possible to see how even if the best solutions

are similar in characteristics, the payback time increases drastically. This is due to the lower difference in cash flow, which makes the investment less profitable.

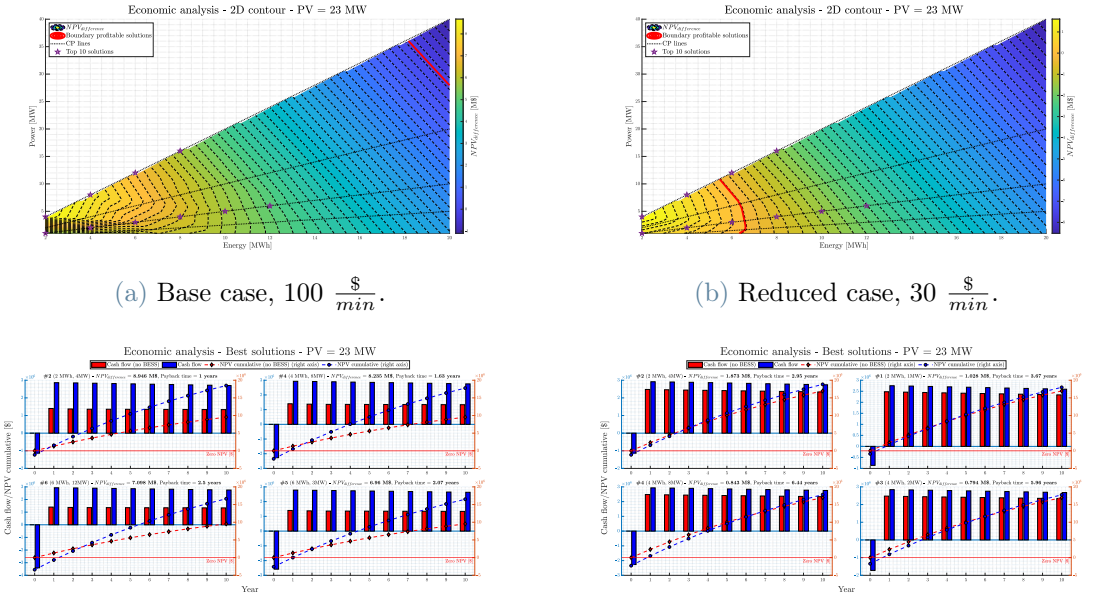

(a) Base case, 100 $\frac{\$}{min}$.

(b) Reduced case, 30 $\frac{\$}{min}$.

(c) Base case, 100 $\frac{\$}{min}$, best solutions.

(d) Reduced case, 30 $\frac{\$}{min}$, best solutions.

Figure 4.6: Energetic mode, analysis on the impact of the violation cost.

To better understand how the PV smoothing algorithm works in the case study, it is possible to take a closer look to how the *BESS* works in detail and comparing the simulation run 1 and 45 that represent two opposite solutions, one with 8450 minutes of violations per year, while the other has 461 minutes. In Figures 4.7a and 4.7b the top plot does not show any detailed information, if not for the red bands which represent a violation event. The bottom one instead shows how the *BESS* works properly inside the *SOC* management region as required. The batteries, which cycle almost once every 2 days in one case and 3 in the other, have as mean *CP* the value of 0.2370 and 0.5221, which is quite low, thus slowing down the cycling ageing. The *DOD* is also limited as well thanks to the aforementioned *SOC* management strategy.

The second row, composed of Figures 4.7c and 4.7d, shows instead a more detailed weekly zoom. This is helpful to address how the *SOC* varies during multiple days, as well as assessing the impact of the auxiliaries which drain the battery during the night.

Lastly, in the third row composed of Figures 4.7e and 4.7f is showing a few minutes of a day. Indeed, it is immediately clear the how the difference in installed power leads to violation on the case on the left, while the one on the right smoothly allows the PV to keep

injecting the power in the grid while not violating the ramp rate constraint. Furthermore, the purple areas on the bars on the left indicate that power has been curtailed, and thus a remuneration loss.

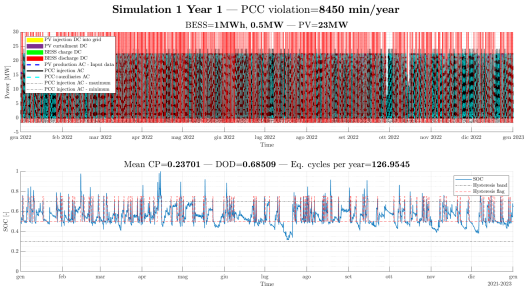

(a) Simulation 1, yearly plot.

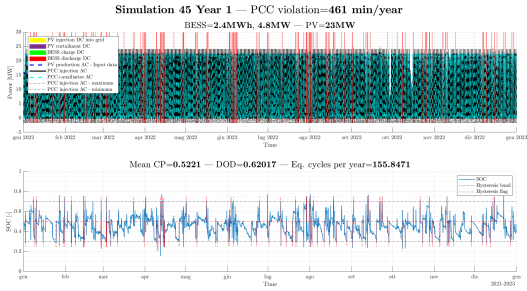

(b) Simulation 45, yearly plot.

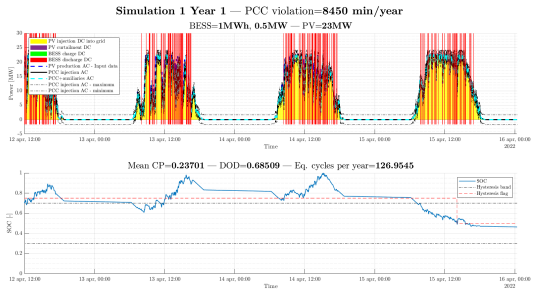

(c) Simulation 1, weekly plot.

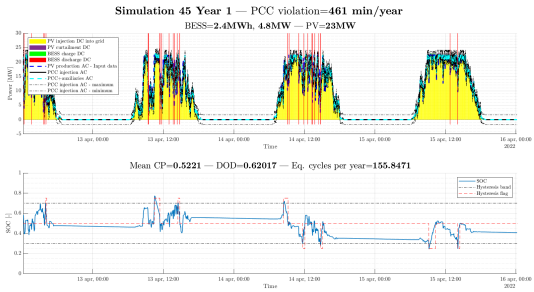

(d) Simulation 45, weekly plot.

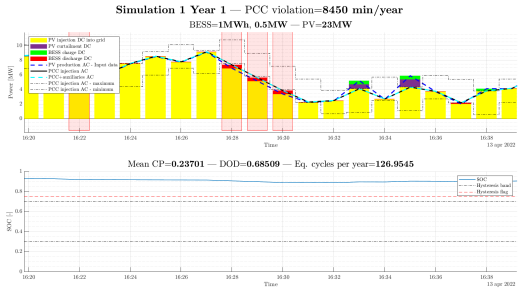

(e) Simulation 1, minutely plot.

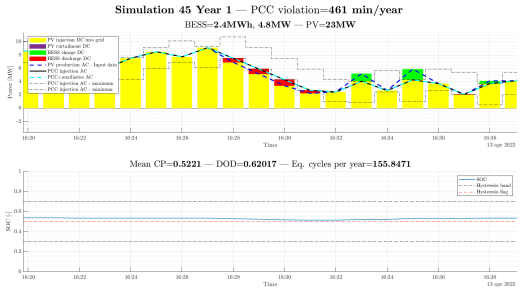

(f) Simulation 45, minutely plot.

Figure 4.7: Energetic mode, detailed analysis of the yearly, daily and minutely plot.

4.1.5. Engineered

The engineered method is, counter-intuitively, easier to setup as all the work is already done in the background during the *Initialize* function of *sMAPPER*. In fact, the only parameters to set are related to the filter, which in this case was disabled, the coupling method, which is AC in this case study, and the same application-dependent parameters as the energetic simulations, such as the PV inverter or HV skid efficiencies.

Prior to the simulation, the space of explorable solutions has to be checked. In Figure 4.8 such space is shown. The first thing that can be spotted is that the size of the solution exceeds in some cases the one required by the case study. This is because some Power Island combinations, even in the minimum quantity, are designed with a high number of containers and battery racks. Indeed, those simulations will perform poorly. The ones which are expected to work at best are the ones on the left-bottom corner, and represent also the ones with higher cost due to the lack of economies of scale and higher *CP*. It needs to be reminded that the best solutions that were found in the *Energetic* mode, that laid on the 2C line, are not available in the *Engineered* mode as the market has shifted since then more towards 2h+ batteries for *BESS* applications.

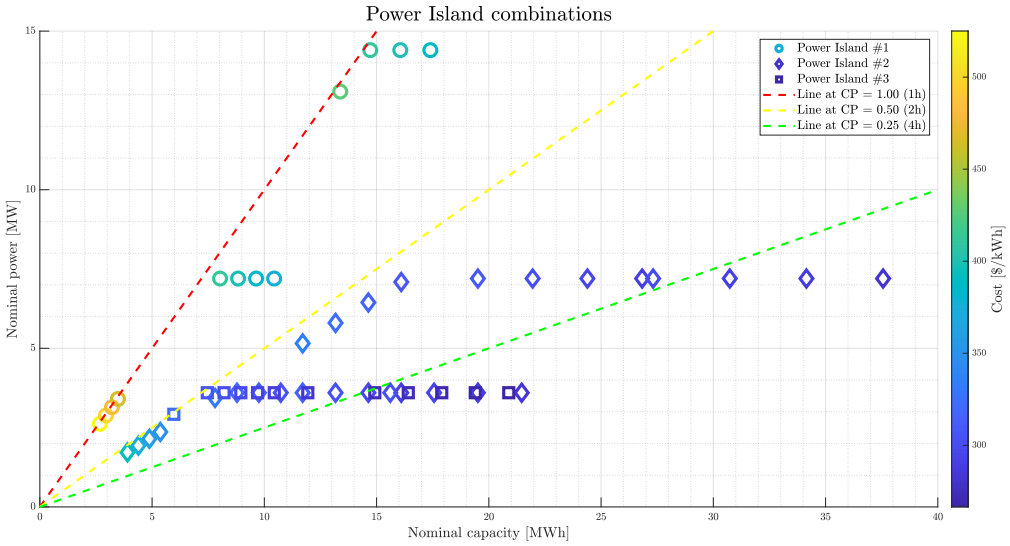

Figure 4.8: *Engineered* Power Island combinations.

Regarding the costs, in the *Engineered* mode they should represent realistically the distribution that is to be expected in a real project. Figure 4.9 shows how different Power Islands have different costs shapes. For instance, solutions with turn-key batteries would allocate more resources to them, while in-house engineered products would share more similar figures. The right-most solutions have a higher battery share due to their higher base capacity, that reduces the impacts of fixed costs and conversion units.

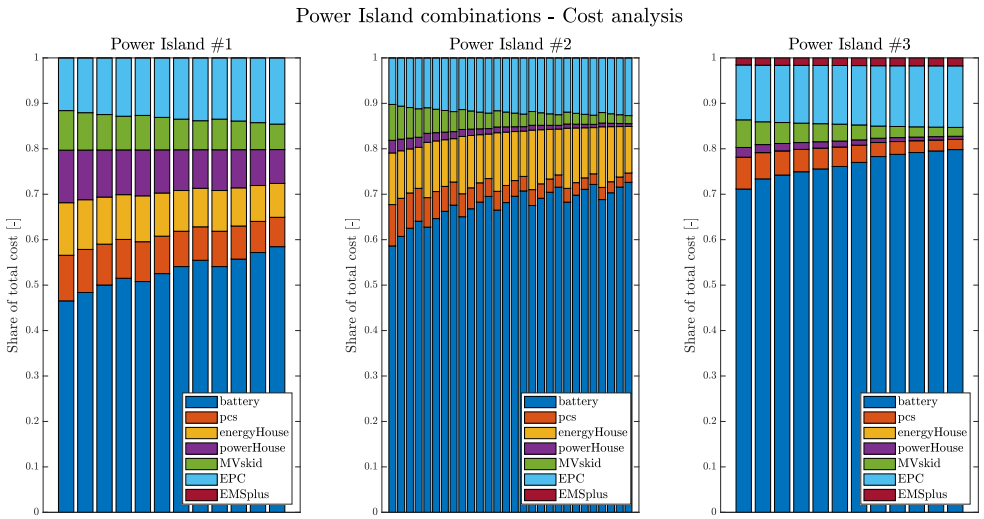

Figure 4.9: *Engineered* Power Island share of costs.

Subsequently, the simulation can be run which, in the end, it took $\sim 7000s$ to explore 52 candidates for 10 years, more than doubling the time with respect to the energetic one. The solutions, as already anticipated by Figure 4.8, has many simulations which will be oversized, and thus will not be reported as they are clearly poor solutions. The main results are reported below in Figures 4.10 and 4.11. As for the *Energetic* case, the best solutions are to be found in the smaller *BESS* sizes and at high CP rates. The contour plot in Figure 4.10 shows a more erratic line in accordance to the non-homogeneous space in the *Engineered* solutions. As before, the best solutions here are heavily influenced by the violation cost, and running a sensitive analysis yielded the same results as the *Energetic* one.

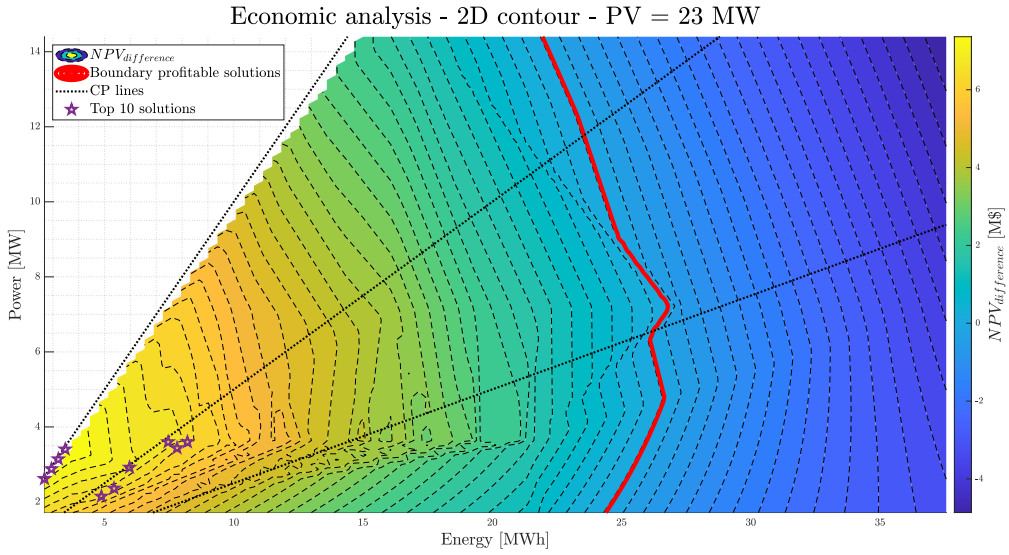

Figure 4.10: Engineered mode, contour map.

Figure 4.11 shows a more realistic estimate of costs and sizes of different *BESS*s. Indeed, if in future developments the Top-Up strategy will be implemented, this chart will become even more significant, showing how a second investment mid-life influences the overall cash flow and *NPV*.

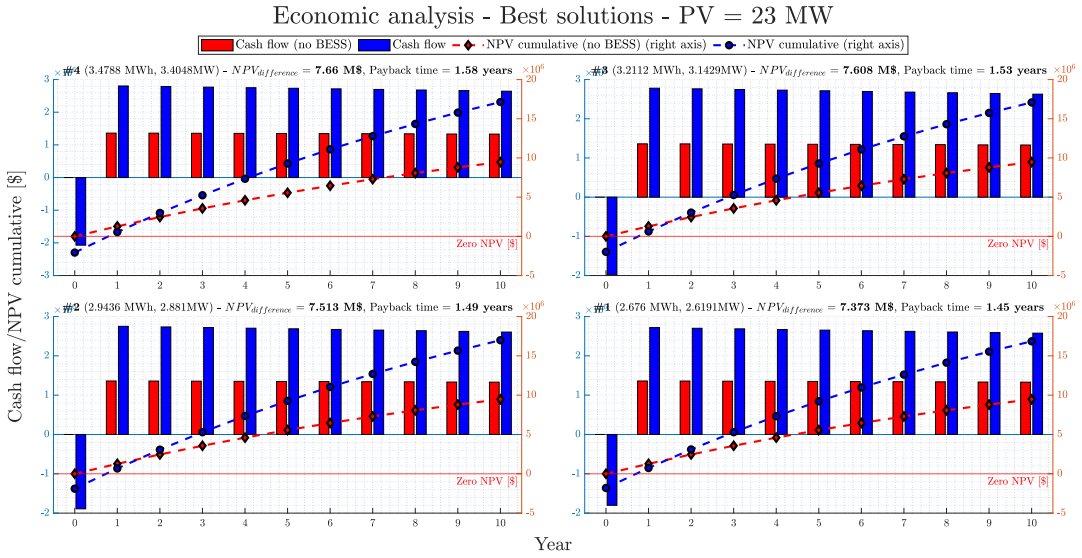

Figure 4.11: Engineered mode, best solutions.

Regarding the yearly plots, the shape is pretty similar as the *EMS* is the same. In Figure 4.12 it is reported an example of one of the optimal simulation that meets the constraint

of violation time under the 0.1%. Indeed, as the battery capacity is oversized, the amount of cycles per year is very low at about 35. This is a clear sign of under-utilization of the *BESS* and thus making a good argument to implement another service along the PV smoothing which makes use of its high capacity. In fact it is not rare to couple services like this one other ones which are energy intensive, such as Peak Shaving. This approach would be the most profitable one, but also the most complex to implement in a simulation framework. For this reason, the multi-application is one of the first future improvements of *sMAPPER*.

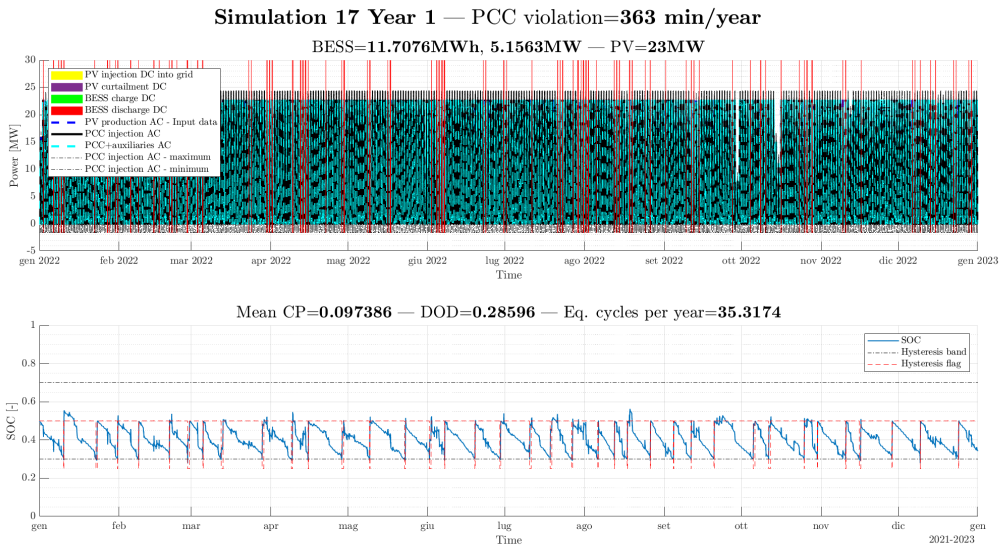

Figure 4.12: Engineered mode, simulation 17, year 1, yearly plot.

It is interesting to note that as the years go by, the performances of the *BESS* improve in terms of violation per year. As shown in Figure 4.13, the installed power does not fade, while the PV power plant does, leaving to smaller absolute ramps which are compensated by the *BESS* more easily. The capacity, which decreases with ageing, is not impactful here due to the oversizing.

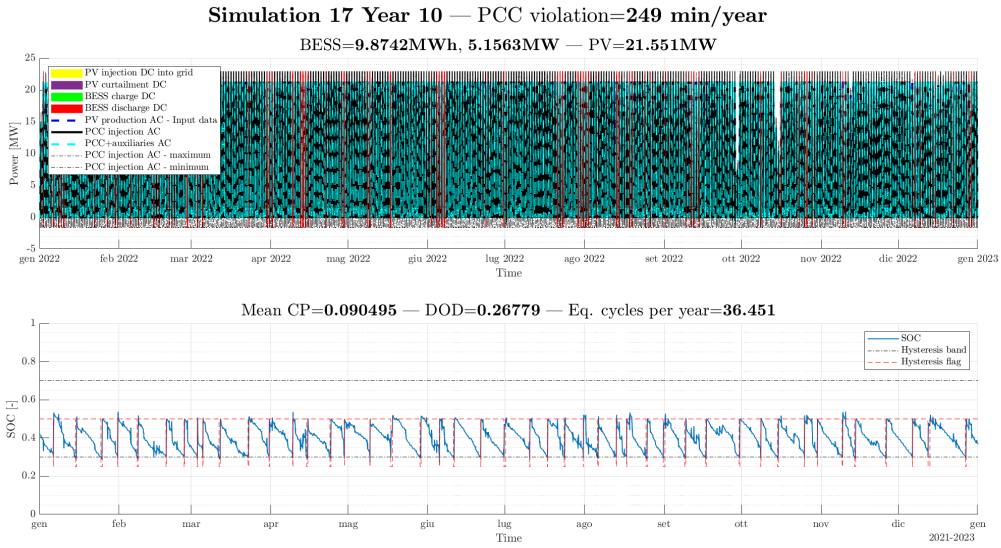

Figure 4.13: Engineered mode, simulation 17, year 10, yearly plot.

The best and more significant results are reported in Table 4.7. It is interesting to see that what would be defined as the best solution is the simulation 17 which has an installed power of 5.2 MW, exactly the same as the one installed in 2019 in *Sol de Insurgentes*. This combination, while being bigger in capacity, still retains the same performances while having a lower cost compared to the other compliant candidates.

Simulation number	Power Island	Nominal energy [MWh]	Nominal power [MW]	Cost [$/kWh]	Violations [min/year]	Eq. cycles [cycles/year]	Mean CP [-]	DOD [-]	PV produced DC [MWh]	PV curtailed DC [MWh]
2	1	3	2.9	500.998	1428.000	107.9	0.3	0.5	57787.4	32.5
6	**1**	**15**	**14.4**	**411.635**	**0.200**	**30.2**	**0.1**	**0.3**	**57819.9**	**0.0**
9	**1**	**8**	**7.2**	**411.732**	**77.800**	**50.5**	**0.2**	**0.4**	**57818.7**	**1.2**
13	2	4	1.7	391.496	3244.800	72.4	0.2	0.5	57733.6	86.4
17	**2**	**12**	**5.2**	**334.444**	**306.600**	**36.4**	**0.1**	**0.3**	**57814.6**	**5.3**
22	2	9	3.6	321.021	812.100	42.4	0.1	0.4	57801.4	18.5

Table 4.7: Results averaged over the 10 years of the Engineered simulation.

Following the same reasoning as in the *Energetic* case, it is not a given that the best solution will also be compliant to the 0.1% limit. Indeed, looking at Table 4.8, it is clear how the highest NPV solution (highlighted in yellow) is not compliant, but rather follow the strategy of smaller size as possible to achieve lower investment costs. It is noteworthy to see that the remuneration loss does not decrease with bigger *BESS*s, but rather increases. This is not due to the more curtailed energy as it is clear from Table 4.7, but rather from an higher auxiliary consumption related to the bigger *BESS*, which leads to more "wasted" energy from the PV power plant.

Simulation number	Nominal energy [MWh]	Nominal power [MW]	Violations [min/year]	Cost [$/kWh]	Remuneration [$/year]	Auxiliary consumption [MWh/year]	Remuneration loss [$/year]	Violation cost [$/year]	NPV cumulative [$]
2	2.9436	2.880960151	1428	501.0	$ 2,857,081	34.98	$ 5,005	$ 142,800	$ 9,627,845
6	**14.718**	**14.4**	**0**	**411.6**	**$ 2,853,027**	**140.24**	**$ 9,059**	**$ 20**	**$ 4,276,610**
9	**8.028**	**7.2**	**78**	**411.7**	**$ 2,855,776**	**88.40**	**$ 6,310**	**$ 7,780**	**$ 7,837,821**
13	3.902545455	1.718774655	3245	391.5	$ 2,853,404	65.83	$ 8,682	$ 324,480	$ 8,742,893
17	**11.70763636**	**5.156323964**	**307**	**334.4**	**$ 2,854,392**	**119.64**	**$ 7,693**	**$ 30,660**	**$ 6,915,071**
22	8.780727273	3.6	812	321.0	$ 2,856,162	73.45	$ 5,924	$ 81,210	$ 8,128,075

Table 4.8: Economic results averaged over the 10 years (except for the NPV cumulative) of the Engineered simulation.

Lastly, some more advanced analysis is available for the user if required for both simulation modes in the form of charts, reported in Figure 4.14 and Figure 4.15. They concern both the *SOC* distribution, the rest *SOC*, and the power distribution. Their focus is to analyze in which conditions the BESS works throughout the year, allowing more insights regarding the battery working regions, as well as checking on compliance on particular parameters.

More in detail, Figure 4.14 shows on the top the *SOC* distribution over the year, with the y-axis representing the hours per year. The bars allow the user to have, at a glance, if the *SOC* management strategy works properly, along with understanding if the battery is not undersized and thus often fully discharged. The bottom plot shows instead the power distribution. While it may seems at first that the plot is empty, the reality is that the battery most of the time is either idle or working at very low power values, thus the single tall bar at the 0 x-axis. To overcome this, a log plot is drawn inside showing how the peaks coincide with some notable points: battery at idle at the 0 power, battery charging power during the SOC management at $\sim -0.5MW$(10% of installed power), and the two peaks at the extremes that represent the moments in which the *BESS* works at its maximum (thus representing also the cases in which the BESS cannot comply with the ramp rate).

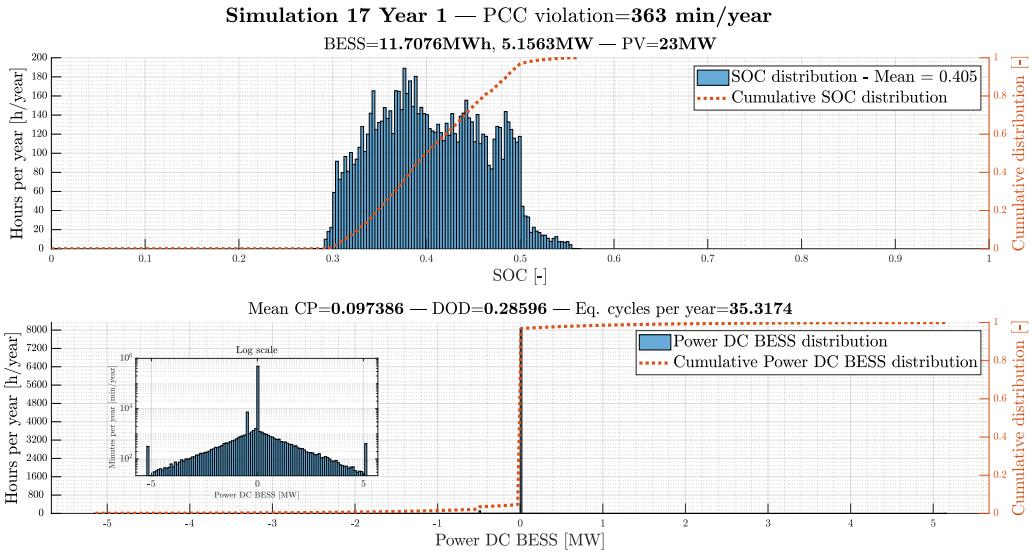

Figure 4.14: Engineered mode, simulation 17, year 1, SOC and power distribution.

On the other hand, Figure 4.15 reports data about the rest *SOC*. The top chart reports a similar shape as the previously described one, as this represents the SOC distribution indirectly. Thus, while it may not be directly useful, it comes in handy when assessing the battery ageing, which rely also on the rest *SOC* time and value. Indeed, this chart gives insights about this matter. The bottom chart reports the rest time, and in particular its distribution. The x-axis represents the rest time (namely the number of consecutive minutes in which the battery is idle), while the y-axis represents for how many hours per year this behavior happens.

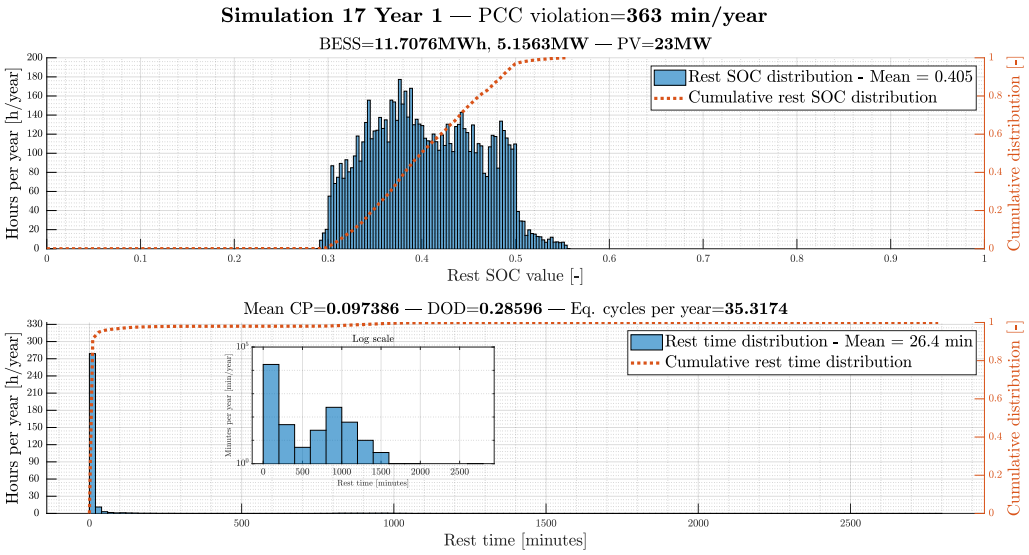

Figure 4.15: Engineered mode, simulation 17, year 1, rest SOC distribution.

5 | Conclusions and future developments

Within this work, this presented. *sMAPPER* provides a state-of-the-art energy storage model and combines it with the modularity of multiple topologies as well as the periphery of an *ESS*. This paper summarizes the structure as well as the capabilities of *sMAPPER*. Storage technology models based on current research for lithium-ion batteries are presented in detail. In addition, HVAC systems and containers models are depicted. Power electronics are represented with *AC-DC* and *DC-DC* converters mapping the main losses of power electronics within a storage system. Additionally, auxiliary components like *MV* skid are considered. A standard use case like *PV smoothing* is discussed in this work. The analysis is provided by technical and economic evaluations illustrated by *KPI*s. *sMAPPER*'s capabilities are demonstrated through the discussion of a case study mapped to the applications of *PV* smoothing. It is demonstrated how different energy storage system topologies as well as various performance indicators can be investigated and analyzed with *sMAPPER*. In the future, more detailed performance and aging models for all types of storage systems will be implemented. Investigations into other operational strategies that correspond to nationally and globally recognized derivatives of application scenarios are also possible.

5.1. Results

The results are very promising, producing an output that closely matches the sizing proposed and built by *NHOA* in 2019 in Mexico. This shows how even a simpler approach, the *Energetic* one, yield excellent results in line with the case study proposed within reasonable simulation timeframes. The economic analysis, while not being robust enough to evaluate it directly due to the confidentiality, gives nevertheless an insight of the best cases. Other results have to be checked as well to ensure the compliance of the solutions, such as the number of violations per year. Indeed, The capability of *sMAPPER* to produce high-level analysis as well as minute per minute simulation plots allow the

user to asses every aspect of the project in an accurate manner. Furthermore, the *Engineered* simulation produced even more realistic results, providing an optimal solution with components and subsystems very similar to the one built in the study case back in 2019 despite the difference in battery technologies.

5.2. Future developments

Some aspects, which are not essential, were left out but nonetheless taken into account when designing the use of the tool for the future. Hereafter some of them are discussed. Among the many features that are meant to be implemented, *sMAPPER* is furthermore intended to be used in combination with other internal simulation tools, such as the internal platform Modular Multi-Service Model (*MMSM*), which could be called parametrically through sMAPPER to explore the impact of different system architectures or set of operating parameters (e.g., alternative service plans) on the overall system performance. Hereafter some of them are discussed:

- **Sensitive analysis**: as of today, the sensitive analysis is possible only on the main parameters such as installed capacity, installed power and PV DC peak power. While these cover the main sensitive analysis that one would study, other interesting parameters could be assessed to further improve the simulation. For instance, being able to assess different ramp rate limits or PV degradation rates would allow to understand how they impact the solution. Indeed, once a general method could be established, any variable or parameter could be part of a sensitive analysis.
- **Application**: for the moment, only the PV smoothing (and the *PFR*, but not reported in this thesis due to it being incomplete) is implemented. In the future, it will be possible to add more algorithms such as peak shaving, which copes very well with the other present services. In fact, one big improvement would be to implement the possibility to use multi-applications in a single simulation. Indeed, this would allow to make use of a *BESS* even better.
- **Top-Up strategy**: this technique is very important when it comes to planning over the next 5 to 10 years. The *BESS* capacity fades over the years, and for this reason it is usually oversized to account for this. Since the warranties in the contract impose minimum capacities according to the different year, it usually happens that the best compromise in time between oversizing more and revamping the power plant too early is about 3 to 5 years. The trade-off comes from the fact that while (intuitively) a bigger initial investment increases the payback time and return rate, revamping comes with its challenges too. Indeed, it requires re-doing all the *EPC*. Also the land

footprint plays an important role. Nevertheless, the most important aspect when performing the Top-Up strategy is to decide whether to exploit the empty free racks left when designing the *BESS*, or to install new containers. This decision is based on many issues that come up due to logistics, spacing and designing. In particular, to install new batteries in the same containers it is required first that all the battery racks inside are transferred and split among other container, grouping them by the same degradation state as this is mandatory. Then, the empty container has to be filled with new battery racks that increase the overall capacity of the *BESS*. Furthermore, as manufacturers and battery chemistries change, problems about compatibility may arise.

- **Stochasticity**: since *sMAPPER* can work with applications such as *PV smoothing* or *PFR*, the input data is usually given as it is, and all the simulations rely always on the same numbers. The idea of introducing a controlled stochasticity environment where the randomness is controlled by seeds to allow repeatability of the runs is a valuable one. Indeed, it would make the simulations more robust to different scenarios conditions that may not have arisen from the gathered data. This approach needs some effort in order to be able to induce random variations, while keeping the same shape of the original data.

- **Simulation optimization**: there are many ways to optimize the computational time of the simulations. The first one would be to improve the code of each application, as well as structure the workspace such that it can be accessed easily by Matlab and thus reducing the overhead. Another interesting follow-up would be to implement some heuristics that would spot during a simulation if the latter is a sub-optimal case, without needing to run the whole time horizon. While this would reduce the number of results in the output, the speed would drastically increase as usually many candidates from the different *Power Islands* are not the right ones from the beginning. This will be especially crucial when implementing more complex and advanced *EMS* strategies inside *sMAPPER* that will increase the computational time even more.

Bibliography

[1] Volkmar Lauber and Staffan Jacobsson. The politics and economics of constructing, contesting and restricting socio-political space for renewables – the german renewable energy act. *Environmental Innovation and Societal Transitions*, 18:147–163, 3 2016. ISSN 22104224. doi: 10.1016/j.eist.2015.06.005.

[2] Hannah E. Murdock, Duncan Gibb, and Thomas Andre. Renewables 2021 - global status report. Technical report, France, 2021. URL `http://inis.iaea.org/search/search.aspx?orig_q=RN:52059346`.

[3] International Renewable Energy Agency. *Renewable Power Generation Costs in 2021*. Clarendon Press, 2021. ISBN 978-92-9260-452-3.

[4] P. Denholm, E. Ela, B. Kirby, and M. Milligan. Role of energy storage with renewable electricity generation. Technical report, National Renewable Energy Laboratory (NREL), 1 2010.

[5] Stefan Englberger, Andreas Jossen, and Holger Hesse. Unlocking the potential of battery storage with the dynamic stacking of multiple applications. *Cell Reports Physical Science*, 1:100238, 11 2020. ISSN 26663864. doi: 10.1016/j.xcrp.2020.100238.

[6] Dimitrios Zafirakis, Konstantinos J. Chalvatzis, Giovanni Baiocchi, and Georgios Daskalakis. The value of arbitrage for energy storage: Evidence from european electricity markets. *Applied Energy*, 184:971–986, 12 2016. ISSN 03062619. doi: 10.1016/j.apenergy.2016.05.047.

[7] Raymond H. Byrne, Ricky J. Concepcion, and Cesar A. Silva-Monroy. Estimating potential revenue from electrical energy storage in pjm. pages 1–5. IEEE, 7 2016. ISBN 978-1-5090-4168-8. doi: 10.1109/PESGM.2016.7741915.

[8] Annette Evans, Vladimir Strezov, and Tim J. Evans. Assessment of utility energy storage options for increased renewable energy penetration. *Renewable and Sustainable Energy Reviews*, 16:4141–4147, 8 2012. ISSN 13640321. doi: 10.1016/j.rser.2012.03.048.

[9] Tjark Thien, Daniel Schweer, Denis vom Stein, Albert Moser, and Dirk Uwe Sauer. Real-world operating strategy and sensitivity analysis of frequency containment reserve provision with battery energy storage systems in the german market. *Journal of Energy Storage*, 13:143–163, 10 2017. ISSN 2352152X. doi: 10.1016/j.est.2017.06.012.

[10] Alexandre Oudalov, Rachid Cherkaoui, and Antoine Beguin. Sizing and optimal operation of battery energy storage system for peak shaving application. pages 621–625. IEEE, 7 2007. ISBN 978-1-4244-2189-3. doi: 10.1109/PCT.2007.4538388.

[11] Joern Hoppmann, Jonas Volland, Tobias S. Schmidt, and Volker H. Hoffmann. The economic viability of battery storage for residential solar photovoltaic systems – a review and a simulation model. *Renewable and Sustainable Energy Reviews*, 39: 1101–1118, 11 2014. ISSN 13640321. doi: 10.1016/j.rser.2014.07.068.

[12] IRENA. Electricity storage and renewables: Costs and markets to 2030, international renewable energy agency, abu dhabi, 2017. URL `https://www.irena.org/-/media/Files/IRENA/Agency/Publication/2017/Oct/IRENA_Electricity_Storage_Costs_2017_Summary.pdf`. Last accessed 10 September 2022.

[13] Holger Hesse, Rodrigo Martins, Petr Musilek, Maik Naumann, Cong Truong, and Andreas Jossen. Economic optimization of component sizing for residential battery storage systems. *Energies*, 10:835, 6 2017. ISSN 1996-1073. doi: 10.3390/en10070835.

[14] Stefan Englberger, Holger Hesse, Daniel Kucevic, and Andreas Jossen. A techno-economic analysis of vehicle-to-building: Battery degradation and efficiency analysis in the context of coordinated electric vehicle charging. *Energies*, 12:955, 3 2019. ISSN 1996-1073. doi: 10.3390/en12050955.

[15] Olga Moraes Toledo, Delly Oliveira Filho, and Antônia Sônia Alves Cardoso Diniz. Distributed photovoltaic generation and energy storage systems: A review. *Renewable and Sustainable Energy Reviews*, 14:506–511, 1 2010. ISSN 13640321. doi: 10.1016/j.rser.2009.08.007.

[16] Marc Möller, Daniel Kucevic, Nils Collath, Anupam Parlikar, Petra Dotzauer, Benedikt Tepe, Stefan Englberger, Andreas Jossen, and Holger Hesse. Simses: A holistic simulation framework for modeling and analyzing stationary energy storage systems. *Journal of Energy Storage*, 49, 5 2022. ISSN 2352152X. doi: 10.1016/j.est.2021.103743.

[17] Bruce Dunn, Haresh Kamath, and Jean-Marie Tarascon. Electrical energy storage

for the grid: A battery of choices. *Science*, 334:928–935, 11 2011. ISSN 0036-8075. doi: 10.1126/science.1212741.

[18] T. Tjaden Weniger. Performance-simulationsmodell für ac-gekoppelte pv-batteriesysteme (permodac): Dokumentation | version 1.0, hochschule fürtechnik und wirtschaft h.t.w. berlin, berlin, 2017. URL `https://solar.htw-berlin.de/wp-content/uploads/HTW-PerMod-Dokumentation.pdf`. Last accessed 17 August 2022.

[19] Nirmal-Kumar C. Nair and Niraj Garimella. Battery energy storage systems: Assessment for small-scale renewable energy integration. *Energy and Buildings*, 42: 2124–2130, 11 2010. ISSN 03787788. doi: 10.1016/j.enbuild.2010.07.002.

[20] A.P.S. Ramalakshmi Sureshkumar, P.S. Manoharan. Economic cost analysis ofhybrid renewable energy system using homer. In *IEEE-International Conferenceon Advances in Engineering, Science and Management*, pages 94–99, 2012.

[21] Intregra Sources. Efficient energy management and energy saving with a bess (battery energy storage system), 2021. URL `https://www.integrasources.com/blog/energy-management-and-energy-saving-bess/`. Last accessed 10 September 2022.

[22] Joonki Song. Charged choices: The lfp vs nmc question. URL `https://www.ihiterrasun.com/charged-choices-the-lfp-vs-nmc-question/`. Last accessed 03 September 2022.

[23] Deutsches Zentrum für Luft-und Raumfahrt (DLR) / German Aerospace Centre. greenius: Green energy system analysis. URL `https://www.dlr.de/sf/en/desktopdefault.aspx/tabid-11688/20442_read-44865/`. Last accessed 04 September 2022.

[24] Battery University. Bu-802b: What does elevated self-discharge do?, 2021. URL `https://batteryuniversity.com/article/bu-802b-what-does-elevated-self-discharge-do`. Last accessed 17 August 2022.

[25] Eduardo Redondo-Iglesias, Pascal Venet, and Serge Pelissier. Measuring reversible and irreversible capacity losses on lithium-ion batteries. 5:2016–2026, 2016. doi: 10.1109/VPPC.2016.7791723Ãŕ. URL `https://dx.doi.org/10.1109/VPPC.2016.7791723`.

[26] *Lithium ion*. SANYO, 2006. Available at `https://web.archive.org/web/`

20060312062815/http://www.rathboneenergy.com/articles/sanyo_lionT_E.pdf. Last accessed 18 August 2022.

[27] Haiyu Liao, Bixiong Huang, Yan Cui, Huan Qin, Xintian Liu, and Huayuan Xu. Research on a fast detection method of self-discharge of lithium battery. *Journal of Energy Storage*, 55:105431, 11 2022. ISSN 2352152X. doi: 10.1016/j.est.2022.105431. URL https://linkinghub.elsevier.com/retrieve/pii/S2352152X22014232.

[28] A.H. Zimmerman. Self-discharge losses in lithium-ion cells. *IEEE Aerospace and Electronic Systems Magazine*, 19:19–24, 2 2004. ISSN 0885-8985. doi: 10.1109/MAES.2004.1269687. URL http://ieeexplore.ieee.org/document/1269687/.

[29] *Harding Battery Handbook For Quest ® Rechargeable Cells and Battery Packs*. Harding Energy, 2010. Available at http://nic.vajn.icu/PDF/battery/Rechargeable_Batteries.pdf. Last accessed 18 August 2022.

[30] Matthias Vetter and Stephan Lux. *Rechargeable Batteries with Special Reference to Lithium-Ion Batteries*. Elsevier, 2016. doi: 10.1016/B978-0-12-803440-8.00011-7.

[31] Keysight. Self-discharge measurement solutions, 2021. URL https://www.keysight.com/us/en/products/application-specific-test-systems/lithium-ion-battery-self-discharge-measurement-solutions.html. Last accessed 18 August 2022.

[32] DNK. Myth or fact: Lithium-ion batteries self-discharge after being fully charged, 2018. URL https://www.dnkpower.com/myth-or-fact-lithium-ion-batteries-self-discharge/. Last accessed 18 August 2022.

[33] I Bloom, B.W Cole, J.J Sohn, S.A Jones, E.G Polzin, V.S Battaglia, G.L Henriksen, C Motloch, R Richardson, T Unkelhaeuser, D Ingersoll, and H.L Case. An accelerated calendar and cycle life study of li-ion cells. *Journal of Power Sources*, 101:238–247, 10 2001. ISSN 03787753. doi: 10.1016/S0378-7753(01)00783-2.

[34] K. Jalkanen, J. Karppinen, L. Skogström, T. Laurila, M. Nisula, and K. Vuorilehto. Cycle aging of commercial nmc/graphite pouch cells at different temperatures. *Applied Energy*, 154:160–172, 9 2015. ISSN 03062619. doi: 10.1016/j.apenergy.2015.04.110.

[35] M. Broussely, Ph. Biensan, F. Bonhomme, Ph. Blanchard, S. Herreyre, K. Nechev, and R.J. Staniewicz. Main aging mechanisms in li ion batteries. *Journal of Power Sources*, 146:90–96, 8 2005. ISSN 03787753. doi: 10.1016/j.jpowsour.2005.03.172.

[36] Soo Seok Choi and Hong S Lim. Factors that affect cycle-life and possible degradation mechanisms of a li-ion cell based on licoo2. *Journal of Power Sources*, 111:130–136, 9 2002. ISSN 03787753. doi: 10.1016/S0378-7753(02)00305-1.

[37] D Aurbach, B Markovsky, I Weissman, E Levi, and Y Ein-Eli. On the correlation between surface chemistry and performance of graphite negative electrodes for li ion batteries. *Electrochimica Acta*, 45:67–86, 9 1999. ISSN 00134686. doi: 10.1016/S0013-4686(99)00194-2.

[38] Victor Agubra and Jeffrey Fergus. Lithium ion battery anode aging mechanisms. *Materials*, 6:1310–1325, 3 2013. ISSN 1996-1944. doi: 10.3390/ma6041310.

[39] Sung-Kyun Jung, Hyeokjo Gwon, Jihyun Hong, Kyu-Young Park, Dong-Hwa Seo, Haegyeom Kim, Jangsuk Hyun, Wooyoung Yang, and Kisuk Kang. Understanding the degradation mechanisms of lini _{0.5} co _{0.2} mn _{0.3} o ₂ cathode material in lithium ion batteries. *Advanced Energy Materials*, 4:1300787, 1 2014. ISSN 16146832. doi: 10.1002/aenm.201300787.

[40] Petr Novák, Felix Joho, Martin Lanz, Beat Rykart, Jan-Christoph Panitz, Dario Alliata, Rüdiger Kötz, and Otto Haas. The complex electrochemistry of graphite electrodes in lithium-ion batteries. *Journal of Power Sources*, 97-98:39–46, 7 2001. ISSN 03787753. doi: 10.1016/S0378-7753(01)00586-9.

[41] Pallavi Verma, Pascal Maire, and Petr Novák. A review of the features and analyses of the solid electrolyte interphase in li-ion batteries. *Electrochimica Acta*, 55:6332–6341, 9 2010. ISSN 00134686. doi: 10.1016/j.electacta.2010.05.072.

[42] Christoph R. Birkl, Matthew R. Roberts, Euan McTurk, Peter G. Bruce, and David A. Howey. Degradation diagnostics for lithium ion cells. *Journal of Power Sources*, 341:373–386, 2 2017. ISSN 03787753. doi: 10.1016/j.jpowsour.2016.12.011.

[43] J. Vetter, P. Novák, M.R. Wagner, C. Veit, K.-C. Möller, J.O. Besenhard, M. Winter, M. Wohlfahrt-Mehrens, C. Vogler, and A. Hammouche. Ageing mechanisms in lithium-ion batteries. *Journal of Power Sources*, 147:269–281, 9 2005. ISSN 03787753. doi: 10.1016/j.jpowsour.2005.01.006.

[44] Gang Ning and Branko N. Popov. Cycle life modeling of lithium-ion batteries. *Journal of The Electrochemical Society*, 151:A1584, 2004. ISSN 00134651. doi: 10.1149/1.1787631.

[45] Gang Ning, Ralph E. White, and Branko N. Popov. A generalized cycle life model

of rechargeable li-ion batteries. *Electrochimica Acta*, 51:2012–2022, 2 2006. ISSN 00134686. doi: 10.1016/j.electacta.2005.06.033.

[46] M. Safari, M. Morcrette, A. Teyssot, and C. Delacourt. Multimodal physics-based aging model for life prediction of li-ion batteries. *Journal of The Electrochemical Society*, 156:A145, 2009. ISSN 00134651. doi: 10.1149/1.3043429.

[47] R. Spotnitz. Simulation of capacity fade in lithium-ion batteries. *Journal of Power Sources*, 113:72–80, 1 2003. ISSN 03787753. doi: 10.1016/S0378-7753(02)00490-1.

[48] Qi Zhang and Ralph E. White. Capacity fade analysis of a lithium ion cell. *Journal of Power Sources*, 179:793–798, 5 2008. ISSN 03787753. doi: 10.1016/j.jpowsour.2008.01.028.

[49] Matthew B. Pinson and Martin Z. Bazant. Theory of sei formation in rechargeable batteries: Capacity fade, accelerated aging and lifetime prediction. *Journal of The Electrochemical Society*, 160:A243–A250, 2013. ISSN 0013-4651. doi: 10.1149/2.044302jes.

[50] E. Prada, D. Di Domenico, Y. Creff, J. Bernard, V. Sauvant-Moynot, and F. Huet. A simplified electrochemical and thermal aging model of lifepo ₄ - graphite li-ion batteries: Power and capacity fade simulations. *Journal of The Electrochemical Society*, 160:A616–A628, 2 2013. ISSN 0013-4651. doi: 10.1149/2.053304jes.

[51] John Christensen and John Newman. Stress generation and fracture in lithium insertion materials. *Journal of Solid State Electrochemistry*, 10:293–319, 5 2006. ISSN 1432-8488. doi: 10.1007/s10008-006-0095-1.

[52] Rutooj Deshpande, Mark Verbrugge, Yang-Tse Cheng, John Wang, and Ping Liu. Battery cycle life prediction with coupled chemical degradation and fatigue mechanics. *Journal of The Electrochemical Society*, 159:A1730–A1738, 1 2012. ISSN 0013-4651. doi: 10.1149/2.049210jes.

[53] K. Smith, E. Wood, S. Santhanagopalan, G. Kim, Jeremy Neubauer, and Ahmad Pesaran. Models for battery reliability and lifetime. *Battery Congr.*, pages 15–16, 01 2013.

[54] Izaro Laresgoiti, Stefan Käbitz, Madeleine Ecker, and Dirk Uwe Sauer. Modeling mechanical degradation in lithium ion batteries during cycling: Solid electrolyte interphase fracture. *Journal of Power Sources*, 300:112–122, 12 2015. ISSN 03787753. doi: 10.1016/j.jpowsour.2015.09.033.

[55] Michael Koller, Theodor Borsche, Andreas Ulbig, and Goran Andersson. Defining a degradation cost function for optimal control of a battery energy storage system. pages 1–6. IEEE, 6 2013. ISBN 978-1-4673-5669-5. doi: 10.1109/PTC.2013.6652329.

[56] O. Erdinc, B. Vural, and M. Uzunoglu. A dynamic lithium-ion battery model considering the effects of temperature and capacity fading. pages 383–386. IEEE, 6 2009. ISBN 978-1-4244-2543-3. doi: 10.1109/ICCEP.2009.5212025.

[57] Scott B. Peterson, Jay Apt, and J.F. Whitacre. Lithium-ion battery cell degradation resulting from realistic vehicle and vehicle-to-grid utilization. *Journal of Power Sources*, 195:2385–2392, 4 2010. ISSN 03787753. doi: 10.1016/j.jpowsour.2009.10.010.

[58] Miguel A. Ortega-Vazquez. Optimal scheduling of electric vehicle charging and vehicle-to-grid services at household level including battery degradation and price uncertainty. *IET Generation, Transmission & Distribution*, 8:1007–1016, 6 2014. ISSN 1751-8687. doi: 10.1049/iet-gtd.2013.0624.

[59] Anderson Hoke, Alexander Brissette, Dragan Maksimovic, Annabelle Pratt, and Kandler Smith. Electric vehicle charge optimization including effects of lithium-ion battery degradation. pages 1–8. IEEE, 9 2011. ISBN 978-1-61284-248-6. doi: 10.1109/VPPC.2011.6043046.

[60] Bolun Xu, Alexandre Oudalov, Andreas Ulbig, Göran Andersson, and Daniel S. Kirschen. Modeling of lithium-ion battery degradation for cell life assessment. *IEEE Transactions on Smart Grid*, 9:1131–1140, 2018. ISSN 19493053. doi: 10.1109/TSG.2016.2578950.

[61] Power Electronics. Energy storage power quality, . URL `https://www.power-electronics.co.nz/assets/brochures/Storage-Brochure-Sept2019.pdf`. Last accessed 04 September 2022.

[62] Power Electronics. Pure energy: Solar solutions, . URL `https://www.nuovaelva.it/docs/Power%20Electronics/Solar%20Brochure.pdf`. Last accessed 06 September 2022.

[63] ABB. Secondary skid unit (ssu): Solar power collection application with central inverter. URL `https://library.e.abb.com/public/fda25b0b072b48a5ab2275610a130030/SSU_central_inverter_data_sheet_rev_A_1YNE182002.pdf`. Last accessed 06 September 2022.

[64] REN21 Secretariat. Renewables 2019: Global status report, ren21 secretariat.

[65] LAZARD. Lazard's levelized cost of energy analysis—version 13.0; 2019, .

[66] LAZARD. Lazard's levelized cost of energy analysis—version 5.0; 2019, .

[67] EIA. Levelized cost and levelized avoided cost of new generation resources in the annual energy outlook 2020, u.s. energy information administration; 2020.

[68] Ward Jewell and R. Ramakumar. The effects of moving clouds on electric utilities with dispersed photovoltaic generation. *IEEE Transactions on Energy Conversion*, EC-2:570–576, 12 1987. ISSN 0885-8969. doi: 10.1109/TEC.1987.4765894.

[69] Rakibuzzaman Shah, N. Mithulananthan, R.C. Bansal, and V.K. Ramachandaramurthy. A review of key power system stability challenges for large-scale pv integration. *Renewable and Sustainable Energy Reviews*, 41:1423–1436, 1 2015. ISSN 13640321. doi: 10.1016/j.rser.2014.09.027.

[70] Javier Marcos, Luis Marroyo, Eduardo Lorenzo, David Alvira, and Eloisa Izco. Power output fluctuations in large scale pv plants: One year observations with one second resolution and a derived analytic model. *Progress in Photovoltaics: Research and Applications*, 19:218–227, 3 2011. ISSN 10627995. doi: 10.1002/pip.1016.

[71] Javier Marcos, Iñigo de la Parra, Miguel García, and Luis Marroyo. Control strategies to smooth short-term power fluctuations in large photovoltaic plants using battery storage systems. *Energies*, 7:6593–6619, 10 2014. ISSN 1996-1073. doi: 10.3390/en7106593.

[72] I. de la Parra, J. Marcos, M. García, and L. Marroyo. Control strategies to use the minimum energy storage requirement for pv power ramp-rate control. *Solar Energy*, 111:332–343, 1 2015. ISSN 0038092X. doi: 10.1016/j.solener.2014.10.038.

[73] Kari Lappalainen and Seppo Valkealahti. Output power variation of different pv array configurations during irradiance transitions caused by moving clouds. *Applied Energy*, 190:902–910, 3 2017. ISSN 03062619. doi: 10.1016/j.apenergy.2017.01.013.

[74] Kari Lappalainen, Guang C. Wang, and Jan Kleissl. Estimation of the largest expected photovoltaic power ramp rates. *Applied Energy*, 278:115636, 11 2020. ISSN 03062619. doi: 10.1016/j.apenergy.2020.115636.

[75] Ana Cabrera-Tobar, Eduard Bullich-Massagué, Mònica Aragüés-Peñalba, and Oriol Gomis-Bellmunt. Review of advanced grid requirements for the integration of large scale photovoltaic power plants in the transmission system. *Renewable and Sustainable Energy Reviews*, 62:971–987, 9 2016. ISSN 13640321. doi: 10.1016/j.rser.2016.05.044.

[76] S.M. Chalmers, M.M. Hitt, J.T. Underhill, P. Anderson, P. Vogt, and R. Ingersoll. The effect of photovoltaic power generation on utility operation. *IEEE Transactions on Power Apparatus and Systems*, PAS-104:524–530, 3 1985. ISSN 0018-9510. doi: 10.1109/TPAS.1985.318968.

[77] Gondia Sokhna Seck, Vincent Krakowski, Edi Assoumou, Nadia Maïzi, and Vincent Mazauric. Embedding power system's reliability within a long-term energy system optimization model: Linking high renewable energy integration and future grid stability for france by 2050. *Applied Energy*, 257:114037, 1 2020. ISSN 03062619. doi: 10.1016/j.apenergy.2019.114037.

[78] PREPA. Puerto rico electric power authority minimum technical requirements for photovoltaic generation (pv) projects, puerto rico electric power authority; 2012.

[79] CRE. Anexo 3: Requerimientos tecnicos para interconexion de centrales solares fotovoltaicas al sistema electrico nacional, in: Reglas generales de interconexion al sistema electrico nacional, comision reguladora de energia, mexico; 2014.

[80] CNE. National electricity rules version 150, australian energy market commission, australia; 2019.

[81] AEMC. Lazard's levelized cost of energy analysis—version 5.0; 2019.

[82] NERSA. Grid connection code for renewable power plants (rpps) connected to the electricity transmission system (ts) or the distribution system (ds) in south africa. version 3.0, national energy regulator of south africa, south africa, 2019.

[83] S. Shivashankar, Saad Mekhilef, Hazlie Mokhlis, and M. Karimi. Mitigating methods of power fluctuation of photovoltaic (pv) sources – a review. *Renewable and Sustainable Energy Reviews*, 59:1170–1184, 6 2016. ISSN 13640321. doi: 10.1016/j.rser.2016.01.059.

[84] Yu Jiang, John Fletcher, Patrick Burr, Charles Hall, Bowen Zheng, Da-Wei Wang, Zi Ouyang, and Alison Lennon. Suitability of representative electrochemical energy storage technologies for ramp-rate control of photovoltaic power. *Journal of Power Sources*, 384:396–407, 4 2018. ISSN 03787753. doi: 10.1016/j.jpowsour.2018.03.013.

[85] Bloomberg New Energy Finance. Curry c. lithium-ion battery costs and market; 2017.

[86] Richard Perez, Thomas Hoff, John Dise, David Chalmers, and Sergey Kivalov. The cost of mitigating short-term pv output variability. *Energy Procedia*, 57:755–762, 2014. ISSN 18766102. doi: 10.1016/j.egypro.2014.10.283.

[87] IEEE Trans Energy Convers. Beltran h, tomas garcia i, alfonso-gil jc, perez e. levelized cost of storage for liion batteries used in pv power plants for ramp-rate control. 2019;34(1):554–61.

[88] Shivashankar Sukumar, Marayati Marsadek, K.R. Agileswari, and Hazlie Mokhlis. Ramp-rate control smoothing methods to control output power fluctuations from solar photovoltaic (pv) sources—a review. *Journal of Energy Storage*, 20:218–229, 12 2018. ISSN 2352152X. doi: 10.1016/j.est.2018.09.013.

[89] D. Jordan and Sarah Kurtz. Photovoltaic degradation rates—an analytical review. *Progress in Photovoltaics: Research and Applications*, 21, 01 2013. doi: 10.1002/pip.1182.

[90] Wei Luo, Yong Sheng Khoo, Peter Hacke, Dirk Jordan, Lu Zhao, Seeram Ramakrishna, Armin G. Aberle, and Thomas Reindl. Analysis of the long-term performance degradation of crystalline silicon photovoltaic modules in tropical climates. *IEEE Journal of Photovoltaics*, 9:266–271, 1 2019. ISSN 2156-3381. doi: 10.1109/JPHOTOV.2018.2877007.

[91] Francesco Lo Franco, Antonio Morandi, Pietro Raboni, and Gabriele Grandi. Efficiency comparison of dc and ac coupling solutions for large-scale pv+bess power plants. *Energies*, 14:4823, 8 2021. ISSN 1996-1073. doi: 10.3390/en14164823.

[92] Power Technology. Sol de insurgentes solar pv park, mexico, 2022. URL `https://www.power-technology.com/marketdata/sol-de-insurgentes-solar-pv-park-mexico/`. Last accessed 11 September 2022.

[93] Suntech. 120 half-cell polycrystalline module, 2022. URL `https://www.suntech-power.com/wp-content/uploads/download/product-specification/EN_SuperPoly_STP300_60_Wfh.pdf`. Last accessed 11 September 2022.

[94] Green Tech Media. Solar stuns in mexico's first clean energy auction, 2016. URL `https://www.greentechmedia.com/articles/read/solar-stuns-in-mexicos-first-clean-energy-auction-1860-mw-won-at-50-7-p`. Last accessed 11 September 2022.

List of Figures

List of Tables